Copyright Warning & Restrictions

The copyright law of the United States (Title 17, United States Code) governs the making of photocopies or other reproductions of copyrighted material.

Under certain conditions specified in the law, libraries and archives are authorized to furnish a photocopy or other reproduction. One of these specified conditions is that the photocopy or reproduction is not to be "used for any purpose other than private study, scholarship, or research." If a, user makes a request for, or later uses, a photocopy or reproduction for purposes in excess of "fair use" that user may be liable for copyright infringement,

This institution reserves the right to refuse to accept a copying order if, in its judgment, fulfillment of the order would involve violation of copyright law.

Please Note: The author retains the copyright while the New Jersey Institute of Technology reserves the right to distribute this thesis or dissertation

Printing note: If you do not wish to print this page, then select "Pages from: first page # to: last page #" on the print dialog screen

ABSTRACT

INTERVENTIONS OF WATERJET TECHNOLOGY IN SKIN INCISIONS

by
Nadi Atalla

This research explores the use of waterjet (WJ) technology in performing skin incisions. The study defines the analytical relationships between the skin properties and the operating parameters of the WJ which include the skin thickness, its elastic modulus, the WJ pressure, the nozzle's orifice diameter, its stand-off distance and the traverse speed of the WJ as well as the duration of applying the WJ pressure. An analytical model is developed to measure the depth incision of the skin, the water pressure and the water velocity, while using a WJ. Systemization and optimization models that determine the optimal operating parameters levels to maximize the depth of incision as well as a specific target, accompany the analytical model.

The study also validates the developed models using literature as well as experimental verification. In the literature verification of previous work done using WJ to cut through bone cement, the percent error between the calculated depth of cut and the measured depth of cut ranged from as low as 2% to 11% error. The experimental verification uses a local WJ device to make cow skin and bone incisions. The percent error between the calculated depth of cut and the measured depth of cut ranged from as low as 9% to 23% error.

In order to illustrate the accuracy of the proposed models, they are applied to a case study: Cesarean section procedure. The analysis of results shows that the most significant factors that affect the depth of cut are the nozzle's orifice diameter, the water pressure, the

nozzle's loss coefficient and the traverse speed of the WJ. Using the results of the study, it is concluded that to make a 2.30 mm deep abdomen skin incision when the elastic modulus is 1 GPa, the optimal WJ operating parameters are 12.5 MPa water pressure with 0.3 mm nozzle's orifice diameter, 17 mm/s traverse speed and 0.15 nozzle's loss coefficient.

INTERVENTIONS OF WATERJET TECHNOLOGY IN SKIN INCISIONS

by
Nadi Atalla

A Dissertation
Submitted to the Faculty of
New Jersey Institute of Technology
in Partial Fulfillment of the Requirements for the Degree of
Doctor of Philosophy in Industrial Engineering

Department of Mechanical and Industrial Engineering

May 2019

APPROVAL PAGE

INTERVENTIONS OF WATERJET TECHNOLOGY IN SKIN INCISIONS

Nadi Atalla

Dr. George Abdou, Dissertation Advisor Associate Professor of Mechanical and Industrial Engineering, NJIT	Date
Dr. Paul Ranky, Committee Member Professor of Mechanical and Industrial Engineering, NJIT	Date
Dr. Athanassios Bladikas, Committee Member Associate Professor of Mechanical and Industrial Engineering, NJIT	Date
Dr. Ismet Esra Buyuktahtakin-Toy, Committee Member Associate Professor of Mechanical and Industrial Engineering, NJIT	Date
Dr. Sergei Adamovich, Committee Member Professor of Biomedical Engineering, NJIT	Date

BIOGRAPHICAL SKETCH

Author: Nadi Atalla

Degree: Doctor of Philosophy

Date: May 2019

Undergraduate and Graduate Education:

- Doctor of Philosophy in Industrial Engineering,
  New Jersey Institute of Technology, Newark, NJ, 2019

- Master of Science in Biomedical Engineering,
  New Jersey Institute of Technology, Newark, NJ, 2011

- Bachelor of Science in Biomedical Engineering,
  Rutgers University, New Brunswick, 2008

Major: Industrial Engineering

Presentations and Publications:

N. Atalla and G. Abdou, "Physical Experimentation using Waterjet for Animal Skin Incision," *International Journal of Advanced Manufacturing Technology,* submitted, April 2019.

N. Atalla and G. Abdou, "Analytical Model of Waterjet for Skin Incisions," *International Journal of Production Research,* submitted, April 2019.

N. Atalla and G. Abdou, "Applying Waterjet Technology in Surgical Procedures," in *Future Technologies Conference*, Vancouver, CA, 2018, pp. 616-625: Springer.

N. Atalla, "Non-Invasive Interventions to Reduce Low Back Dysfunction," in *IEEE 37th Annual Northeast Bioengineering Conference (NEBEC)*, Troy, NY, 2011: IEEE.

H. Chaudhry, N. Atalla, V. K. Singh, M. Roman, and T. Findley, "Evaluation of the Rotational Stiffness and Visco-Elasticity of the Low Back and Improving the Low Back Visco-Elasticity," *International Journal of Experimental and Computational Biomechanics,* vol. 1, no. 4, 2011.

H. J. Lee *et al*., "Gemini Vitamin D Analogs Inhibit Estrogen Receptor Positive and Estrogen Receptor Negative Mammary Tumorigenesis Without Hypercalcemic Toxicity," *American Association for Cancer Research,* vol. 68, no. 9, 2008.

This dissertation is dedicated to the people who stood by me during my ups and downs during the course of working on this dissertation. I am thankful to my wife, Katrina, my parents, Soheir and Atalla, my sister, Nadine and my whole family, my teachers and my friends who were there for me and gave me hope to reach this point in my life.

This dissertation is also dedicated to Theodore.

المسيح قام. حقاً قام.

ACKNOWLEDGMENT

I would like to thank Dr. George Abdou for not only being my advisor for my dissertation, but also for being my advisor in life by giving me general advice and by helping me not give up.

I would like to thank Dr. Sanchoy Das for all of his guidance and help throughout my PhD. I am honored and thankful to have Dr. Paul Ranky, Dr. Athanassios Bladikas, Dr. Ismet Esra Buyuktahtakin-Toy and Dr. Sergei Adamovich on my committee and for showing extreme interest in this research. I would also to specially thank Dr. Adamovich for funding my final semester's tuition.

I would like to thank the Industrial Engineering Department for funding the experiment at the makerspace laboratory.

I would like to recognize Professor Daniel Brateris and his team at the makerspace lab for their time and allowing me to use the waterjet machine to run my experiment, especially Mr. Christopher Eugenio. A special thanks to Mr. Aristides Chavez for fabricating the apparatus that was used for the experiment.

Finally, I would like to acknowledge the help of my family, friends and everyone who supported me in various ways during my research, especially Samir Arida, Anthony Fanous, Phillip Murphy and Rima Bandeli.

TABLE OF CONTENTS

TABLE OF CONTENTS
(Continued)

LIST OF TABLES

LIST OF TABLES
(Continued)

LIST OF FIGURES

LIST OF FIGURES
(Continued)

LIST OF FIGURES
(Continued)

CHAPTER 1

CLINICAL ASPECT

In today's medical field, doctors aim to conduct minimally invasive surgical procedures which suggest smaller incisions. There are two main types of minimally invasive surgical procedures: Robotic and Endoscopic. In a robotic-assisted surgery, computer software replaces the surgeon's actual hand movement. The surgeon operates a console that is two controllers that maneuver four robotic arms while viewing the images in 3-D on the console. In endoscopic surgery, the surgeon operates through small incisions that are made in various locations. Thin flexible tube with a video camera is inserted through the incised location as well as tiny surgical instruments that are necessary for the procedures [1]. In addition to the patient's preference, minimal invasive surgical procedures have many advantages: they cause lower blood loss, less scarring, lower chance of complications such as wound infections. Furthermore, with small incisions the recovery time is significantly shorter.

Waterjet (WJ) technology can be used to accomplish minimally invasive incisions in surgical procedures. The two main benefits of WJ technology are variability and simplicity. The sheer variety of materials and thicknesses that a WJ can cut illustrates the versatility. On the other hand, the simplicity of using the WJ technology is best illustrated when compared to laser, plasma and flame cutting [2]. While WJ is currently used for cutting a wide range of materials and applied to all kind of industries, only the medical field is being highlighted, and the focus of the research is its application in skin incisions. This chapter introduces the clinical aspects of the use of WJ technology. First, an overview

of the skin, its various properties and measurements are presented. Second, the different types of skin incisions are defined. Lastly, the different tools for the different skin incisions are introduced including the advantages and disadvantages of the WJ tool.

1.1 Human Skin Overview

Skin is the largest organ of the human body, it makes up 16% of body weight, with a surface area of 1.8 m^2 [3]. The human skin is a non-homogeneous, anisotropic, non-linear viscoelastic material whose properties vary with age, from site to site and per person [4]. As seen in Figure 1.1, the human skin is composed of several layers. The outer layer is the epidermis which serves as the physical and chemical barrier that protects the interior body from the exterior environment. The dermis is the deeper layer, it provides the structural support of the skin. Below the dermis layer is the subcutis layer or hypodermis which consists of the loose connective tissue and is an important depot of fat. Table 1.1 summarizes the different skin layers [3].

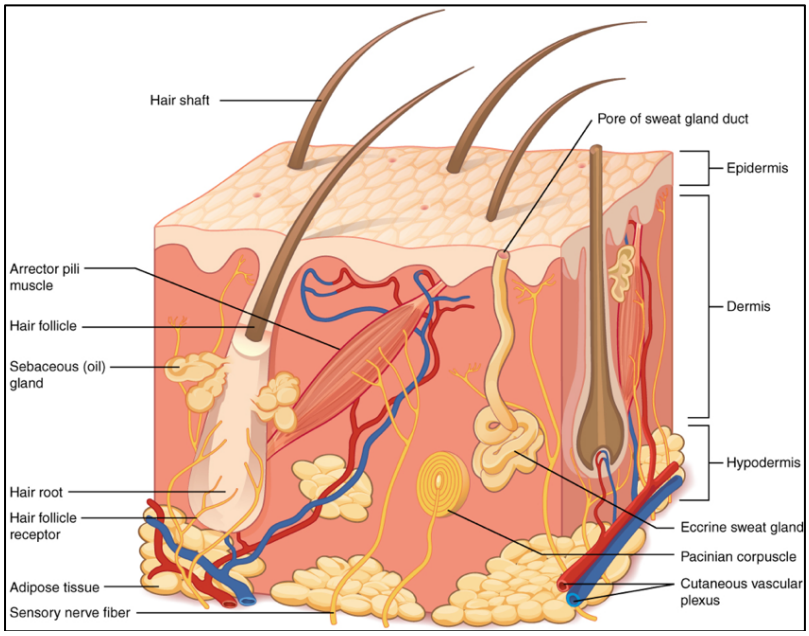

Figure 1.1 Anatomy of the human skin.
Source: [5].

Table 1.1 Different Human Skin Layers

Skin Layer	Description
Epidermis	The external layer mainly composed of layers of keratinocytes but also containing melanocytes, Langerhans cells and Merkel cells
Basement Membrane	The multilayered structure forming the dermoepidermal junction
Dermis	The area of supportive connective tissue between the epidermis and the underlying subcutis: contains sweat glands, hair roots, nervous cells and fibers, blood and lymph vessels
Subcutis	The layer of loose connective tissue and fat beneath the dermis

The epidermis' main cells are the keratinocytes, these cells synthesize the protein keratin. Desmosomes are protein bridges that connect the keratinocytes; they are in a constant state of transition from the deeper layers to the superficial layers. The epidermis is composed of four separate layers, which are formed by the differing stages of keratin

maturation. These layers are the stratum basale (most inner layer), the stratum spinosum, the stratum granulosum and the stratum corneum (most outer layer). The thickness of the epidermis varies from 0.05 mm on the eyelids to 0.8 ± 1.5 mm on the soles of the feet and palms of the hand [3].

The basement membrane is a 20 nm thick multilayered membrane is found between the epidermis and dermis [6].

The dermis is found below the epidermis and is composed of a tough, supportive cell matrix. The dermis is composed of two layers: A thin papillary layer and a thicker reticular layer. The papillary dermis lies below and connects with the epidermis. It is made up of thin collagen fibers that are loosely arranged. Running parallel to the skin surface in the deeper reticular layer are thicker bundles of collagen; they extend from the base of the papillary layer to the subcutis tissue. The dermis consists of fibroblasts that produce collagen, elastin and structural proteoglycans, together with immunocompetent mast cells and macrophages. 70% of the dermis is made up of collagen fibers which gives it strength and toughness [3]. These collagen fibers are characterized by high stiffness with a 0.1 to 1 GPa Young's modulus in the linear region and low extensibility which rupture at strains in the order of 5-6% [7]. The second main component of the dermis are the elastin fibers; they are less stiff than collagen and show reversible strains of more than 100% [7]. The normal elasticity and flexibility of the dermis is maintained by elastin while the viscosity and hydration are provided by proteoglycans. The dermal vasculature, lymphatics, nervous cells and fibers, sweat glands, hair roots and small quantities of striated muscle are embedded within the fibrous tissue of the dermis. The thickness of the dermis can vary from 0.6 mm on the eyelids to 3 mm on the back, palms and soles [3].

The subcutis is found below the dermis, which is made up of loose connective tissue and fat, which can be up to 3 cm thick on the abdomen [3].

Epidermal thickness differs by age, sex, gender, skin type, porcine mentation, blood content, smoking habits, body site, geographical location and many other variables [8]. Table 1.2 presents the average skin thickness of the triceps, anterior abdomen as well as anterior thigh for 297 healthy adult humans [9]. Figure 1.2 also breaks down the data to show the difference in skin thickness for males and females [9].

Table 1.2 Skin Thickness at Different Body Locations

	Triceps	Anterior Abdomen	Anterior Thigh
Epidermis + Dermis	1.87 ± 0.34 mm	2.30 ± 0.43 mm	1.89 ± 0.41 mm
Subcutaneous Adipose Tissue	6.06 ± 5.49 mm	15.18 ± 9.65 mm	7.72 ± 6.19 mm

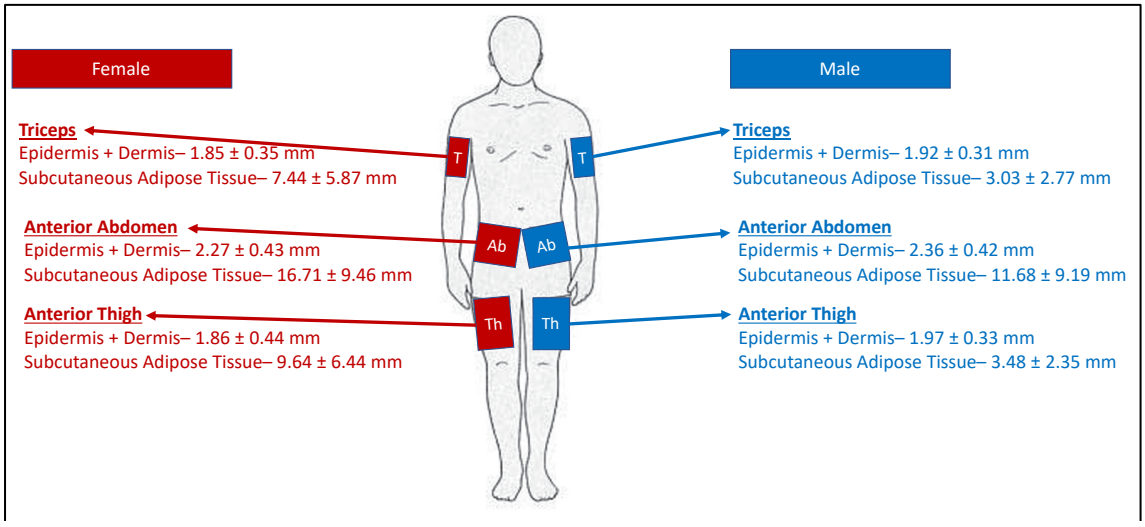

Figure 1.2 Skin thickness at different human body sites for males and females.

Tables 1.3, 1.4 and 1.5 show the different epidermis and dermis thickness of humans of the thigh, waist, deltoid and suprascapular according to their age, body type as well as their ethnic origin [10].

Table 1.3 Epidermis and Dermis Thickness at Different Body Locations According to Age

	Thigh	Waist	Deltoid	Suprascapular
18 – 30 years	1.64 mm	1.97 mm	2.12 mm	2.60 mm
31 – 40 years	1.59 mm	2.01 mm	2.09 mm	2.56 mm
41 – 50 years	1.61 mm	1.94 mm	2.10 mm	2.55 mm
51 – 70 years	1.60 mm	1.90 mm	2.13 mm	2.55 mm

Table 1.4 Epidermis and Dermis Thickness at Different Body Locations According to Body Type

	Thigh	Waist	Deltoid	Suprascapular
Underweight	1.59 mm	1.78 mm	1.93 mm	2.46 mm
Normal	1.54 mm	1.88 mm	2.02 mm	2.54 mm
Overweight	1.58 mm	1.96 mm	2.08 mm	2.56 mm
Obese	1.74 mm	2.20 mm	2.42 mm	2.70 mm

Table 1.5 Epidermis and Dermis Thickness at Different Body Locations According to Ethnic Origin

	Thigh	Waist	Deltoid	Suprascapular
Caucasian	1.71 mm	1.91 mm	2.12 mm	2.58 mm
Black	1.57 mm	1.94 mm	2.10 mm	2.58 mm
Asian	1.55 mm	2.02 mm	2.12 mm	2.53 mm

In order to accurately measure the skin thickness, skin imaging is necessary. Skin imaging was started by Alexander and Miller in 1979; using an unfocused transducer with a 15 MHz frequency, they were able to measure the thickness of the skin [11]. High frequency Ultrasound was later introduced with 20 MHz and higher transducers. High-frequency apparatuses are equipped with single element mechanical transducers with the frequency of 20- 100 MHz. All three layers of the skin are visible and may be distinguished in an ultrasound image of healthy skin. Figure 1.3 shows an example of a high frequency ultrasound image. The higher the resolution, the lower the depth of ultrasound beam penetration into the skin. This allows one to visualize greater number of details and for a more thorough assessment of the skin [12].

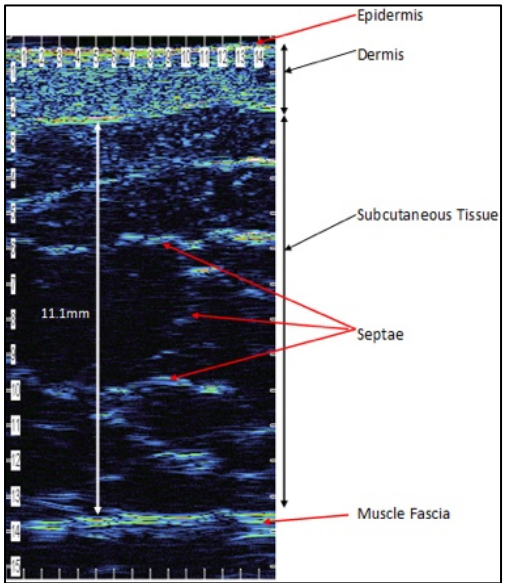

Figure 1.3 High frequency ultrasound image of the skin.
Source: [13].

The mechanical properties of the skin can vary due to individual factors such as exposure to Ultraviolet (UV) radiation, the use of creams, individual health and nutritional status [14]. There are three phases to describe a non-linear stress strain curve for the skin. The loading phase, where the fibers are unaligned, in that phase, low applied load causes

large deformation to the skin. The skin stiffness gradually increases in the second phase due to the fibers' alignment in the direction of the applied load. The skin stiffness increases rapidly due to the alignment of the collagen fibers which cause this phase to be almost linear. The overall mechanical response of the skin becomes dependent on the mechanical properties of the collagen fibers [15].

1.2 Types of Human Skin Incisions

Since the whole human body is covered with skin, it is the first incision that a surgeon has to make in almost any surgical procedure. This makes improving upon the ways and tools to incise the skin an interesting and attractive area of research. The length of the skin incision can vary from one surgery to another. For example, in a minimally invasive total hip replacement surgery (Figure 1.4), the length of incision can range from 5.1 cm to 12.7 cm [16], while the length of incision required for a laparoscopy procedure (Figure 1.5) is no more than 1.3 cm [17].

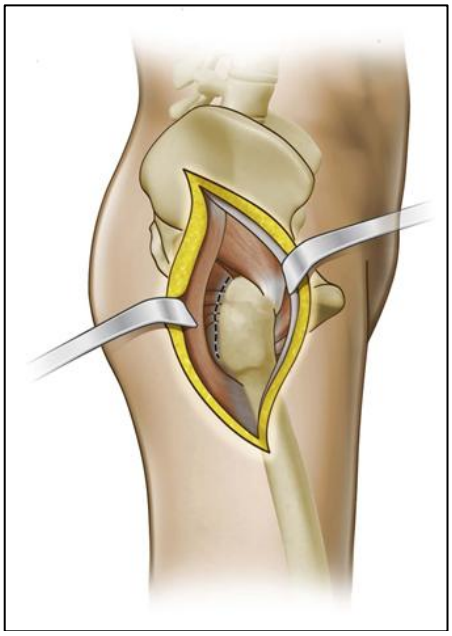

Figure 1.4 Example of total hip replacement surgery incision.
Source: [18].

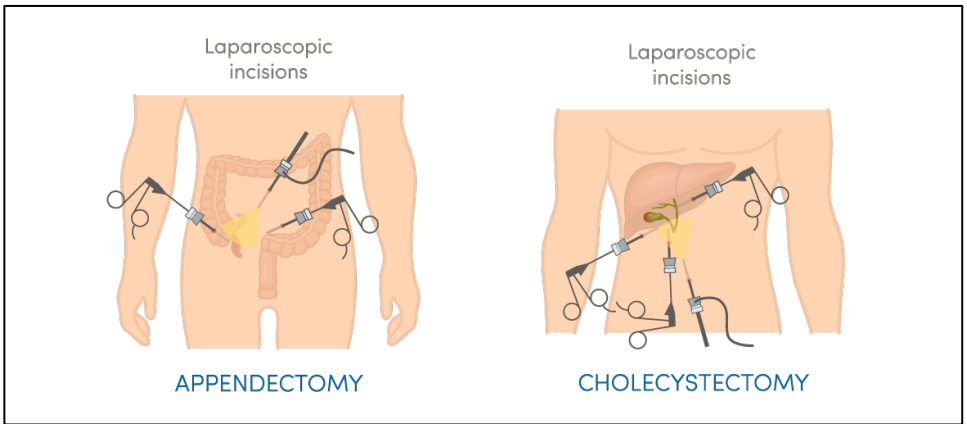

Figure 1.5 Example of incisions for different laparoscopy procedures.
Source: [19].

The three types of skin incisions described in this research are cutting, drilling and debridement. Cutting is the most common type of skin incision, it can be transverse, vertical or oblique. The advantages of transverse incision are providing the best cosmetic results, offering the least interference with postoperative respirations as well as being less painful. However transverse incisions are more time consuming, more hemorrhagic and

compromise the ability to explore upper abdominal cavity. Additionally, a transverse incision's division of multiple layers of fascia and muscle and nerves may result in potential spaces with hematoma or seroma.

The advantages of vertical incisions include excellent exposure, extendibility, and minimum nerve damage. The disadvantages of vertical incisions include more frequent wound dehiscence ahernia and poorer cosmetic results. Median and paramedian are two types of vertical incisions. Median incision is least hemorrhagic with rapid entry into abdomen and pelvis. Paramedian incision has higher infection rates, hemorrhage and operative time [4].

While drilling in surgical procedures is mainly done on bones, skin drilling occurs during such processes as burr hole surgery, when the skull as well as the skin are penetrated using a special air drill. Drilled holes make it possible to make certain incisions in the skull without risking penetrating trauma to the brain tissues [20].

Surgical debridement may not be considered a traditional type of skin incision, but it does involve removal of the skin and treating skin wounds and burns (Figure 1.6). The different types of surgical debridement include wound cleaning, removing all hyperkeratotic, infected and nonviable tissues and foreign debris and residual material from dressings [21].

Figure 1.6 Debridement of loose epidermis between fingers using WJ.
Source: [22].

1.3 Tools for Making Skin Incisions

There are several tools that are used to make minimally invasive skin incisions: Traditional tools and non-traditional tools. Traditional tools include scalpels, surgical scissors and surgical air drills while non-traditional tools include CO_2 laser, diathermy and harmonic scalpels. WJ technology is considered a non-traditional tool for making surgical incisions. While it is not usually used for skin incisions, it has the potentials and advantages to accomplish such task.

The depth and length of skin incisions depend on the tools that are utilized to make such incisions. The most traditional and commonly used tool for skin incision, whether for cutting or debridement, is the scalpel. A scalpel's number refers to the size of the scalpel's blade size. Each blade varies in length and shape of the cutting edge to suit different

purposes. There are two main methods for skin incisions using a scalpel: press cutting and slide cutting [23].

Another traditional type of surgical tool used for skin cutting and debridement is the surgical scissors. Scissor blades can either be curved or straight. In order to achieve the best wound healing when using surgical scissors, the surgeon should cut exactly at the point where the blades meet. A disadvantage of the surgical scissors is they are designed primarily for right-handed users [24].

The surgical air drill is used for drilling holes through the skin and bone in various procedures. An advantage of the specialized air drill, which is used to drill the skull, is that it has a feedback system that is designed to stop drilling automatically once the skull is penetrated. This design prevents injuries to the brain [20].

CO_2 laser is a non-traditional tool that is used for skin incision. The way a CO_2 laser works is by vaporizing water that is found in the skin and other soft tissue. One thin layer of skin at a time is removed when using CO_2 laser which causes no damages to the surrounding areas. CO_2 laser enables high precision in removing the tissue while simultaneously providing sufficient hemostasis [25].

Diathermy which is also known as electrocautery is an alternative non-traditional way that is used for skin incision. Continuous high frequency current of 100 kHz or above of sufficient voltage that ranges from 200 to 500 V is used for skin incision. The diathermy tool allows for faster incisions and reduced bleeding while causing less postoperative pain over a traditional scalpel [26].

A newer non-traditional tool used for skin incision is the harmonic scalpel. The harmonic scalpel uses ultrasonic energy to simultaneously cut and cauterize tissues including sealing the veins. The main advantages of the harmonic scalpel is precise dissection, reliable hemostasis in addition to less lateral thermal spread [27].

While the non-traditional processes for skin incision tools have shown several advantages to justify their use over the traditional scalpel, surgical scissors and drills, some disadvantages still pose a hindrance. Such disadvantages include producing burning of variable depth in the tissues which may affect outcome of surgical wound [26]. Additionally, the patients can smell their skin burning which can be unpleasant and unsettling. Furthermore, the use of intraoperative energized dissection can result in surgical smoke containing potentially carcinogenic and irritant chemicals [28].

A WJ tool has the same advantages of the non-traditional tools to justify using it over traditional tools for minimally invasive skin incision but without the thermal damage to the separated tissue due to its coolant ability [29]. The technique of the WJ tool is simply moving the tool in a line to apply the pressure and the cut, rendering the main advantage of WJ incision its precision. The WJ tool has an essential advantage over laser scalpels due to its ability to control and change the water pressure during an incision making it more selective. For example, a WJ tool is able to cut liver tissue (Figure 1.7) without cutting a vein [30]. Furthermore, the WJ washes away blood which eliminates any extra tools necessary for this action which would be required in a regular cut [31]. According to Dr. Matthew Hanna, Neuropathologist at Memorial Sloan Kettering Cancer Center, while providing the same or better precision as a traditional scalpel, WJ can augment or replace current surgical tools for skin incisions [32].

Figure 1.7 An example of liver resection using WJ.
Source: [29].

The advantages of the WJ use are summarized as follows:

- Precision in incision
- Reducing blood loss
- Quicker and more selective
- Washing away blood
- Less environmental pollution
- Water is cheap, non-toxic and always available
- Operating and maintenance expenses are low
- Safe to use

The disadvantages of the WJ use are summarized as follows:

- No feedback provided while making an incision
- Does not have the ability seal bleeding vessels
- Initial cost is high

The next chapter discusses the previous work that has been done using WJ technology in various surgical procedures.

CHAPTER 2

LITERATURE REVIEW

Over the past 30 years, WJ techniques have been developed into a revolutionary cutting tool in variety types of surgery [33]. WJ can be used in precision cutting of skin for any type of surgery. WJ technology in surgical procedures was first reported in 1982 for liver resections. Throughout the years, WJ machining process has become a recognized technique in different surgical areas. Clinically, WJ technique is used for cutting softs tissues for instance, liver tissues. Experimentally, WJ technique is used for dissecting spleen, kidney tissue and brain tissues. While these tissues can be cut at low water pressures, WJ techniques can also cut bone and bone cement at much higher water pressures [34]. Applications of this include dentistry, wound cleaning and other surgical operations. Table 2.1 summarizes some of the applications of WJ cutting in the medical field [29].

The performance of WJ machining process is dependent on the water pressure of the jet and the elastic properties of the material. The initial impact is considered to be the highest impact; it can be achieved when the WJ hits the tissue. After that, the water starts flowing radially and the impact of the jet decreases [35].

WJ technology can be used for surgical wound debridement and surgical interventions where selective cutting is necessary. Surgical wound debridement uses devices on the market such as VersaJet and Debritom while surgical interventions use devices on the market such as Jet Cutter 4, Helix Hydro-Jet and ErbeJet2 [35].

Table 2.1 Overview of Using WJ Technology in Medicine

Type of Surgery	Operation Description	Benefits
Orthopaedic	Cutting endoprosthese and bone	Below the critical temperature by cutting
Dental	Cutting and grinding of dental materials	Reduces the risk of jagged teeth and reduces the need for anesthesia
General	Resection of soft tissues: liver, gallbladder, brain, kidney, prostate, cleaning wounds	Blood vessels and nerve fibers remain in the defined pressure maintained, minimal bleeding, intact edges and precise cuts, lack of necrotic edge, reduce the duration of myocardial ischemia
Plastic	Cleaning skin graft, removal of tattoos, liposuction	Separation of the layers of tissue, higher accuracy of results without edema and contour changes
Dermatology	Removing dead skin	Possibility of direct dose medications in a water jet

Liver Resection

The first recorded WJ use in a surgical procedure was reported by Papachristou and Barters in 1982. In this study, the authors performed four liver resections using a jet of normal saline generated by a standard agriculture electric sprayer. Other than reduced blood loss, this technique washed away the intrahepatic parenchyma while not damaging the ducts and vessels [36].

Skin Incision Finite Element Analysis (FEA)

In 1998, a research thesis by Vichyavichien, conducted computational nonlinear analyses using FEA to compute the effect of WJ on the skin layers. The results of the FEA analysis showed that the skin started to shear at a pressure of 40 MPa with a 0.2 mm nozzle's orifice diameter [37].

Kidney Surgery

In 2000, Basting *et al*. used Helix Hydro-Jet WJ on 24 patients who underwent various open surgeries such as partial nephrectomy for renal-cell cancer and nephrolithotomy for kidney stones. Sharp dissection lines were produced by the WJ; when compared to laser or electric cautery, WJ resulted in less trauma to adjacent tissues [38].

Fatty Tissue Dissection

Wanner *et al*. performed a study in 2002 to investigate the optimal technical parameters for WJ cutting abdominal fat tissue. With a 0.120 mm nozzle diameter and cutting speed of 12 mm/s, one single pass at cutting pressure between 2 and 6 MPa was able to make an 8 mm deep incision [39].

The study concluded that the optimal pressure for dissecting fatty tissues using WJ is between 3 and 4 MPa [39].

Gallbladder Surgery

A study in 2003 by Shekarriz *et al*. compared Helix Hydro-Jet WJ with conventional dissection in laparoscopic cholecystectomy on 80 patients. Reduced complications rates were recorded using the WJ. The authors showed that the reduced complications are due to the improved anatomic dissection in addition to the almost bloodless operating field due to the continuous water flow [40].

Bone and Bone Cement Drilling

Many studies have been done using WJ technology to drill or cut bone or bone cement**.** A 2004 *in vitro* study by Honl *et al*. investigated the use of plain and abrasive WJ as a cutting tool for endoprosthesis revision surgery. Five different (pure and abrasive) water pressure levels of 30, 40, 50, 60 and 70 MPa were applied at two different angles (30° and 90°) to

cut samples of mid-diaphysis of human femora and bone cement. As shown in Figure 2.1, only bone cement was cut with pure WJ (PWJ). When using abrasive WJ (AWJ), significant higher cut depth were recorded in both bone and bone cement [41].

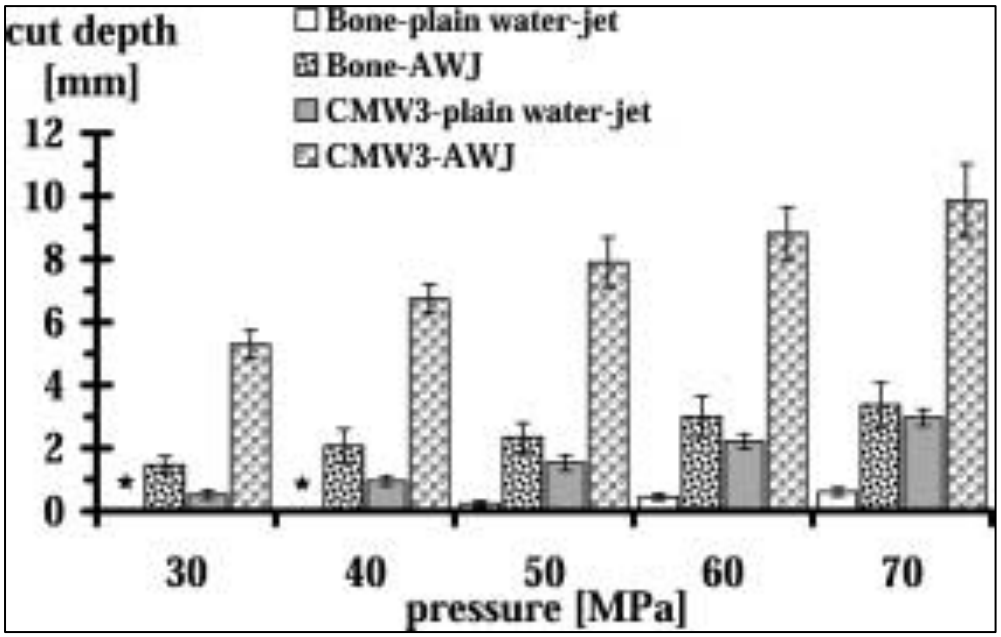

Figure 2.1 Incision depth of bone cement and cortical bone at different WJ pressures.

The study concluded that AWJ would be an alternative tool for cement removal. Additionally, AWJ is advantageous for revision of non-cemented prosthesis due to its possibility for localized cutting at interfaces [41].

Wound Debridement

A study in 2006 introduced Versajet WJ as an alternative to standard surgical excisional techniques for burn wounds. In the study, the Versajet WJ was able to sufficiently debride superficial partial thickness and mid-dermal partial thickness wounds for the subsequent placement of Biobrane. Additionally, the study demonstrated that the Versajet WJ is

beneficial in the surgical treatment of superficial to mid-partial thickness burns in the face, hand and foot [22].

Another study conducted in 2007 reviewed the versatility of the Versajet WJ surgical tool in treating the deep and indeterminate depth face and neck burns. With ex-vivo histologic analysis of depth of debridement on human skin, the study confirmed that predictable and controlled depth of debridement could be obtained by adjusting the apparatus settings [42].

Laparoscopic Liver Dissection

A study by Rau *et al*. in 2008 compared 950 patients' data in which 350 patients underwent liver dissection using a Helix Hydro-Jet WJ. This study concluded that WJ dissection is fast, feasible, reduces blood loss and safe to be used in open and in laparoscopic liver dissection [43]

Neurosurgery

In 2010, Keiner *et al*. published a paper with their research that took place from 1997 to 2009. In the 12-year span, the authors performed 208 procedures on patients with various intracranial neurosurgical pathologies using WJ dissector with pressures ranging from 0.4 to 1.5 MPa. Müritz 1000, Helix Hydro-Jet, and ErbeJet 2 were used in these procedures. The surgeons evaluated the WJ devices used and recorded the differences and limitations in the various pathologies. The surgeons noted that the WJ apparatus was considered to be very helpful in 166 procedures (79.8%) and helpful to some extent in 33 procedures (15.9%). In eight (3.8%) procedures, it was not helpful, and in one procedure (0.5%), the usefulness was not documented by the surgeon [44]. The authors concluded that WJ technology is safe and easy to apply in precise tissue dissection. They also noted in addition

to such precision, the preservation of blood vessels and no greater risk of complications are possible with WJ [44].

Interface Tissue Incision

A study by Kraaij *et al*. in 2014 investigated the feasibility of using WJ technology to cut interface tissue membrane. Using 0.2 mm and 0.6 mm WJ diameter with a stand-off distance of 5 mm and traverse speed of 0.5 mm/s, interface tissue samples were cut in half. The WJ pressure was regulated by changing the flow. The WJ pressure required to cut mean thickness of 2.3 mm was between 10 and 12 MPa with a 0.2 mm nozzle diameter. The WJ pressure required to cut mean thickness of 2.6 mm was between 5 and 10 MPa with a 0.6 mm nozzle diameter [34]. The study has also summarized different materials that were tested in previous studies, the required WJ pressure to cut them as well as the nozzle diameter (Table 2.2) [34].

Table 2.2 Overview of Required WJ Pressures to Cut Different Materials

Material Tested	D_{nozzle} (mm)	Required Pressure (MPa)
Human calcanei	0.6	30
Human femora	0.2	50
	0.3	40
Bone cement	0.2	30
	0.3	40
Human interface tissue	0.2	12
	0.6	10

Skin Incision

Not many studies have focused on using WJ technology on skin incisions. While the research conducted by Vichyavichien in 1998 dealt with skin incisions using WJ, it was only theoretical with an FEA analysis, not experimental. The study conducted by Wanner *et al*. in 2002 using WJ technology to cut abdominal fat tissue is the only experimental study reviewed that utilized WJ technology on a skin layer (the fat tissue). This research focused not only on the application of WJ technology on skin incision theoretically but also experimentally.

CHAPTER 3

OBJECTIVES AND CONTRIBUTIONS

While *in vivo* and *in vitro* experiments on patients and animals have been conducted with continuous WJ at different low pressures, few studies have focused on the skin. Further analyses on the relationship among the operating parameters of WJ, structure, and mechanical properties of the skin should be conducted. The main objectives of this research are to determine the precise depth of incision using WJ technology, verify the existing WJ research results and determine the optimal operating parameter levels to maximize the depth of incision. In order to achieve these objectives, the following models have been developed:

1- Analytical model that incorporates the skin properties and the operating parameters of the WJ in skin incisions. These properties include skin thickness, its modulus of elasticity, WJ pressure, diameter of nozzle orifice, nozzle standoff distance and the traverse speed of the WJ as well as the duration of applying the WJ pressure.

2- Systematic model to conduct both the verification of existing models results and to optimize the different WJ operating parameters in order to maximize the depth of incision. It consists of the following:

   i- Minitab Design of Experiment model (M-DOE) to construct a treatment table of the experiment, as a Microsoft Excel file, which is transferred to the Matlab model.

   ii- Matlab model, after receiving the file from M-DOE, the depth of incision values for the different responses have been calculated and update the Microsoft Excel file to be transferred back to the M-DOE.

   iii- The M-DOE, after receiving the Microsoft Excel output file from Matlab, a full factorial as well as Taguchi Design of Experiment (DOE) are conducted.

In addition, a case study (Cesarean section procedure) has implemented the developed models to illustrate the effectiveness of the research. A comparison between current publications and the developed models is illustrated in Table 3.1.

The methods developed in this study provide more flexible and robust solutions for setting up the WJ apparatus when used in surgical procedures. The models presented may be applied not only to skin but to any location of the human body given its mechanical properties. Moreover, the models are suitable to set up any existing WJ devices. A unique feature is that the models rely on basic manufacturing processes formulation which is verified theoretically and experimentally.

Table 3.1 Features of Previous Works and Developed Models

Authors	Year	Type of Study	Method Used	Apparatus	Water Purity	Pressure	Depth of Incision	Width of Incision	Cuting Velocity	Orifice Diamater	Stand-off Distance	Angle	Feed Rate/ Transverse Speed
Vichyavichien [37]	1999	Skin Incision	Finite Element Analysis	Theoritical	100% Water	Fixed	Generated	Generated	N/A	Fixed	Fixed	Fixed	N/A
Wanner *et al.* [39]	2002	Fat tissue incision	Ex Vivo	Commercial	0.9% Saline	Fixed	Generated	N/A	Fixed	Fixed	Fixed	Fixed	N/A
Rennekampff *et al.* [22]	2006	Debridement of burn wounds	Ex Vivo	Commercial	Sterile Saline	Fixed	N/A	N/A	Fixed	Fixed	N/A	Fixed	N/A
Cubison *et al.* [45]	2006	Debridement of burns	Ex Vivo	Commercial	N/A	Fixed	N/A	N/A	Fixed	Fixed	N/A	N/A	N/A
Tenenhaus *et al.* [42]	2007	Wound debridement	Ex Vivo	Commercial	N/A	Fixed	N/A	N/A	Fixed	Fixed	N/A	N/A	N/A
Keiner *et al.* [44]	2010	Brain tissue dissection	In Vivo	Commercial	0.9% Saline	Fixed	N/A	N/A	N/A	Fixed	N/A	N/A	N/A
Kraaij *et al.* [34]	2015	Interface tissue incision	In Vitro	Custom	100% Water	Fixed	Generated	N/A	Fixed	Fixed	Fixed	Fixed	Fixed
Bahls *et al.* [35]	2017	Various tissue incision or abrasion and removal	In Vivo	Commercial	10% Gelatine	Fixed	N/A	N/A	Fixed	Fixed	Fixed	Fixed	N/A
Proposed	**2019**	**Skin incision**	**Analytical/ Optimization**	**Matlab & Minitab**	**100% Water**	**Variable**	**Generated**	**Variable**	**Generated**	**Generated**	**Variable**	**Fixed**	**Variable**

CHAPTER 4

DEVELOPED MODELS

In this chapter, two models have been developed: analytical and DOE optimization. The developed analytical model incorporates mathematical relationships between the WJ operating parameters and the skin properties. These relationships allow one to produce the desired depth of incision based on specific WJ operating parameters and skin characteristics. The Matlab model's integration with Minitab provides a seamless feature for the optimization model. The M-DOE model provides the ability to test different operating conditions to generate the optimal skin incision depth that is safe for the patient based on their skin characteristics.

4.1 Analytical Model

The WJ incision parameters are affected by process, skin, nozzle and pump characteristics as shown in Table 4.1. The skin incision occurs due to the WJ pressure energy which is defined by the skin characteristics. The pressure energy is translated by the kinetic energy coming out of the nozzle which is defined by the process characteristics as well as the nozzle characteristics. The catcher's kinetic energy is generated from the remaining kinetic energy that is coming out of the nozzle. The kinetic energy of the nozzle is translated by the pressure energy coming out of the pump, which is defined by the pump characteristics.

Table 4.1 WJ Incision Parameters

Process Characteristics	Skin Characteristics	Nozzle Characteristics	Pump Characteristics
Incision Characteristics:	Type of skin	Orifice diameter	Direct drive
Depth of cut	Thickness	Nozzle structure	Hydraulic drive
Width of cut	Hardness	WJ velocity	Oil pressure
WJ Characteristics:	Consistency		Pressure amplification
Traverse speed	Body location		Pressure
Feed rate	Age		Pump efficiency
Stand-off distance	Gender		Power
Pure or abrasive water	Demographic		
Continuous or discontinuous jet	Specific Energy/ Elastic Modulus		

The following sections present the analytical mathematical model that describes the skin incision processes using WJ technology. An overview of the skin incision process is illustrated in Figure 4.1; starting from the skin including its components and parameters to the nozzle including its components and parameters, and all the way to the pump including its parameters and components. The symbols in the figure are described in the following sections.

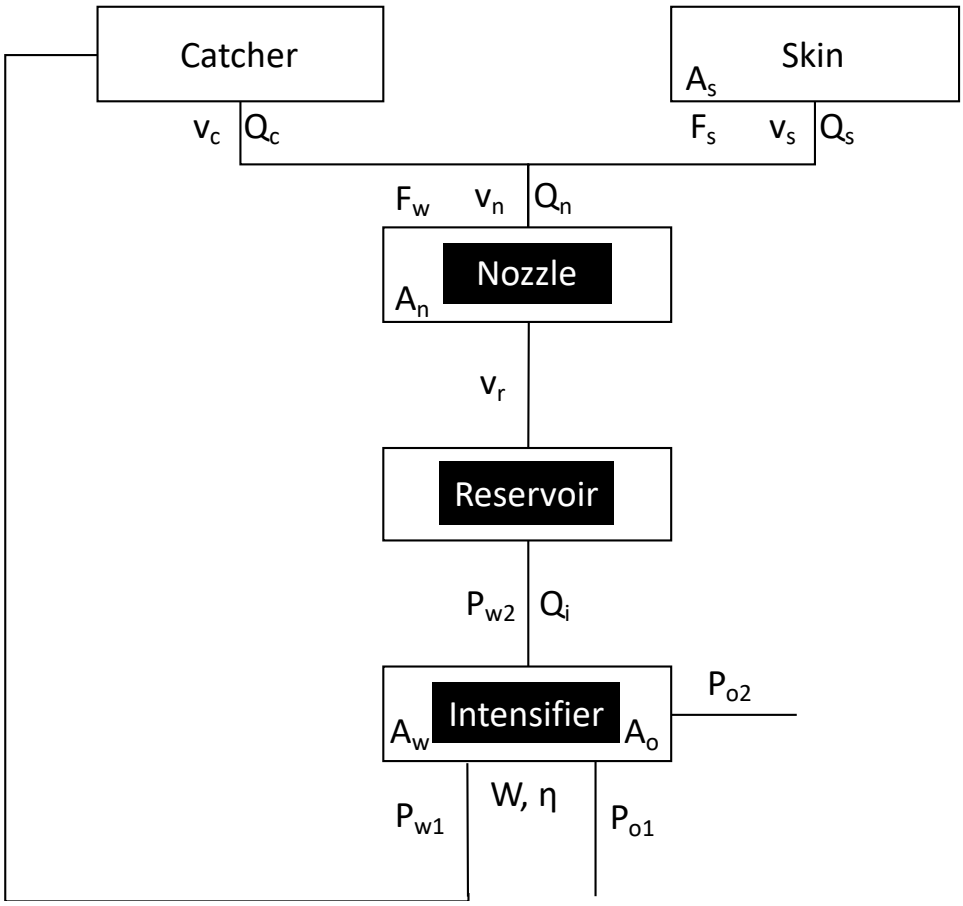

Figure 4.1 WJ components and parameters.

4.1.1 Surgical Incisions Main Components: Operation Characteristics

The two main components for a surgical incision are the width and the depth of incision. Before performing the incision, the one must have these two factors defined. The width of incision is determined based on the individual surgery and the recommended incision specifications. When performing a skin incision, the target depth of incision is determined by the skin thickness. Moreover, the specific energy of the skin must be determined. The specific energy of any material used is defined as the energy per unit mass; in this model it is used for the kinetic energy or potential energy of the material [46]. While the specific energy of many materials is known, it may not be known for organic materials such as the

human skin. Based on the experimental results provided in this study, the specific energy of the skin is assumed to be equal to the elastic modulus.

As discussed in the first chapter, the skin properties vary based on the patient's unique characteristics. For these reasons, a system which can adapt to the differences, must be created. Table 4.2 summarizes the general thickness of each individual skin layer [6].

Table 4.2 Properties of the Different Skin Layers

Skin Layer	Thickness
Skin (theoretical)	6.4 – 8.8 mm
Epidermis	0.1 mm
Basement Membrane	2×10^{-5} mm
Dermis	2 – 5 mm
Subcutis	0.4 – 4 mm

In the preparation before the surgical procedure, the individual's skin thickness can be measured using high frequency ultrasound machine. This provides a range to set up the WJ device's operating parameters. In addition to measuring the skin thickness prior to the procedure, the high frequency ultrasound can also be used to abate the lack of feedback while using the WJ apparatus. While it is not possible for the WJ apparatus to provide feedback while making an incision, attaching a high frequency ultrasound machine to the WJ can get a real-time depth of incision measurement. Using this approach, one is able to visualize the incision being made as well as stop the WJ flow if needed to ensure he is not making an incision deeper than the skin thickness needed to be incised.

After determining the main components for making a skin incision, the relationship between the force of the water coming out of the nozzle (F_w) and the force required for skin incision (F_s) can be formulated as follows:

$$F_w = F_s \tag{4.1}$$

$$P_w \cdot A_n = E \cdot A_s \tag{4.2}$$

where P_w is the pressure of water out of the nozzle, E is the specific energy/elastic modulus of the skin, A_n and A_s are the areas of the nozzle and skin to be cut respectively as follows:

$$A_n = \pi \cdot \frac{d_n^2}{4} \tag{4.3}$$

$$A_s = D_s \cdot w_s \tag{4.4}$$

where d_n is the orifice diameter of the nozzle, D_s is the depth of incision and w_s is the width of incision. The relationship between the nozzle's orifice diameter and the width of incision is given by the following relationship:

$$w_s = d_n \cdot e^{a \cdot x} \tag{4.5}$$

where a is the taper index and x is the standoff distance of the nozzle. Theoretically, the width of incision is the same as the nozzle's orifice diameter.

For example, given the following:

- *Nozzle's orifice diameter (d_n) value of 0.2 mm,*
- *Stand-off distance (x) value of 10 mm*
- *Taper (a) value of 0.25*

The width of incision is calculated to be 0.199 mm.

The total energy required for the skin incision which is converted to pressure energy is formulated as follows:

$$PE = E \cdot Q_s \tag{4.6}$$

where Q_s is the volume flow rate at which the WJ removes the skin, which is calculated as:

For skin cutting and debridement:

$$Q_{s\_cut} = D_s \cdot w_s \cdot s \tag{4.7}$$

For skin drilling:

$$Q_{s\_drill} = \frac{\pi \cdot d_i^2 \cdot f}{4} \tag{4.7a}$$

s is the traverse speed, d_i is the insert diameter and f is the feed rate. Given the length of cut (L_{cut}) or the depth of drill (D_{drill}), the time required to make a certain incision (t) can be calculated as follows:

For skin cutting and debridement:

$$t_{cut} = \frac{L_{cut}}{s} \tag{4.8}$$

For skin drilling:

$$t_{drill} = \frac{D_{drill}}{f} \tag{4.8a}$$

4.1.2 WJ Technology Operating Conditions: Catcher Characteristics

To minimize the process noise, a catcher is necessary. The kinetic energy of the catcher is the remaining energy that is not absorbed by the skin incision process, it is formulated as follows:

$$KE_c = \frac{1}{2} \cdot Q_c \cdot v_c^2 \cdot \rho_w \tag{4.9}$$

where ρ_w is the density of water, Q_c is the volume flow rate at which the residue water is going into the catcher; it is the sum of the volume flow rates of water out of the nozzle Q_n and rate at which the WJ removes the skin Q_s.

The velocity at which the excess water is going to the catcher (v_c) is:

$$v_c = \sqrt{2 \cdot g \cdot x} \tag{4.10}$$

where g is the gravity.

4.1.3 WJ Technology Operating Conditions: Nozzle Characteristics

The kinetic energy of the WJ stream coming out of the nozzle is the sum of the pressure energy required to make the skin incision and the kinetic energy of the catcher:

$$KE_n = PE + KE_c \tag{4.11}$$

To look at the nozzle characteristic of the WJ incision, this kinetic energy (Equation 4.11) will be equal to the following:

Pure WJ

$$KE_n = \frac{1}{2} \cdot Q_n \cdot v_n^2 \cdot \rho_w \cdot k_e \tag{4.12}$$

Abrasive WJ

$$KE_n = \frac{1}{2} \cdot \dot{m}_{abr} \cdot v_n^2 \cdot k_e \tag{4.12a}$$

where v_n is the velocity of the WJ stream coming out of the nozzle, k_e is the loss coefficient and $\dot{m}_{abr}$ is the abrasive mass flow rate.

The WJ nozzle converts high pressure water to a high velocity jet. The performance of WJ incision is affected by several variables such as the nozzle's orifice diameter, water pressure, incision feed rate and standoff distance. In the medical field, WJ incision devices usually use low to medium pressure as well as a small design nozzle that is different from industrial WJ. A relationship between the velocity of the WJ stream coming out of the nozzle (v_n) and the velocity of the WJ stream at the skin (v_s) can be described as follows:

$$v_s = v_n \cdot e^{-a \cdot x} \tag{4.13}$$

Example, given:

- *The velocity of the water coming out of the nozzle (v_n) is 141.42 m/s*
- *The stand-off distance (x) is 10 mm*
- *The taper value (a) is 0.25*

Then the velocity of the water that hits the skin is calculated as 141.07 m/s.

The flow of the water from the nozzle to the atmosphere is affected by the area and the shape of the orifice. Figure 4.2 and Table 4.3 represents the different orifice types and the typical values of discharge (C_d) and loss (k_e) coefficients for the orifices [47].

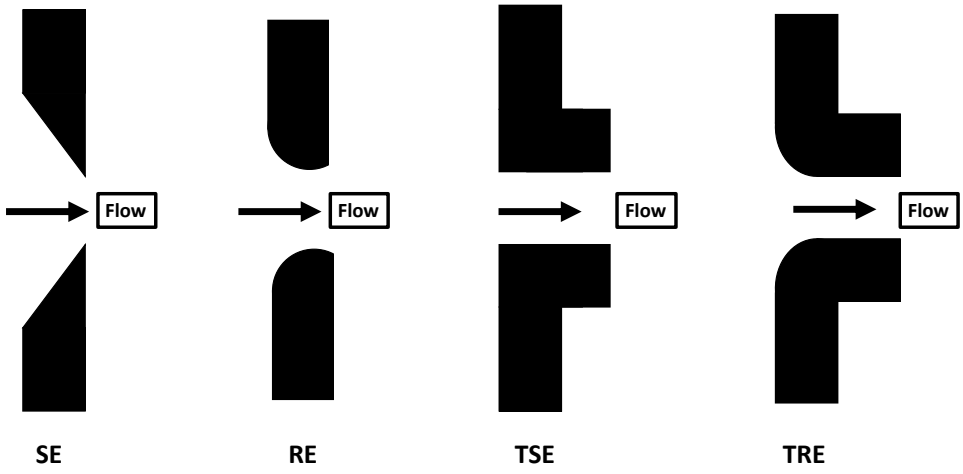

Figure 4.2 Types of orifices.

Table 4.3 Types of Orifices and their Coefficients Values

Orifice	Description	C_d	K_e
SE	Sharp-edged	0.62	0.08
RE	Round-edged	0.98	0.10
TSE	Tube with square-edged	0.61	0.51
TRE	Short tube with rounded entrance	0.54	0.15

The kinetic energy of the nozzle is directly proportional to both discharge and loss coefficients (C_d and K_e) of the orifices. The shape of the orifice can have a significant impact on the flow rate of the water that is coming out of the nozzle.

The relationship between Q_n and v_n is represented by:

$$Q_n = C_d \cdot A_n \cdot v_n \tag{4.14}$$

For example, given the following:

- *The velocity of the water coming out of the nozzle (v_n) is 141.42 m/s*
- *A sharp-edged nozzle orifice with a 0.2 mm orifice diameter (d_n)*

Then the water flow coming out of the nozzle Q_n is calculated to be 3.55 mm^3/s.

The relationship between v_n and the water pressure (P_w) coming out of the nozzle is described as follows:

$$v_n = \sqrt{\frac{2 \cdot P_{w2}}{\rho_w}} \tag{4.15}$$

Re-arranging Equation 4.15, the pressure of the WJ is:

$$P_{w2} = \frac{v_n^2 \cdot \rho_w}{2} \tag{4.16}$$

4.1.4 WJ Technology Operating Conditions: Pump and Intensifier Characteristics:

The relationship between the velocity of the WJ flow coming out of the pump reservoir and the one coming out of the nozzle is calculated as follows:

$$v_r = v_n \cdot e^{-2 \cdot \beta \cdot L_n} \tag{4.17}$$

where L_n is the length of the nozzle, β is the exponential constant which is based on an exponential taper WJ nozzle design (seen in Figure 4.3) and d_o is the diameter of the top of the nozzle:

$$\beta = \frac{-\ln (d_n/d_o)}{L_n} \tag{4.18}$$

.

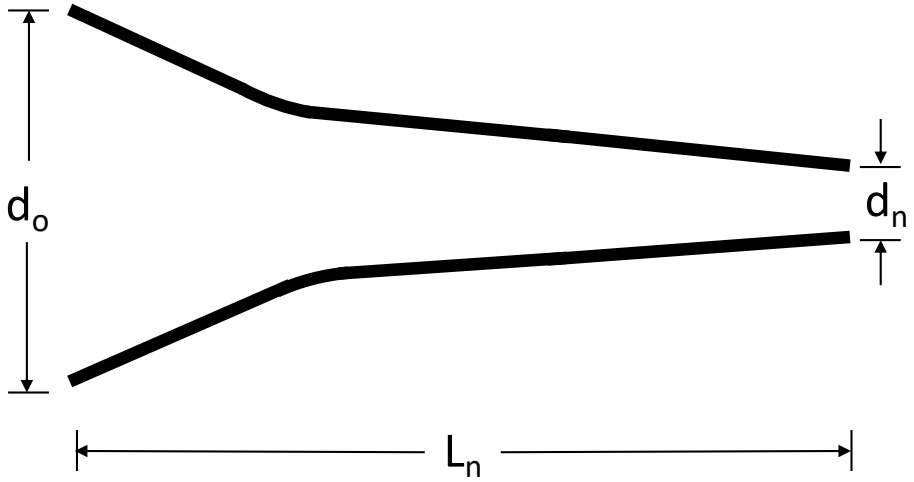

Figure 4.3 Exponential WJ nozzle design.

The pressure ratio (r_p) between the water outlet pressure (P_{w2}) and the oil inlet pressure (P_{o1}) and as well as the oil inlet area (A_o) and the water inlet area (A_w) is described as follows:

$$r_p = \frac{P_{w2}}{P_{o1}} = \frac{A_o}{A_w} \tag{4.19}$$

The WJ flow rate out of the intensifier (Q_i) is equal to the WJ flow rate coming out of the nozzle (Q_n). Thusly, the Power (W) is determined by the water pressure coming out of the intensifier (P_{w2}), the efficiency of the intensifier (η_i) and the flow rate (Q_i) as follows:

$$W = \frac{P_{w2} \cdot Q_i}{\eta_i} \tag{4.20}$$

Equations 4.1 to 4.20 show the association between how much specific WJ pressure is necessary to make a specific incision in the skin based on its mechanical characteristics. These relationships involve the whole setup of the WJ device such as the WJ velocity and the pump power. This model is robust enough to be applied to any new or existing WJ apparatus. The developed model is compatible with the top three WJ brands in surgical procedures: ErbeJet 2 (Figure 4.4), Helix HydroJet (Figure 4.5) and VersaJet (Figure 4.6) or any custom-made WJ.

Figure 4.4 ErbeJet 2 WJ system.
Source: [48].

Figure 4.5 Helix HydroJet WJ system.
Source: [49].

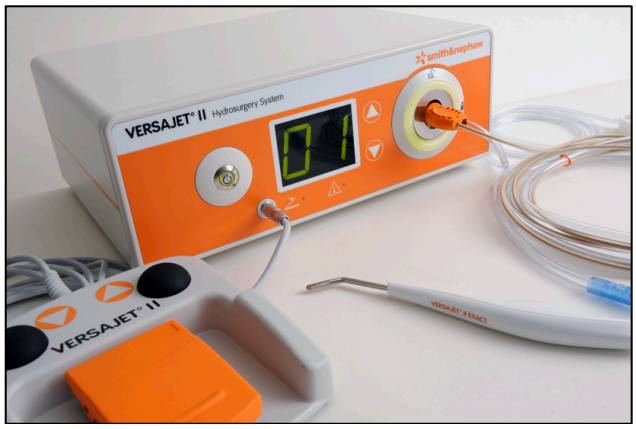

Figure 4.6 VersaJet II WJ system.
Source: [50].

4.1.5 Derived Analytical Relationships

From Equations 4.1 to 4.20, the analytical relationships between the skin characteristics and the WJ operating parameters can be derived. The WJ pressure with pure water is derived as follows:

$$P_{pwj} = \frac{\rho_w}{2} \cdot \left(\frac{8 \cdot Q_s}{c_d \cdot \pi \cdot d_n^2 \cdot \rho_w \cdot k_e}\right)^{\frac{2}{3}} \tag{4.21}$$

For example, given the following:

- *The skin's specific energy/elastic modulus (E) is 1 GPa*
- *The traverse speed (s) is 12 mm/s*
- *The target width of cut (w_s) is 0.2 mm*
- *The stand-off distance (x) is 10 mm*
- *The target depth of cut (D_s) is 2 mm*

Then the WJ pressure is calculated to be 17 MPa.

When re-arranging Equation 4.21, the depth of incision of the skin for pure WJ with given pressure and operating parameters is:

$$D_{s\_pwj} = \frac{c_d \cdot \pi \cdot v_n \cdot \rho_w \cdot d_n^2 \cdot k_e}{8 \cdot E \cdot w_s \cdot s} \tag{4.22}$$

The velocity of the water coming out of the nozzle for pure water with respect to the WJ operating parameters is:

$$v_{n\_pwj} = \sqrt[3]{\frac{8 \cdot Q_s \cdot E}{c_d \cdot \pi \cdot d_n^2 \cdot \rho_w \cdot k_e}} \tag{4.23}$$

The WJ pressure for abrasive WJ incision is calculated as follows:

$$P_{awj} = \frac{4 \cdot D_s \cdot (1+R)^2 \cdot E \cdot d_i \cdot s}{c_d \cdot \pi \cdot d_n^2 \cdot R \cdot k_e} \tag{4.24}$$

where *R* is the loading parameter which is the ratio of the mass flow rate of the abrasive material and the mass flow rate of the water.

$$R = \frac{\dot{m}_{abr}}{\dot{m}_w} \tag{4.25}$$

When re-arranging Equations 4.24 and 4.25, the depth of incision of the skin for abrasive WJ with given pressure and operating parameters is:

$$D_{s\_awj} = \frac{c_d \cdot \pi \cdot v_n^3 \cdot \rho_w \cdot d_n^2 \cdot R \cdot k_e}{8 \cdot (1+R)^2 \cdot E \cdot d_i \cdot s} \tag{4.26}$$

A theoretical example, given the following:

- *10 MPa abrasive WJ pressure*
- *The traverse speed (s) is 0.5 mm/s*
- *The nozzle's orifice diameter (d_n) is 0.1 mm*
- *The insert diameter (d_i) is 0.1 mm*
- *The skin specific energy/elastic modulus (E) is 1 GPa*
- *The mass flow rate of the water is 0.86 kg/min*
- *The mass flow rate of the abrasive material is 1 kg/min*

Then the calculated depth of incision is 21.5 mm.

The velocity of the water coming out of the nozzle for abrasive water with respect to the WJ operating parameters is:

$$v_{n\_awj} = \sqrt{\frac{8 \cdot D_s \cdot (1+R)^2 \cdot E \cdot d_i \cdot s}{c_d \cdot \pi \cdot d_n^2 \cdot \rho_w \cdot R \cdot k_e}} \tag{4.27}$$

Making a skin incision using abrasive WJ is rare due to the minimal pressure necessary to incise the skin. However, the abrasive WJ equations could possibly be used in making incisions in other harder materials such as bones and bone cement as displayed in the literature review chapter. The robustness of the model, allows one to use it for not only skin incision on any animal but on any material, given its properties such as its specific energy or elastic modulus. The operating parameters vary from one material to another

based on its mechanical properties. For example, for a target depth of incision, a material that is stiffer than the skin requires a higher pressure and a different orifice diameter design. Since the skin does not require high water pressure compared to stiffer materials, the orifice diameter design may be adjusted accordingly to provide specific discharge and loss coefficient values to result in more effective pressure and velocity to make the skin incision.

4.2 Systemization and Optimization Models

In order to optimize the process, a Matlab model has been developed to systemize the analytical model. As shown in Figure 4.7, the first input is the skin characteristics: the width of incision and the specific energy/elastic modulus. The other input is the operations characteristics such as the suggested WJ pressure, the transverse speed, stand-off distance and taper value. The model output consists of numerical information as well as graphical relationships of the depth of incision vs. water pressure and nozzle's orifice diameter (Figure 4.8). The slide bars shown under each graph in Figure 4.8 provide the user the flexibility to create a what-if scenario by changing the water pressure or the nozzle's orifice diameter. Appendix A.1 provides the Matlab source code for this model.

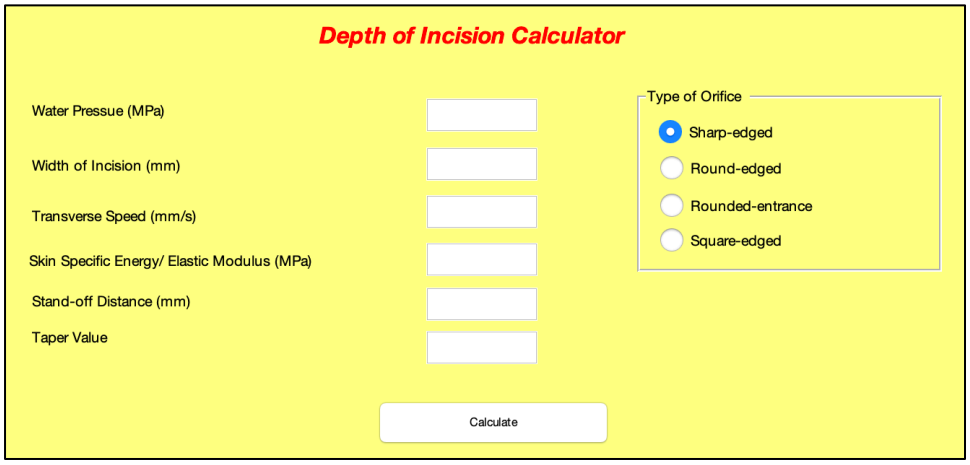

Figure 4.7 Matlab model input example.

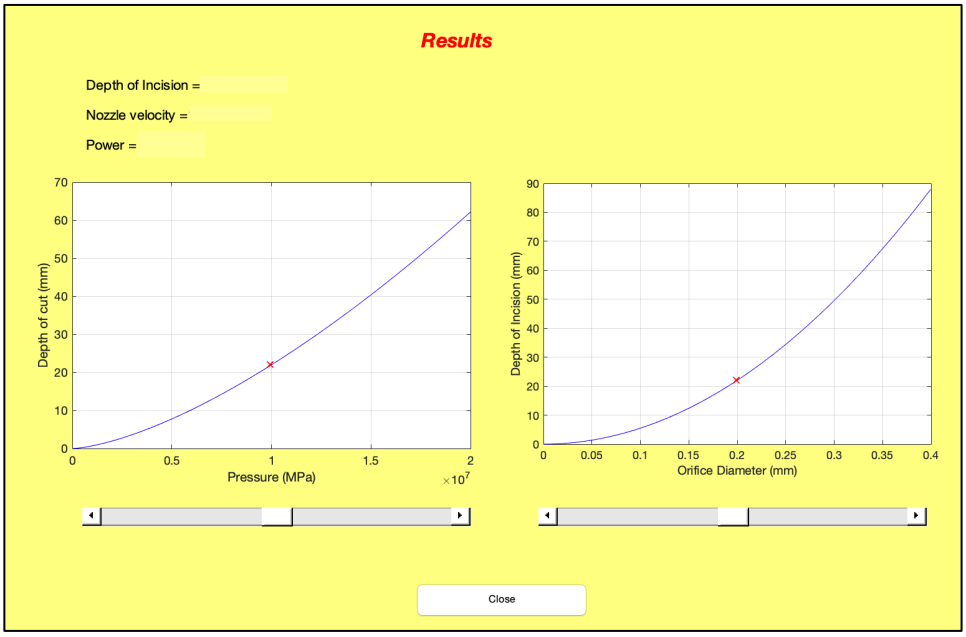

Figure 4.8 Matlab model output example.

In addition to systemizing the analytical model, the Matlab model is also used to be integrated in the M-DOE. Figure 4.9 shows a schematic of the integration between the Matlab Model and the M-DOE optimization model. Once the M-DOE table is set up, the operating parameters are transferred to the Minitab-Matlab integration model to generate the runs' responses. The responses are then transferred back into M-DOE table to be

analyzed. The full Minitab-Matlab integration source code is provided in Appendix A.2.

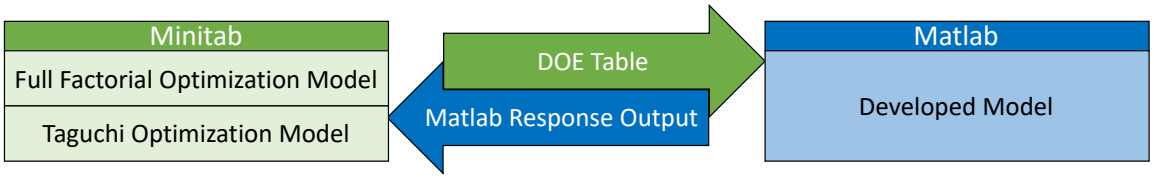

Figure 4.9 Matlab and Minitab integration.

The optimal operating conditions for different skin properties and incisions are determined using Factorial as well as Taguchi DOE analysis. Depending on the numbers of levels and factors, the factorial design can either be 2-level, general full factorial, Placket-Burman or split-plot design while the Taguchi design can be 2, 3, 4, 5-level or mixed level design. The response to be optimized in this study's design is the depth of incision of the skin while the controllable factors may include any of those provided in Table 4.1 such as the width of cut, traverse speed, feed rate, stand-off distance, the skin's characteristics, the nozzle's characteristics as well as the pump's characteristics. The study is robust enough to allow choosing any number of factors and levels constituting orthogonal array.

Full Factorial Design:

To set up full factorial design on Minitab:

1- Select *Stat* > *DOE* > *Factorial* > *Create Factorial Design*.

2- Under Type of Design, select *General full factorial design*.

3- Select the number of factors.

4- Click on *Designs*.

5- Input the name and select the number of levels for each factor (an example is shown in Figure 4.10).

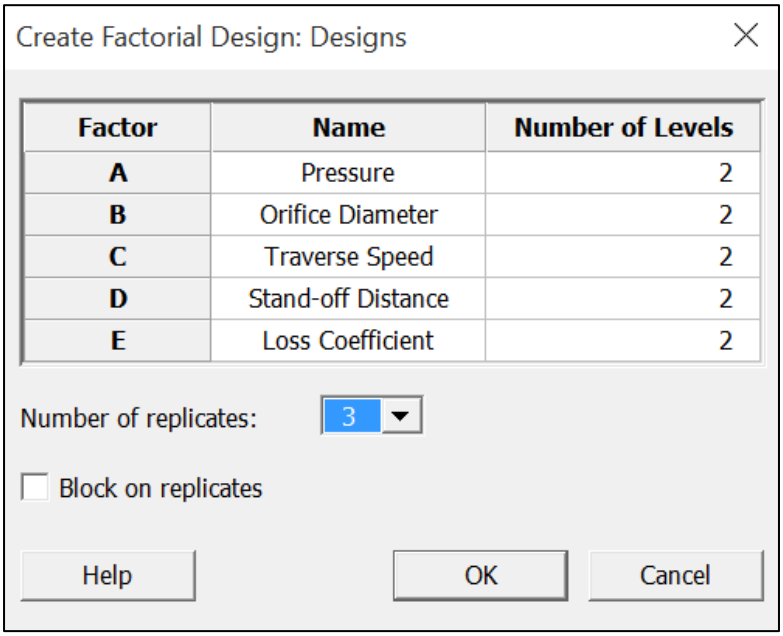

Figure 4.10 Full factorial design: designs set up example.

6- Select the number of replicates.

7- Click on *Factors*.

8- Input the level values for each factor (an example is given in Figure 4.11).

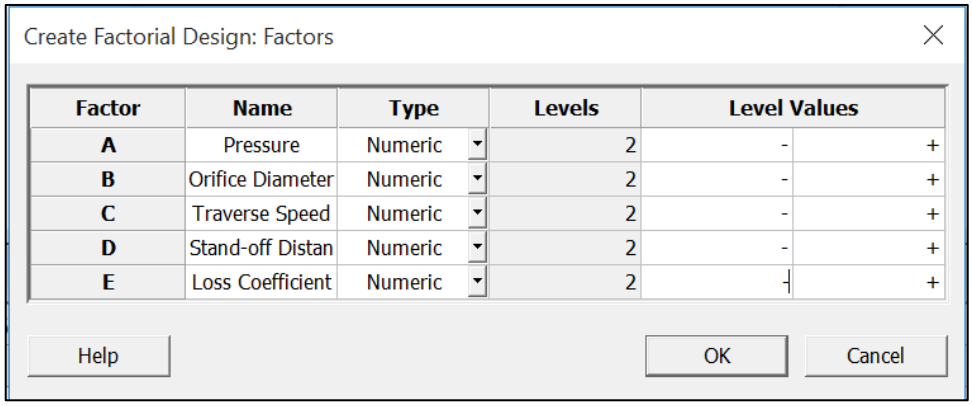

Figure 4.11 Full factorial design: factors set up example.

To help reduce the error of the depth of incision in a full factorial design, a covariate is incorporated to the design. In this study, the covariate chosen is the specific energy/elastic modulus of the skin since *in-vivo* it is measurable, but difficult to control. The number of replicates corresponds to the different levels of the covariates that are added to the design. For example, if two specific energy/elastic modulus levels are selected as covariates, then the number of replicates for this full factorial design should be two as well. Since the experiments are run via the Minitab-Matlab integration, there is no need to block on replicates and randomizing the runs is not necessary. The design table is exported to a Microsoft Excel file and then integrated with the Matlab model to produce the response for each of the runs instantaneously. The response output Microsoft Excel files is then transferred back into Minitab where the DOE analysis is initiated.

To analyze full factorial design on Minitab:

1- Select *Stat > DOE > Factorial > Analyze Factorial Design*.

2- Select the response, in this study it is the depth of incision.

3- Under *terms*, click on *default* to ensure that all factors and their interactions are analyzed.

4- Under *covariates*, select the covariate, in this study it is the specific energy/elastic modulus of the skin.

The M-DOE analysis output illustrates the main effects of the factors as well as the interactions effects between the factors. The most significant levels and factors are identified, a predicted model that optimizes the response is developed and a confirmation test is run. Once the optimized response is generated, the model is used to predict any depth of incision given any WJ operating parameters as well as skin characteristics.

Taguchi Design:

To set up Taguchi design on Minitab:

1- Select *Stat > DOE > Taguchi> Create Taguchi Design*.

2- Under *Type of Design*, select the level, in this study, it is *2-level Design*.

3- Select the number of factors.

4- Click on *Designs*.

5- Select the number of runs, in this study it is *L32*.

6- Click on *Factors*.

7- Input the level values for each factor (an example is given in Figure 4.12).

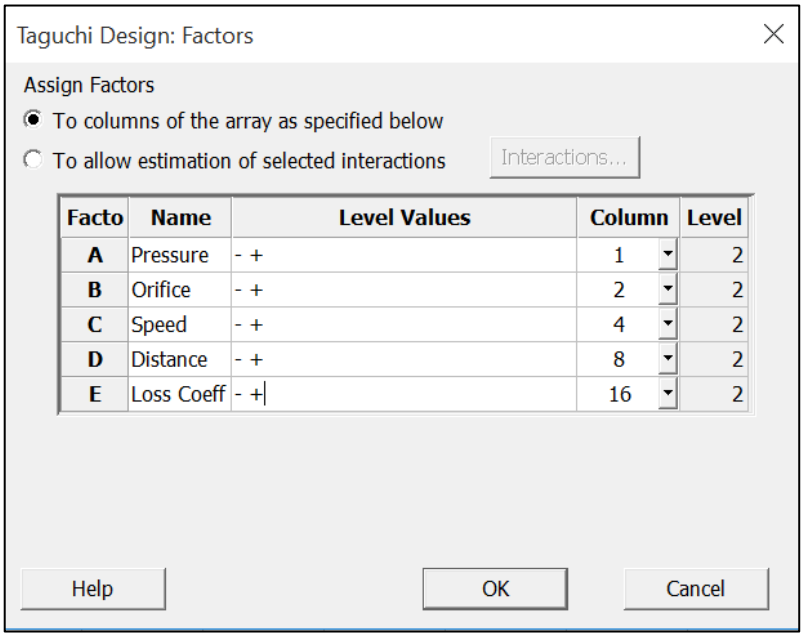

Figure 4.12 Taguchi design: factors set up example.

Similar to the number of replicates in full factorial design, in the Taguchi design, the specific energy/elastic modulus of the skin is considered as the noise factor that causes variability in the performance of the system.

To analyze Taguchi design on Minitab:

1- Select *Stat > DOE > Taguchi > Analyze Taguchi Design*.

2- In *Response data are in*, select the appropriate response, in this study it is the depth of incision.

3- Click *Analysis*.

4- *Under Fit linear model for*, check *Signal to Noise ratios*, *Means*, and *Standard deviations*.

5- Under *Terms*, move all terms to the right side to ensure that all factors and their interactions are analyzed.

5- Under *Options*, select *Larger is better*, under *Signal to Noise Ratio*.

In addition to the results that are generated in the full factorial design, the Taguchi design generates the signal-to-noise (S/N) ratio, the response means and standard deviation. In this study, the goal is to maximizes the S/N ratio as well as the means while minimizing the standard deviation. The response tables show the average of each response characteristic for each level of each factor. In the tables, each factor is ranked based on Delta statistics which compares the relative magnitudes of effects. Using the level averages in the response tables, one can determine the best level of each factor that produces the optimal results.

CHAPTER 5

MODEL VERIFICATION

The analytical model verification is important to ensure the integrity of the mathematical model. Once the model verification is confirmed, it is safe to say that the analytical and optimization models are functional and can be used in real life events.

To verify the developed analytical model, two types of verifications are done: theoretical and experimental. The theoretical verification is conducted using the results of a published previous study that was performed using WJ on bone cement. The experimental verification is done using an industrial WJ, located at the New Jersey Institute of Technology Makerspace laboratory, on animal skin and bone.

5.1 Theoretical Verification

As illustrated in the Literature Review Chapter, the developed analytical model is verified using the experimental work done by Honl *et al* in 2004 where WJ technology is used as a cutting tool for endoprosthesis revision surgery. A specially designed WJ cutting system was used for cutting bone cement at five different water pressures; Table 5.1 summarizes the operating conditions of the study.

Table 5.1 Operating Parameters of Fat Tissue Incision Using WJ

Parameter	Value
WJ Pressure (P)	30, 40, 50, 60 and 70 MPa
Width of cut (w_s)	0.20 mm
Density of water (ρ)	1.00 g/cm^3
Traverse speed (s)	0.5 mm/s
Gravity (g)	9.80 m/s^2
Stand-off distance (x)	5 mm
Taper (a) [47]	0.25

The experiment shows that using WJ pressure of 30, 40, 50, 60 and 70 MPa yield 0.75, 1.10, 1.75, 2.21 and 3.00 mm depth of cut of the bone cement respectively. However, the experiment in the paper did not state the specific energy of the bone cement. Using the analytical Matlab model (Figure 5.1), the specific energy of the bone cement is calculated from the given parameters. At 30 MPa WJ pressure, the specific energy is calculated to be 1.43 x 10^5 MPa. This value is then used to verify the developed analytical model. Table 5.2 shows the calculated depth of cut compared to the published measurements. The percent error between the measured and calculated values ranges between 2% (for 50 and 60 MPa WJ pressure) and 11% (for 40 MPa WJ pressure).

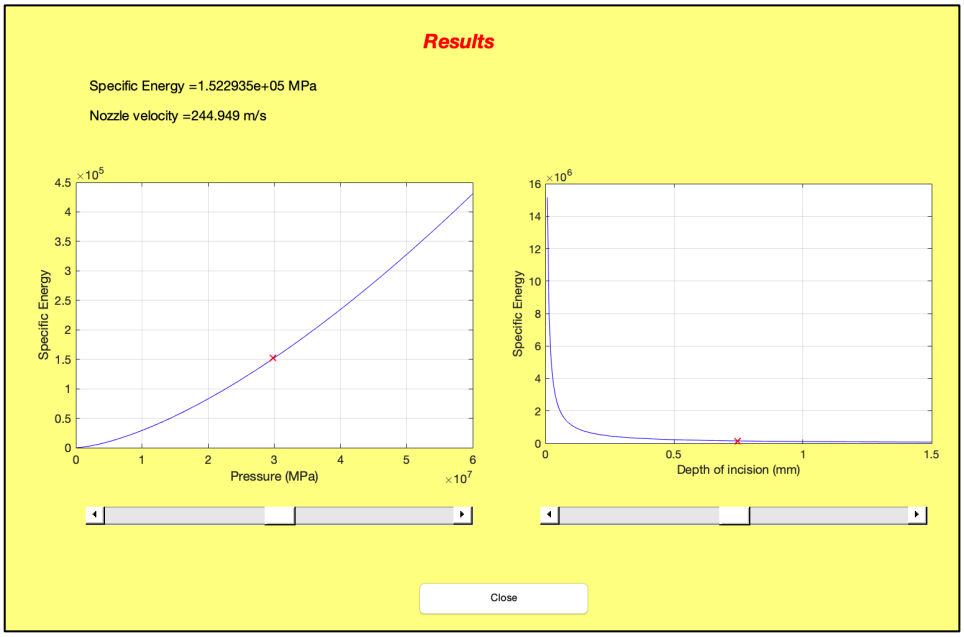

Figure 5.1 Matlab model to calculate the specific energy of the bone cement.

Table 5.2 Measured vs. Calculated Depth of Cut for Bone Cement

Specific Energy	Pressure	Measured Depth of Cut	Calculated Depth of Cut	Percent Error
1.43 x 10^5 MPa	30 MPa	~ 0.75 mm	-	-
1.43 x 10^5 MPa	40 MPa	~ 1.10 mm	**1.23 mm**	11%
1.43 x 10^5 MPa	50 MPa	~ 1.75 mm	**1.72 mm**	2%
1.43 x 10^5 MPa	60 MPa	~ 2.21 mm	**2.26 mm**	2%
1.43 x 10^5 MPa	70 MPa	~ 3.00 mm	**2.85 mm**	5%

5.2 Experimental Verification

While the theoretical verification compared against previous published studies is able to verify the developed analytical model, an experimental verification is recommended. Due to the unavailability of human skin, the experiment is conducted on animal skin using an

industrial type WJ, which is available at the Makerspace laboratory at the New Jersey Institute of Technology. The Makerspace laboratory is 9,500 square feet of state-of-the-art ranging from industrial to small prototyping machines. The Makerspace laboratory recently opened in 2018. The Makerspace laboratory key features include: Product design and prototyping, industry standard computer aided design and machine software, CNC machining, 3D printing, metal work and welding, electronics design, assembly, and manufacturing, industrial metrology, or measurement and verification as well as an industrial WJ machine: The Flow Mach 4c XD 3020 WJ (Figure 5.2) is used to cut the specimen. The WJ apparatus can provide water pressure ranging from 5,000 psi to 60,000 psi (34.5 MPa to 413.7 MPa).

Figure 5.2 Flow Mach 4c XD 3020 WJ.
Source: [51].

5.2.1 Experiment Specification and Preparation

The main components of the machine include a direct drive ultrahigh-pressure HyPlex Prime pump and intensifier (Figure 5.3), a gantry robotic station with a Dynamic WJ XD cutting head (Figure 5.4) and a water catcher tank (Figure 5.5). The pump's power is 50 horsepower (37,285 Watts), while its flow rate is 1 gal/min (6.3×10^{-5} m/s) [51]. The cutting head is where the conversion of water pressure to water velocity occurs. Although they are not used in this experiment, the cutting head also includes a mixing chamber and mixing tube for abrasive cut (Figure 5.6). At the bottom end of the cutting head is the nozzle; many nozzle orifice diameter size options are available. The smallest orifice available is 0.015" (0.38 mm) while the highest is 0.020" (0.51mm). The cutting head is controlled by FlowXpert Software. The software can control the feed rate, traverse speed as well as the stand-off distance as necessary throughout the experiment. The catcher tank is made of stainless steel and measures 3 m x 2 m x 1 m.

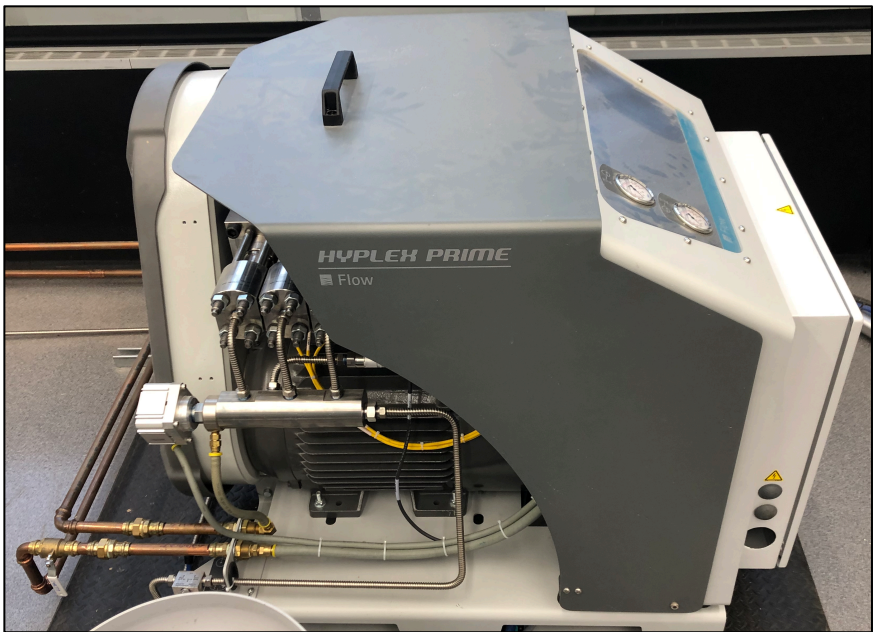

Figure 5.3 HyPlex Prime direct drive pump.

Figure 5.4 WJ cutting head.
Source: [51].

Figure 5.5 Stainless-steel catcher tank.

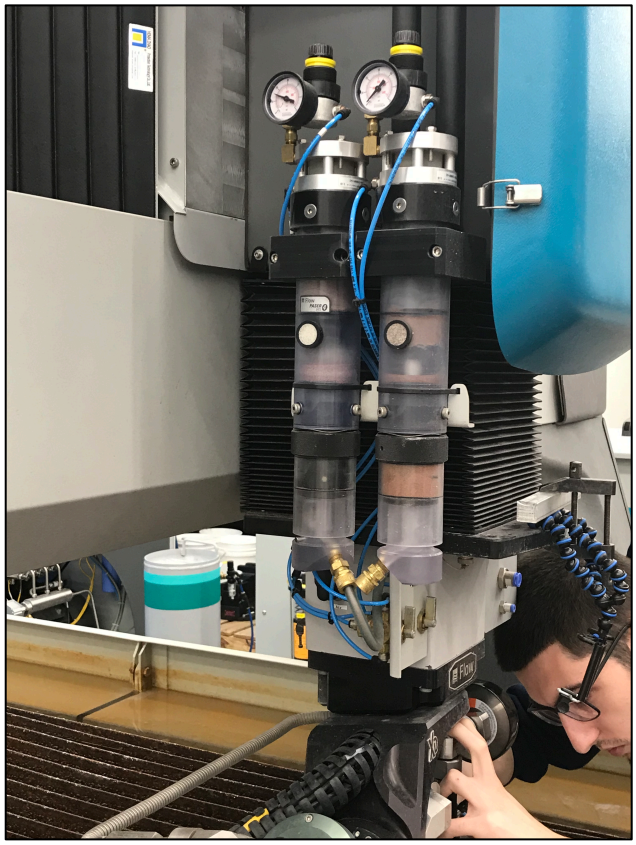

Figure 5.6 Abrasive mixing chamber and mixing tube.

Since the WJ is designed for industrial material cutting not tissue cutting, a downsized water catcher tank is necessary. The smaller water catcher tank (Figure 5.7) is where the specimen securely rests using the attached clamp fixtures. The main advantage of the custom-made catcher tanks is to eliminate any contamination that may occur during the experiment.

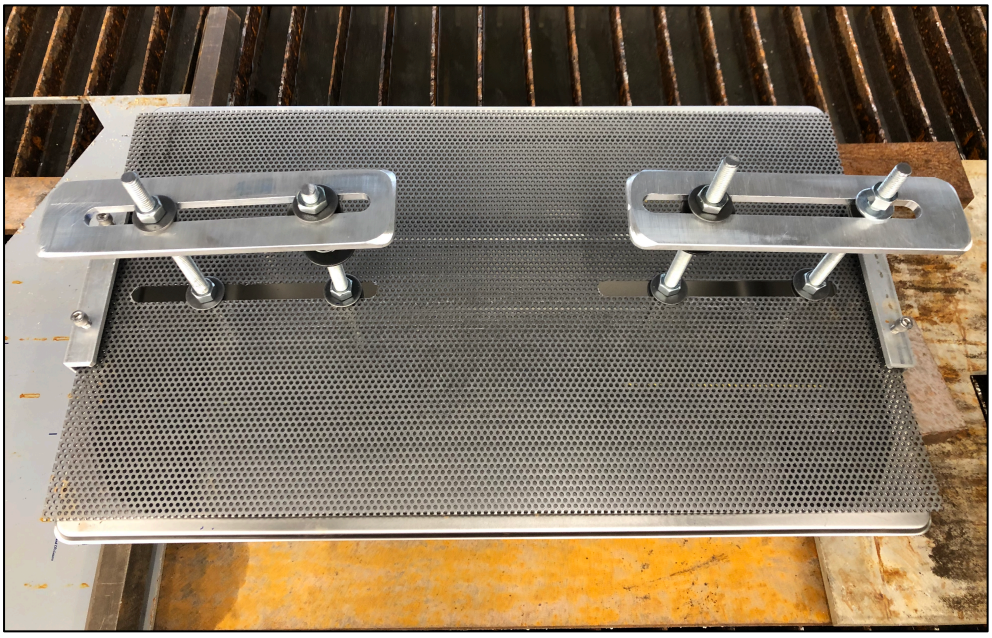

Figure 5.7 Stainless-steel catcher tank with clamp fixtures to hold specimen.

The catcher tank is built locally at the Makerspace laboratory. The tank consists of a stainless-steel pan that is 52.7 cm long, 32.4 cm wide and 15.2 cm deep. This pan is then covered by a 0.19 cm thick steel perforated sheet with 0.24 diameter holes. Two clamp fixtures are welded on each end of the tank.

In order to eliminate any other contamination, the main water catcher tank is covered in plastic wrap. To record the experiment, a GoPro camera is attached to the WJ cutting head to get a top-down view of the experiments. Other GoPro and digital cameras are also used to record the experiments from each side of the main catcher tank (Figure 5.8). Appendix C provides the videos recorded during the experiments.

Figure 5.8: GoPro cameras attached to the cutting head and the side of the tank.

The depth of incision is measured using Absolute Coolant Proof Caliper Series 500 (Figure 5.9). The caliper's length range is between 0 to 150 mm, its accuracy is 0.025 mm [52].

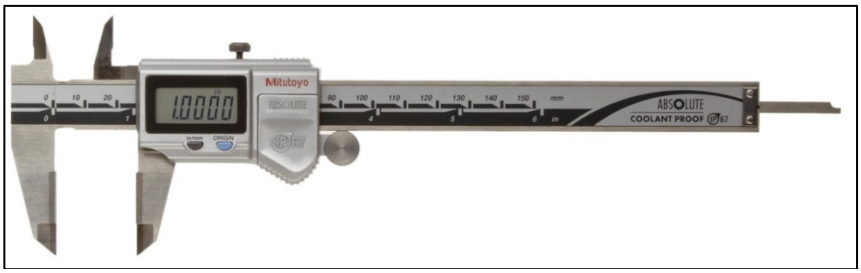

Figure 5.9 Absolute Coolant Proof caliper Series 500 [52].
Source: [52].

While porcine skin may appear to be the best substitute for human skin, the scope of the study only requires any type of animal skin for the experimental model verification. Therefore, based on availability, cow skin and bone are used in this experiment. The specimen used is donated by American Halal Meat, in Newark, New Jersey. The specimen

is provided on the day of the experiment and is transported in a cooling box to keep it fresh. As seen in Figure 5.10, one sample of cow leg is left with its skin intact while the other leg is skinned to allow the WJ to incise the metatarsus bone. It should be noted that the cow skin is covered in hair while the skinned leg has fat tissues intact to the bone.

Figure 5.10 Cow leg skin (left) and cow bone (right).

5.2.2 Experiment Setup and Results

The smallest nozzle's orifice diameter (0.38 mm) is selected and stays constant throughout the experiment. A 0.38 mm orifice allows for better incision precision in addition to mimicking the thickness of traditional skin incision tools that would be used otherwise. The stand-off distance is selected to be constant throughout the experiment at 5 mm which also ensures the incision precision. However, while the stand-off distance is set to be constant, some variation may still exist due to the unevenness of the specimen skin surface. Finally, the feed rate for incision also remains constant throughout the experiment at 16.93

mm/s. Tables 5.3 and 5.4 summarize the experiment setup and results for both skin and bone cutting and drilling.

Table 5.3 Experimental Data and Results for Cow Skin and Bone Cutting

Specimen Location	Pressure (English)	Pressure (Metric)	Depth of Incision	Comments
Cow Skin	6,000 psi	41MPa	0 mm	With Hair
Cow Skin	10,000 psi	69 MPa	10 mm	With Hair
Cow Skin	14,600 psi	101 MPa	15 mm	With Hair
Cow Bone (Fat)	14,700 psi	101 MPa	23 mm (Fat)	First Pass
Cow Bone (Fat)	14,700 psi	101 MPa	1 mm (Fat)	Second Pass
Cow Bone	25,000 psi	172 MPa	28.5 mm	Includes Fat

Table 5.4 Experimental Data and Results for Cow Skin and Bone Drilling

Specimen Location	Pressure (English)	Pressure (Metric)	Depth of Incision	z-direction Distance
Cow Skin	9,000 psi	62 MPa	10 mm	12.4 mm
Cow Skin	15,500 psi	100 MPa	No Effect Observed	12 mm
Cow Bone (Fat)	25,000 psi	172 MPa	12.5 mm (Fat)	7.3 mm

The z-direction distance provided in Table 5.3 refers to the distance that the WJ nozzle traveled vertically during the drilling. It is calculated by subtracting the end position from the start position of the nozzle. These positions are controlled by the cutting head that is adjusted by the WJ software.

As seen in Table 5.2, 6,000 psi (41 MPa) WJ pressure is not able to cut through the cow skin. When increasing the pressure to 10,000 psi (69 MPa) and 14,600 psi (101 MPa),

the WJ is able to cut 10 mm and 15 mm deep through the skin respectively (Figure 5.11). When applying the same pressure of 14,700 psi to cut through the bone, only the fat tissue that is left to the bone is cut (23 mm depth of cut). Applying a second pass of the same pressure in the same location, another 1 mm of fat tissue is cut. When increasing the WJ pressure to 25,000 psi (172 MPa), the water cut through both the fat tissue and the bone with a 28.5 mm depth of cut combined (Figure 5.12). It should be noted that when using the highest pressure to cut the fat and bone, a trapped water bubble appeared under the fat tissue, which can be seen in Figure 5.13.

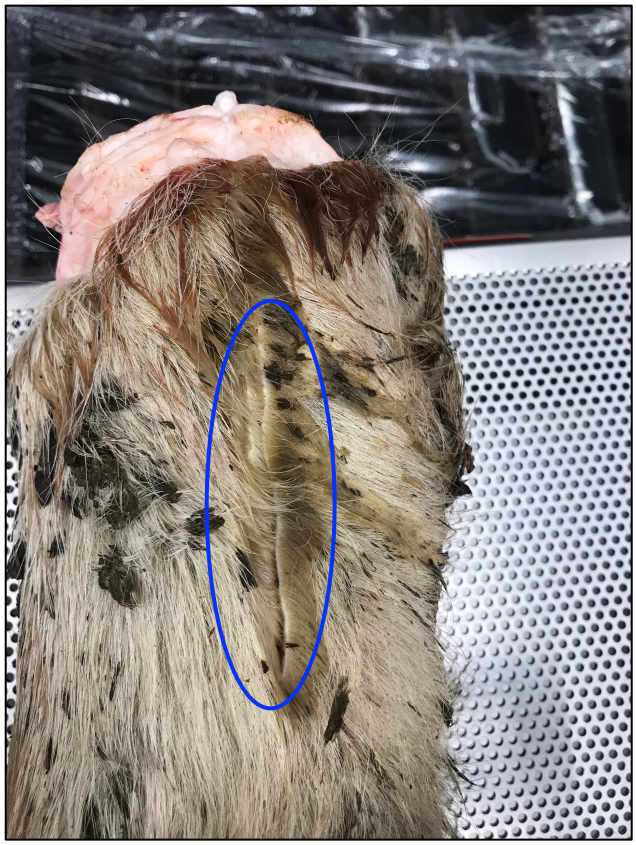

Figure 5.11 Cow skin cut using 101 MPa WJ pressure.

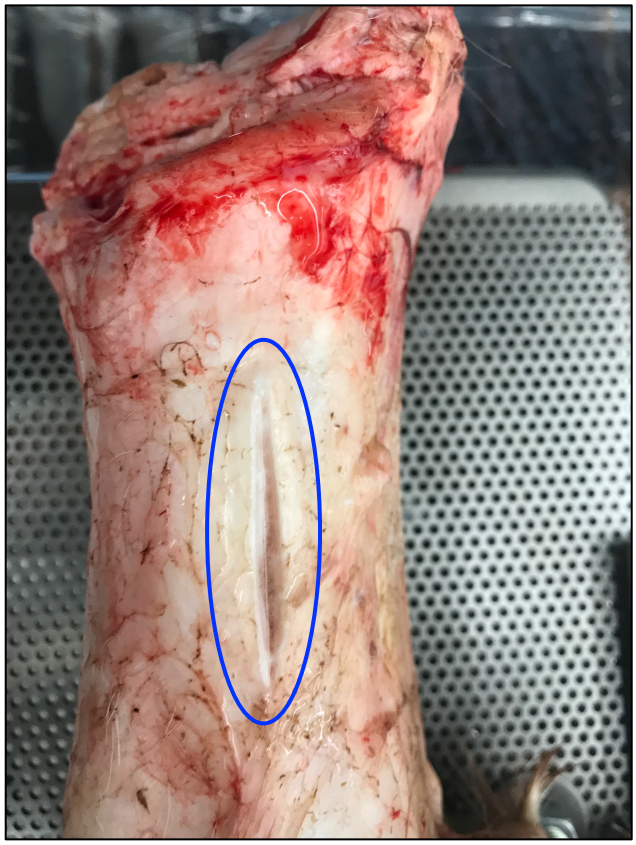

Figure 5.12 Cow fat and bone cut using 172 MPa WJ pressure.

Figure 5.13 Formation of trapped water bubble under the fat tissue.

For drilling, as seen in Table 5.2, the WJ pressure of 9,000 psi (62 MPa) is able to drill through 10 mm of cow skin. At 15,500 psi (100 MPa) no substantial depth of drill reading could be recorded. It should be noted that the thickness of the depth bar of the measuring caliper is 1.9 mm which is larger than width of incision which is 0.38 mm. While this may lead to the inability and inaccuracy of measuring the depth of drill of the specimen, it also demonstrates the precision of the WJ incision. When measuring the depth of drill using 25,000 psi (172 MPa) WJ pressure, 12.5 mm of fat tissue on the bone is recorded. It should be noted that when using the highest pressure to drill the cow skin, another trapped water bubble causes the skin to be raised off the bone, as seen in Figure 5.14.

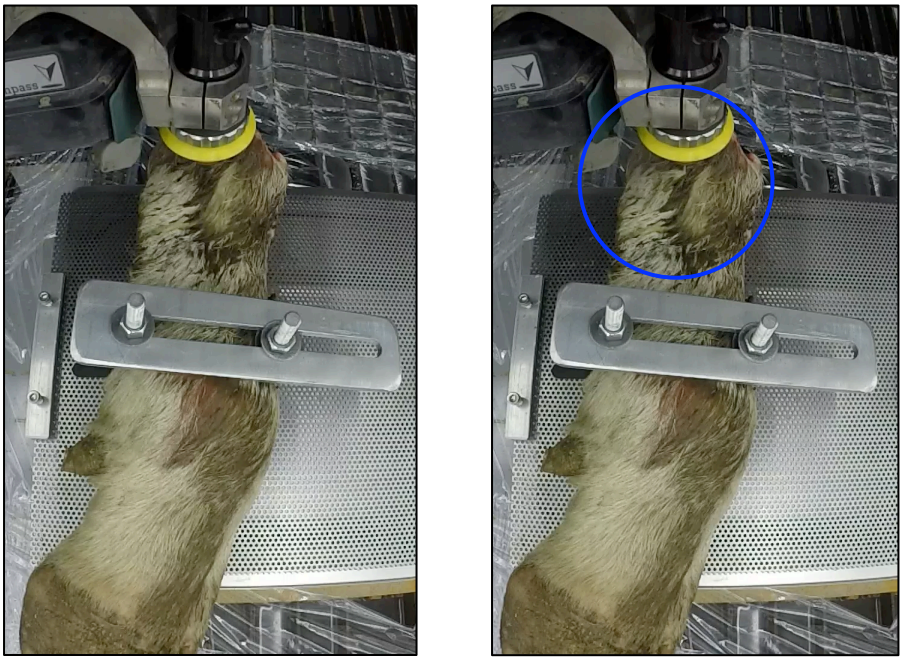

Figure 5.14 (a) Left: skin before WJ drilling, (b) Right: skin raised after WJ drilling.

The trapped water bubbles that are observed open up future research opportunity to add to the analytical model. The current analytical model explores the energy required to make a skin incision as well as the energy of the residue water going into the catcher

(Figure 4.1). Future research should look at the pressure energy (PE_{wb}) of the trapped water that is forming bubbles under the skin. The pressure energy (PE_{wb}) adds another component that is translated by the kinetic energy that is coming out of the nozzle (Figure 5.15).

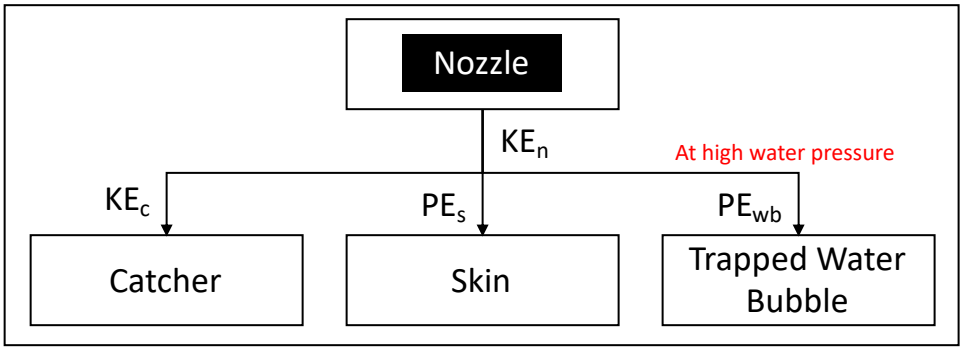

Figure 5.15 The trapped water bubble pressure energy at high water pressure.

5.2.3 Model Verification Using Experimental Results

Since the drilling experiment may not be reliable and might be producing inaccurate results, the analytical model is verified using the cutting experiment only. Meanwhile, the specific energy of the cow skin and bone is not known, the experimental runs are used to determine the specific energy for the cow skin and bone. Using the analytical Matlab model, the specific energy of the cow skin is calculated from the given parameters. At 69 MPa and 101 MPa WJ pressure, the specific energy is calculated to be 2.24 x 10^3 MPa and 2.64 x 10^3 MPa respectively. It can be assumed that the specific energy of organic materials is equal to their elastic modulus. For example, the elastic modulus of cow skin can measure about 2.9 GPa, which is within 16% of the experimentally calculated average specific energy [53]. From previous studies, the elastic modulus of cow bone is measured to be 24.5 GPa [54]. These values are used to verify the developed analytical model. Furthermore, in

the model verification, the same operating parameters from the experiment are used as input into the analytical model using the developed Matlab model (Figure 5.16). Table 5.5 summarizes the results of the analytical model verification using the experimental data. The percent error between the measured depth of cut vs. the calculated depth of cut using the analytical model is shown. The percent error between the measured and calculated values are as low as 9% (101 MPa WJ pressure applied on cow skin) to 23% (for 69 MPa WJ pressure applied on cow skin).

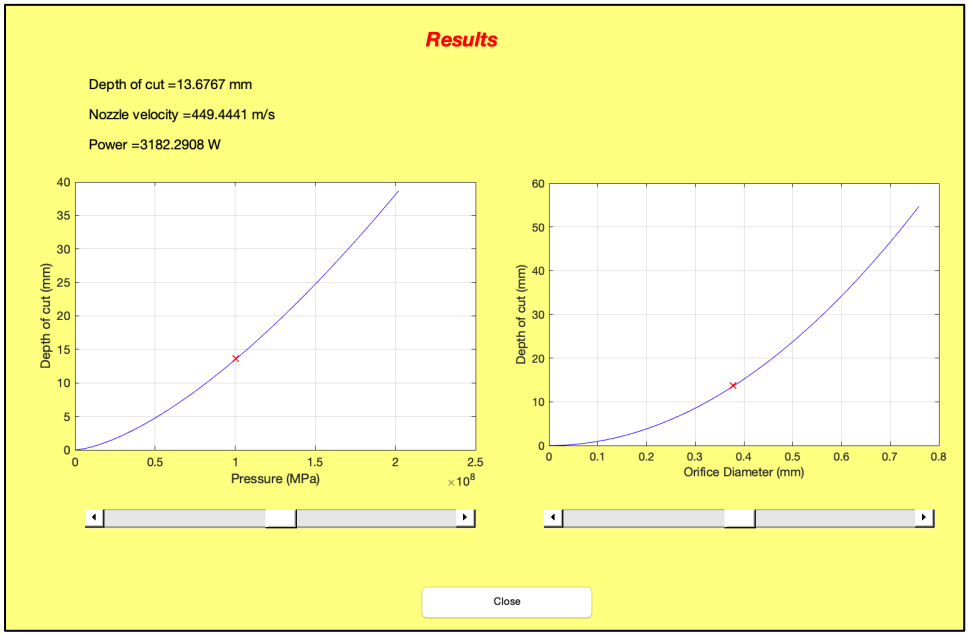

Figure 5.16 Experimental verification model Matlab output.

Table 5.5 Measured vs. Calculated Cow Skin and Bone Depth of Cut

Specimen Location	Specific Energy/ Elastic Modulus	Pressure	Measured Depth of Cut	Calculated Depth of Cut	Percent Error
Cow Skin	2.9 GPa	69 MPa	10 mm	**7.72 mm**	23%
Cow Skin	2.9 GPa	101 MPa	15 mm	**13.67 mm**	9%
Cow Bone	24.5 GPa	172 MPa	4.5 mm	**3.60 mm**	20%

In this experiment, only low profile WJ operating conditions and pressures are used to make skin and bone incisions. It is shown that low WJ pressure is able to cut through skin and fat, however, higher pressure is required for bone incision. For example, an additional experiment is conducted using 30,000 psi (207 MPa) to make an incision in the cow's hoof which resulted in minimal depth of cut that is not measurable (Figure 5.17). While such pressure used might not have a high impact on the depth of incision, there is room for experimenting at higher pressures, especially with stronger materials.

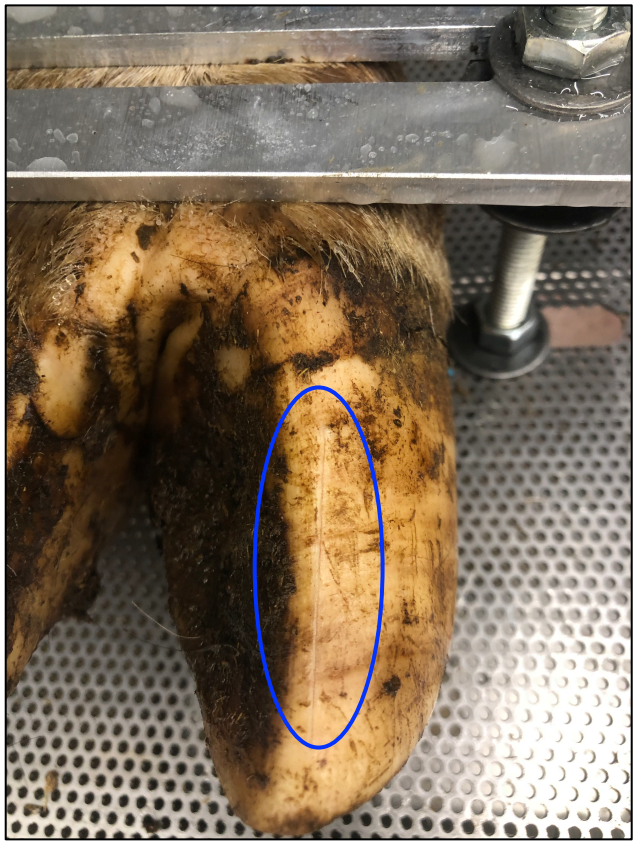

Figure 5.17 Minimal effect on the cow's hoof using 30,000 psi WJ pressure.

In addition to the analytical model verification, the physical experimentation provides proof of the concept that the WJ technology is able to make skin and bone incisions. However, the number of experiments does not provide enough data points to draw any inferences about the percent error between the measured and calculated depth of incision. By increasing the number of experiments and replicates in future work, more statistical inference can be extracted about the depth of incision errors. Additionally, Measurement System Analysis (MSA) to consider:

1- The selection of the correct approach of measuring the depth of incision and assessing the measuring device.

2- The assessment of procedures, operators and any measurement interactions.

3- The Calculation of the measurement uncertainty of individual measurement devices and/or measurement systems.

From the MSA one can recognize whether the percent error is due to measurement error or due to variations in the analytical model.

Although there are no published records of the cow's fat tissue's specific energy/elastic modulus, the developed analytical model has the capability to calculate it. Given the WJ's operating parameters as well as the experimentally measured depth of cut, the developed analytical model can compute any specimen's specific energy/elastic modulus. This model provides an innovative way to measure mechanical properties of organic materials that are difficult to measure using the traditional ways.

CHAPTER 6

CASE STUDY AND ANALYSIS OF RESULTS

The developed models can be applied to any type of surgical procedure to allow to identify the skin characteristics and behavior, given specific WJ operating parameters, before performing a certain incision. A case study is presented to demonstrate the findings of the developed analytical model. In addition to computing the skin behavior given certain WJ operating parameters and water pressures, the optimal operating conditions are determined using the optimization models.

6.1 Analytical Matlab Model

The case study presented in this section is to demonstrate the use of the WJ technology to make the skin incision during a Cesarean section procedure. Table 6.1 summarizes the surgery's operating parameters and skin characteristics. In this case study, the depth of skin cut is measured using different WJ pressure: 5 MPa, 10 MPa, 15 MPa and 20 MPa.

Table 6.1 Cesarean Section Operation Characteristics

Parameter	Value
Width of cut (w_s)	0.20 mm
Specific Energy/ Elastic Modulus (E)	1 GPa
Density of water (ρ)	1.00 g/cm^3
Traverse speed (s)	12 mm/s
Gravity (g)	9.80 m/s^2
Stand-off distance (x)	5 mm
Taper (a) [47]	0.25

The operations characteristics inputted into the Matlab model yield the suggested operating parameters that would make the Cesarean section incision, as seen in Figure 6.1. Table 6.2 summarizes the effect of the tested WJ pressures on the depth of cut of the skin, as well as the velocity of the nozzle and the power used.

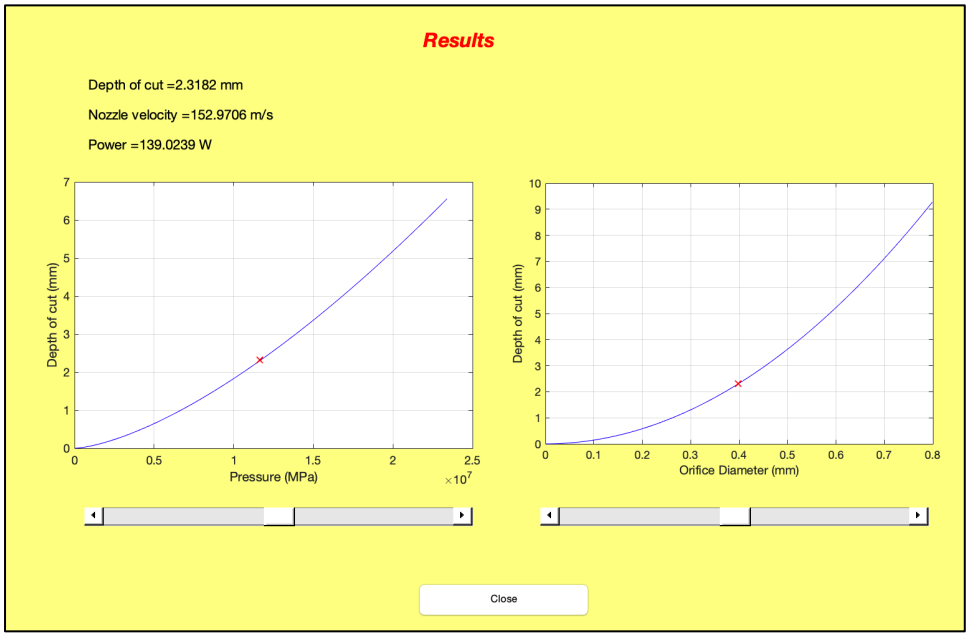

Figure 6.1 Matlab model output for Cesarean section operation.

Table 6.2 Cesarean Section Model Results

WJ Pressure	Skin Depth of Cut	Nozzle Velocity
5 MPa	0.65 mm	100 m/s
10 MPa	1.83 mm	141.4 m/s
15 MPa	3.36 mm	173.2 m/s
20 MPa	5.18 mm	200 m/s

As seen in Figure 6.1 and Table 6.2, with a nozzle's orifice diameter of 0.4 mm and 10 MPa WJ pressure, the depth of cut of the skin is 1.83 mm while the WJ velocity coming out of the nozzle is 141.4 m/s. The calculated power required for this incision is 110 Watts. To make an incision that is exactly 2.30 mm deep, the required WJ pressure is 12 MPa with WJ velocity coming out of the nozzle at 152.6 m/s and 138 Watts of power.

6.2 Systemization and Optimization Models

In order to determine the optimal operating conditions for the WJ a full factorial as well as Taguchi DOE are applied. The design's response is the depth of skin incision while the number of factors is five. Each factor consists of two levels: water pressure (P= 10 and 15 MPa), nozzle's orifice diameter (d_n= 0.2 and 0.4 mm), traverse speed (s= 12 and 17 mm/s) stand-off distance (x= 5 and 10 mm) and loss coefficient (k_e =0.08 and 0.15).

6.2.1 Taguchi DOE

An L32 orthogonal array is created to maximize the S/N ratio. The skin depth of cut is the response while the nozzle's orifice diameter, traverse speed, stand-off distance and the nozzle's loss coefficient are the controllable factors. The skin's elastic modulus in this design is considered to be the noise factor. Using the Minitab-Matlab integration model, 32 experiments are run for each noise factor (E= 0.75, 1 and 1.25 GPa), and the response results are recorded into Minitab. Table 6.3 summarizes the design of experiment as well as the response generated. Appendix B.1 provide the full analysis of the Taguchi DOE model.

Table 6.3 Cesarean Section Taguchi Model Design and Response

Pressure	Orifice Diameter	Traverse Speed	Stand-off Distance	Loss Coefficient	0.75 GPa	1 GPa	1.25 GPa
10	0.2	12	5	0.08	1.22	0.92	0.73
10	0.2	12	5	0.15	1.99	1.49	1.20
10	0.2	12	10	0.08	1.22	0.91	0.73
10	0.2	12	10	0.15	1.99	1.49	1.19
10	0.2	17	5	0.08	0.86	0.65	0.52
10	0.2	17	5	0.15	1.41	1.06	0.84
10	0.2	17	10	0.08	0.86	0.64	0.52
10	0.2	17	10	0.15	1.40	1.05	0.84
10	0.4	12	5	0.08	2.44	1.83	1.46
10	0.4	12	5	0.15	3.99	2.99	2.39
10	0.4	12	10	0.08	2.44	1.83	1.46
10	0.4	12	10	0.15	3.98	2.98	2.39
10	0.4	17	5	0.08	1.72	1.29	1.03
10	0.4	17	5	0.15	2.81	2.11	1.69
10	0.4	17	10	0.08	1.72	1.29	1.03
10	0.4	17	10	0.15	2.81	2.11	1.68
15	0.2	12	5	0.08	2.24	1.68	1.35
15	0.2	12	5	0.15	3.66	2.75	2.20
15	0.2	12	10	0.08	2.24	1.68	1.34
15	0.2	12	10	0.15	3.65	2.74	2.19
15	0.2	17	5	0.08	1.58	1.19	0.95
15	0.2	17	5	0.15	2.58	1.94	1.55
15	0.2	17	10	0.08	1.58	1.18	0.95
15	0.2	17	10	0.15	2.58	1.93	1.55
15	0.4	12	5	0.08	4.48	3.36	2.69
15	0.4	12	5	0.15	7.32	5.49	4.39
15	0.4	12	10	0.08	4.47	3.36	2.68
15	0.4	12	10	0.15	7.31	5.48	4.38
15	0.4	17	5	0.08	3.17	2.37	1.90
15	0.4	17	5	0.15	5.17	3.88	3.10
15	0.4	17	10	0.08	3.16	2.37	1.89
15	0.4	17	10	0.15	5.16	3.87	3.09

When analyzing the mean yields, as seen in Figures 6.2 and 6.3, the Taguchi design shows that the most significant factors that affect the depth of skin incision are the nozzle's orifice diameter, the water pressure, the nozzle's loss coefficient and the traverse speed respectively. Additionally, the interaction between the water pressure and the nozzle's orifice diameter, the nozzle loss coefficient and traverse speed are significant as well as the interactions between the nozzle's orifice diameter and traverse speed. Finally, the interaction between the traverse speed and the nozzle loss coefficient is also significant.

The figures also show that neither the stand-off distance nor any interactions with it have any effect on the depth of skin incision.

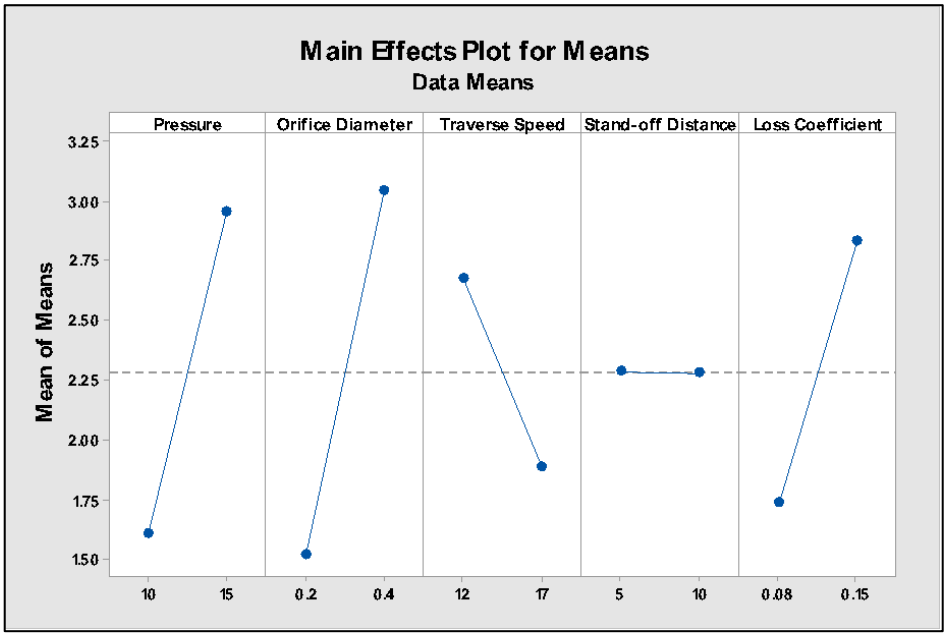

Figure 6.2 Taguchi main effects plot for means for depth of skin incision.

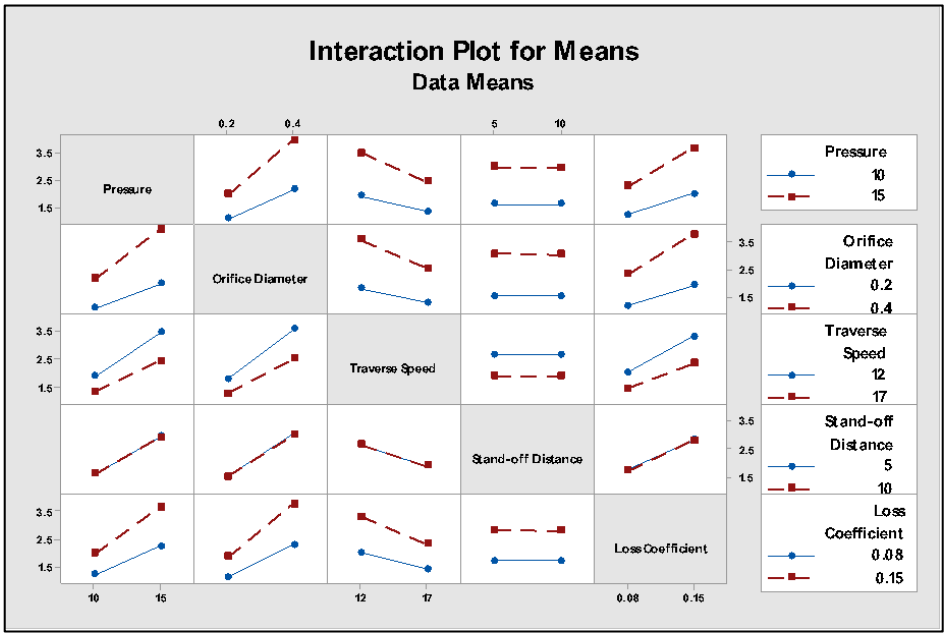

Figure 6.3 Taguchi interaction plot for means for depth of skin incision

The S/N ratio is used to identify the control factor settings that minimize the variability caused by the noise factors (elastic modulus of the skin). In this case study, the "Larger is better" S/N ratio option is selected in order to minimize the standard deviation and maximize the S/N ratio and the means. Tables 6.4-6.6 present the Taguchi response for S/N ratios, means and standard deviation respectively. To indicate the relative effect of the three factors on the depth of cut, the Delta values (the difference between the highest and lowest average response values for each factor) are ranked from high to low. The nozzle's orifice diameter has the largest effect on S/N ratio, mean and standard deviation with highest Delta values, followed by the WJ pressure, loss coefficient, traverse speed and stand-off distance.

Table 6.4 Taguchi Response for S/N Ratios

Level	Pressure	Orifice Diameter	Traverse Speed	Stand-off Distance	Loss Coefficient
1	2.672	2.303	6.826	5.324	3.183
2	7.955	8.324	3.801	5.303	7.444
Delta	5.283	6.021	3.025	0.022	4.260
Rank	2	1	4	5	3

Table 6.5 Taguchi Response for Means

Level	Pressure	Orifice Diameter	Traverse Speed	Stand-off Distance	Loss Coefficient
1	1.608	1.521	2.675	2.285	1.733
2	2.955	3.042	1.888	2.279	2.830
Delta	1.346	1.521	0.787	0.006	1.097
Rank	2	1	4	5	3

Table 6.6 Taguchi Response for Standard Deviations

Level	Pressure	Orifice Diameter	Traverse Speed	Stand-off Distance	Loss Coefficient
1	0.4149	0.3924	0.6901	0.5893	0.4471
2	0.7623	0.7848	0.4871	0.5879	0.7301
Delta	0.3473	0.3924	0.2030	0.0015	0.2830
Rank	2	1	4	5	3

Using Taguchi to predict the results to maximize the response, the skin depth of cut measures 5.57 mm. The optimal operating parameters are 15 MPa WJ pressure, 0.4 mm nozzle's orifice diameter with 12 mm/s traverse speed and loss coefficient value of 0.15.

6.2.2 Full Factorial DOE

In the full factorial DOE, the selected number of replicates is three: each replicate uses a different value of the skin's elastic modulus (E= 0.75, 1 and 1.25 GPa) as covariate for the design. Using the Matlab model, 96 experiments are run, recorded and the response results are transferred into Minitab. Table 6.7 summarizes the design of experiment as well as the response generated. Appendix B.2 provides the full analysis of the full factorial DOE model.

Table 6.7 Cesarean Section Full Factorial Design and Response

StdOrder	RunOrder	CenterPt	Blocks	Pressure	Orifice Diameter	Traverse Speed	Stand-off Distance	Loss Coefficient	Depth of Cut	Elastic Modulus
1	1	1	1	10	0.2	12	5	0.08	1.22	0.75
2	2	1	1	15	0.2	12	5	0.08	2.24	0.75
3	3	1	1	10	0.4	12	5	0.08	2.44	0.75
4	4	1	1	15	0.4	12	5	0.08	4.48	0.75
5	5	1	1	10	0.2	17	5	0.08	0.86	0.75
6	6	1	1	15	0.2	17	5	0.08	1.58	0.75
7	7	1	1	10	0.4	17	5	0.08	1.72	0.75
8	8	1	1	15	0.4	17	5	0.08	3.17	0.75
9	9	1	1	10	0.2	12	10	0.08	1.22	0.75
10	10	1	1	15	0.2	12	10	0.08	2.24	0.75
11	11	1	1	10	0.4	12	10	0.08	2.44	0.75
12	12	1	1	15	0.4	12	10	0.08	4.47	0.75
13	13	1	1	10	0.2	17	10	0.08	0.86	0.75
14	14	1	1	15	0.2	17	10	0.08	1.58	0.75
15	15	1	1	10	0.4	17	10	0.08	1.72	0.75
16	16	1	1	15	0.4	17	10	0.08	3.16	0.75
17	17	1	1	10	0.2	12	5	0.15	1.99	0.75
18	18	1	1	15	0.2	12	5	0.15	3.66	0.75
19	19	1	1	10	0.4	12	5	0.15	3.99	0.75
20	20	1	1	15	0.4	12	5	0.15	7.32	0.75
21	21	1	1	10	0.2	17	5	0.15	1.41	0.75
22	22	1	1	15	0.2	17	5	0.15	2.58	0.75
23	23	1	1	10	0.4	17	5	0.15	2.81	0.75
24	24	1	1	15	0.4	17	5	0.15	5.17	0.75
25	25	1	1	10	0.2	12	10	0.15	1.99	0.75
26	26	1	1	15	0.2	12	10	0.15	3.65	0.75
27	27	1	1	10	0.4	12	10	0.15	3.98	0.75
28	28	1	1	15	0.4	12	10	0.15	7.31	0.75
29	29	1	1	10	0.2	17	10	0.15	1.40	0.75
30	30	1	1	15	0.2	17	10	0.15	2.58	0.75
31	31	1	1	10	0.4	17	10	0.15	2.81	0.75
32	32	1	1	15	0.4	17	10	0.15	5.16	0.75
33	33	1	1	10	0.2	12	5	0.08	0.92	1
34	34	1	1	15	0.2	12	5	0.08	1.68	1
35	35	1	1	10	0.4	12	5	0.08	1.83	1
36	36	1	1	15	0.4	12	5	0.08	3.36	1
37	37	1	1	10	0.2	17	5	0.08	0.65	1
38	38	1	1	15	0.2	17	5	0.08	1.19	1
39	39	1	1	10	0.4	17	5	0.08	1.29	1
40	40	1	1	15	0.4	17	5	0.08	2.37	1
41	41	1	1	10	0.2	12	10	0.08	0.91	1
42	42	1	1	15	0.2	12	10	0.08	1.68	1
43	43	1	1	10	0.4	12	10	0.08	1.83	1
44	44	1	1	15	0.4	12	10	0.08	3.36	1
45	45	1	1	10	0.2	17	10	0.08	0.64	1
46	46	1	1	15	0.2	17	10	0.08	1.18	1
47	47	1	1	10	0.4	17	10	0.08	1.29	1
48	48	1	1	15	0.4	17	10	0.08	2.37	1
49	49	1	1	10	0.2	12	5	0.15	1.49	1
50	50	1	1	15	0.2	12	5	0.15	2.75	1
51	51	1	1	10	0.4	12	5	0.15	2.99	1
52	52	1	1	15	0.4	12	5	0.15	5.49	1
53	53	1	1	10	0.2	17	5	0.15	1.06	1
54	54	1	1	15	0.2	17	5	0.15	1.94	1
55	55	1	1	10	0.4	17	5	0.15	2.11	1
56	56	1	1	15	0.4	17	5	0.15	3.88	1
57	57	1	1	10	0.2	12	10	0.15	1.49	1
58	58	1	1	15	0.2	12	10	0.15	2.74	1
59	59	1	1	10	0.4	12	10	0.15	2.98	1
60	60	1	1	15	0.4	12	10	0.15	5.48	1
61	61	1	1	10	0.2	17	10	0.15	1.05	1
62	62	1	1	15	0.2	17	10	0.15	1.93	1
63	63	1	1	10	0.4	17	10	0.15	2.11	1
64	64	1	1	15	0.4	17	10	0.15	3.87	1
65	65	1	1	10	0.2	12	5	0.08	0.73	1.25
66	66	1	1	15	0.2	12	5	0.08	1.35	1.25
67	67	1	1	10	0.4	12	5	0.08	1.46	1.25
68	68	1	1	15	0.4	12	5	0.08	2.69	1.25
69	69	1	1	10	0.2	17	5	0.08	0.52	1.25
70	70	1	1	15	0.2	17	5	0.08	0.95	1.25
71	71	1	1	10	0.4	17	5	0.08	1.03	1.25
72	72	1	1	15	0.4	17	5	0.08	1.90	1.25
73	73	1	1	10	0.2	12	10	0.08	0.73	1.25
74	74	1	1	15	0.2	12	10	0.08	1.34	1.25
75	75	1	1	10	0.4	12	10	0.08	1.46	1.25
76	76	1	1	15	0.4	12	10	0.08	2.68	1.25
77	77	1	1	10	0.2	17	10	0.08	0.52	1.25
78	78	1	1	15	0.2	17	10	0.08	0.95	1.25
79	79	1	1	10	0.4	17	10	0.08	1.03	1.25
80	80	1	1	15	0.4	17	10	0.08	1.89	1.25
81	81	1	1	10	0.2	12	5	0.15	1.20	1.25
82	82	1	1	15	0.2	12	5	0.15	2.20	1.25
83	83	1	1	10	0.4	12	5	0.15	2.39	1.25
84	84	1	1	15	0.4	12	5	0.15	4.39	1.25
85	85	1	1	10	0.2	17	5	0.15	0.84	1.25
86	86	1	1	15	0.2	17	5	0.15	1.55	1.25
87	87	1	1	10	0.4	17	5	0.15	1.69	1.25
88	88	1	1	15	0.4	17	5	0.15	3.10	1.25
89	89	1	1	10	0.2	12	10	0.15	1.19	1.25
90	90	1	1	15	0.2	12	10	0.15	2.19	1.25
91	91	1	1	10	0.4	12	10	0.15	2.39	1.25
92	92	1	1	15	0.4	12	10	0.15	4.38	1.25
93	93	1	1	10	0.2	17	10	0.15	0.84	1.25
94	94	1	1	15	0.2	17	10	0.15	1.55	1.25
95	95	1	1	10	0.4	17	10	0.15	1.68	1.25
96	96	1	1	15	0.4	17	10	0.15	3.09	1.25

When running and analyzing the full factorial design, as seen in Figures 6.4 and 6.5, the significant factors and their interactions are found to be the same as thus of the Taguchi design.

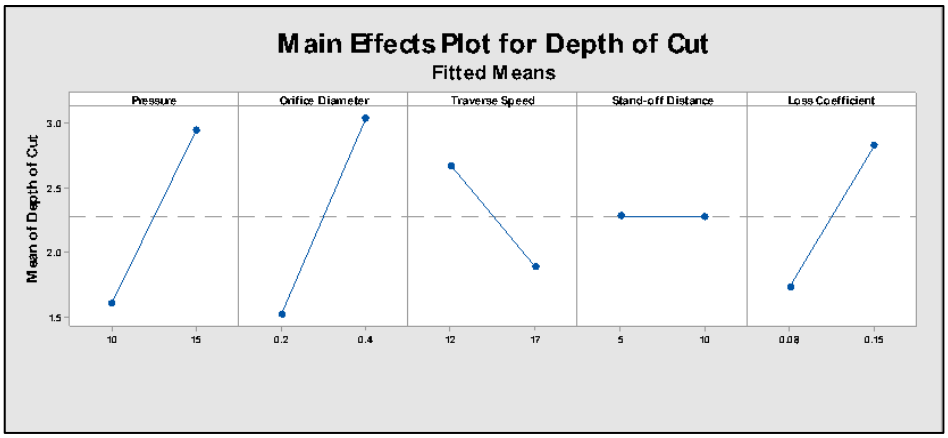

Figure 6.4 Full factorial design main effect plot for depth of skin incision

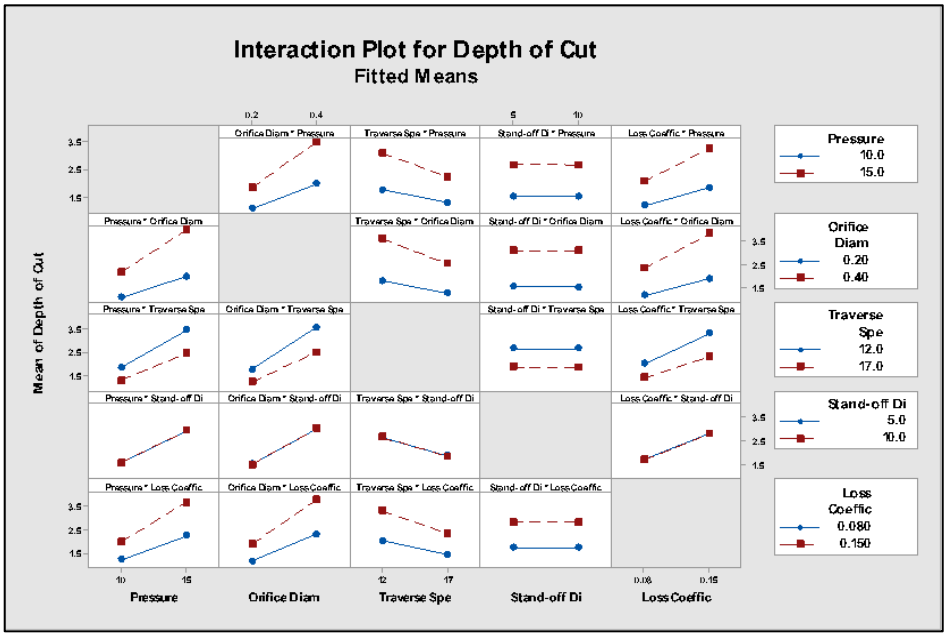

Figure 6.5 Full factorial design interaction plot for depth of skin incision.

A stepwise regression for the analyzed factorial design is performed for the purpose of identifying a useful subset of the terms. Figures 6.6 and 6.7 show the normal plot and the Pareto chart of the main and interaction effects on the depth of skin. An additional 3-way interaction between the water pressure, the nozzle's orifice diameter and the nozzle's loss coefficient has become significant resulting from the stepwise regression.

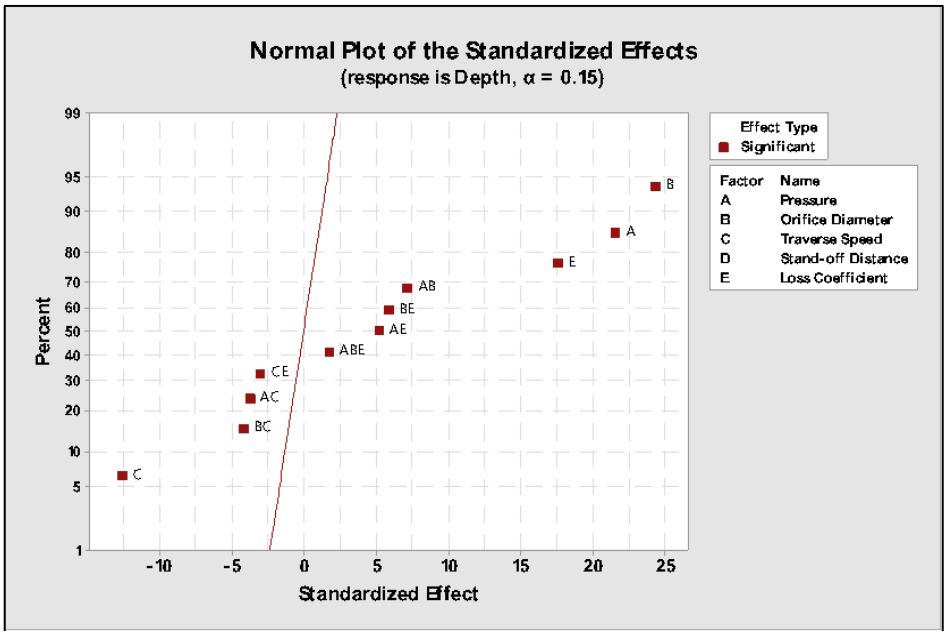

Figure 6.6 Full factorial design normal plot for the standardized effects.

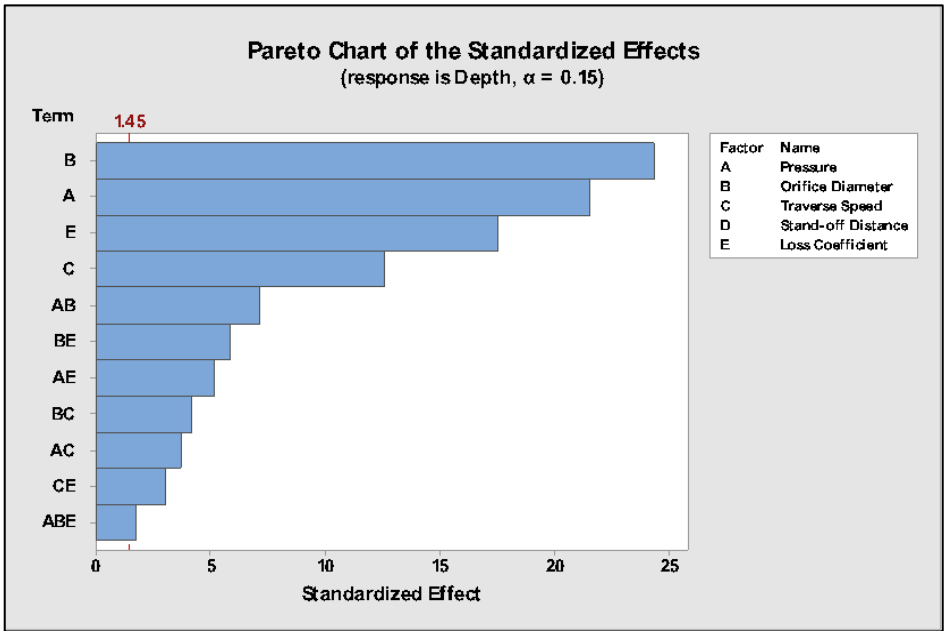

Figure 6.7 Full factorial design pareto for the standardized effects.

The model's regression equation to predict the response is formulated as follows:

$$Depth\ of\ Cut = -1.04 + 2.330 \cdot E + 0.2693 \cdot P + 3.99 \cdot d_n + 0.2322 \cdot s + 0.549 \cdot k_e$$
$$+ 0.898 \cdot P \cdot d_n - 0.01857 \cdot P \cdot s - 0.525 \cdot d_n \cdot s - 0.87 \cdot d_n \cdot k_e$$
$$- 0.0378 \cdot s \cdot k_n + 0.216 \cdot P \cdot d_n \cdot k_e$$

The regression model equation is used to predict the skin depth of cut for different WJ pressures: 5 MPa, 10 MPa, 15 MPa and 20 MPa. Using the same operating parameters shown in Table 6.1, the results of the DOE analysis and the Matlab model analysis are compared in Table 6.7. The percent error, between the two model ranges, decreases with higher water pressure; while the percent error measures 46% for 5 MPa water pressure, it decreases dramatically to 6%, 5% and 1% for 10 MPa, 15 MPa and 20 MPa water pressures respectively.

Table 6.8 Skin Depth of Cut Results Using DOE vs. Matlab Model

WJ Pressure	Skin Depth of Cut (DOE)	Skin Depth of Cut (Matlab Model)	Percent Error
5 MPa	0.35 mm	0.65 mm	46%
10 MPa	1.94 mm	1.83 mm	6%
15 MPa	3.54 mm	3.36 mm	5%
20 MPa	5.13 mm	5.18 mm	1%

Using the response optimizer of the M-DOE model and set the goal to maximize the depth of cut, yields value of 5.62 mm. The predicted optimal WJ operating parameters are as follows: 15 MPa WJ pressure, 0.4 mm nozzle's orifice diameter with 12 mm/s traverse speed and 0.15 nozzle loss coefficient value when the skin's elastic modulus is 1 GPa. Figure 6.8 shows the optimization plot for maximizing the skin depth of cut.

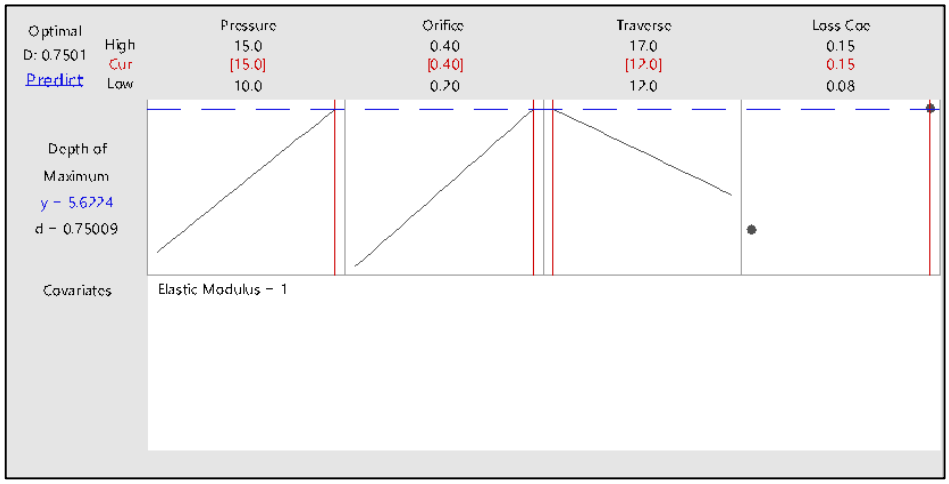

Figure 6.8 Optimization plot for maximizing the skin depth of incision.

When comparing the predicted results using Taguchi's analysis and the response optimizer using the full factorial analysis, both yield the same optimal operating parameters that maximize the skin depth of cut to 5.6 mm.

When running the confirmation test using the Matlab model, using the optimal operating parameters that resulted from both M-DOE models:

- WJ pressure (P_W)= 15 MPa
- Nozzle's orifice diameter (d_n)= 0.4 mm
- Traverse speed (s)= 12 mm/s
- Loss Coefficient value (K_e)= 0.15

The calculated depth of cut is 5.5 mm (shown in Figure 6.9) which is within 2% percent error of the predicted value of the M-DOE.

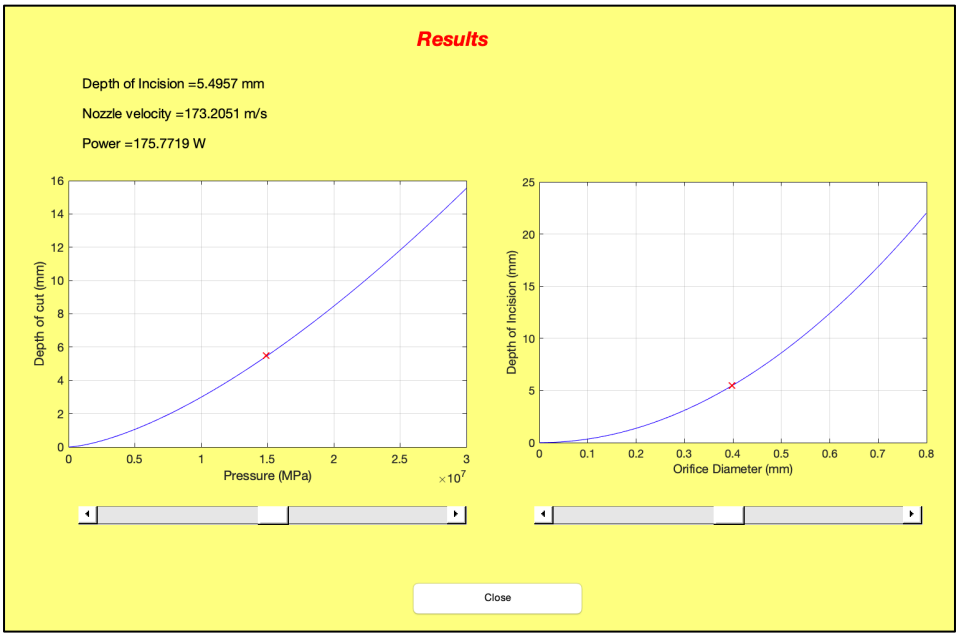

Figure 6.9 Confirmation test results.

Furthermore, when setting the depth of cut target to 2.30 mm (which is the average abdomen skin thickness of a woman that would need to be incised for a Cesarean section procedure), the predicted optimal WJ operating parameters are as follows:

- 12.5 MPa WJ pressure
- 0.3 mm nozzle's orifice diameter
- 17 mm/s traverse speed
- 0.15 nozzle loss coefficient value

when the skin's elastic modulus is 1 GPa. Figure 6.10 shows the optimization plot.

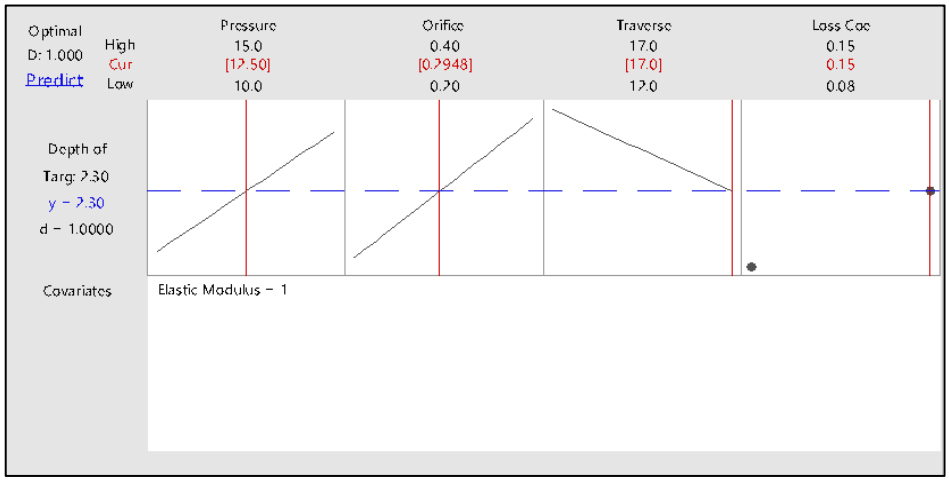

Figure 6.10 Optimization plot for target skin depth of incision.

CHAPTER 7

CONCLUSION AND RECOMMENDATIONS

This research has proven to explore the theoretical and analytical aspects of WJ technology that helps achieve the feasibility of skin incisions, without the costs or the risks. The developed models have presented a new approach to WJ incisions process for different types of skins. The models are based on fundamentals of the machining process of the WJ incisions. Two-interfaced program: Matlab and Minitab, has been used to develop an optimization model. The results obtained were verified with the results published in the literature and a physical experiment on cow skin and bone. Several treatments and characteristics were included to prove the effectiveness of the model.

The most significant operating parameters to make a skin incision were determined to be the nozzle's orifice diameter, the WJ pressure, the nozzle's loss coefficient and the traverse speed. The stand-off distance between the nozzle and the skin did not have a significant effect on the depth of cut. Additionally, the optimal operating parameters required to make a target skin incision of 2.30 mm in the abdomen is calculated to be 12.5 MPa WJ pressure, 0.3 mm orifice diameter with 17 mm/s traverse speed and a 0.15 nozzle loss coefficient value when the skin's elastic modulus is 1 GPa. This study has also revealed an alternative way to measure the specific energy/elastic modulus of any material using the developed analytical model.

The research conducted has unraveled new opportunities for the use of WJ technology. New applications may include using WJ in minimally invasive veterinary

surgeries, such as laparoscopy and thoracoscopy as well as in food cutting businesses which would be more sanitary.

There is still a need for further research to be done in the field. Further modifications and addition of other characteristics will be developed for the model to enhance its capabilities to determine the optimum results for the WJ incisions to be implemented in real life.

Further research may include verifying the developed model using porcine skin, since its material properties are similar to that of human skin. Additionally, verifying the model using a WJ apparatus that is specified for medical procedures with lower water pressure is recommended for more accurate results. Moreover, a larger sample size of experiments is recommended as well as MSA to ensure the integrity of the results.

APPENDIX A

MATLAB SOURCE CODES

A.1 Calculating the Depth of Incision of the Skin

```
function varargout = depth_calc(varargin)
% depth_calc MATLAB code for depth_calc.fig
%      depth_calc, by itself, creates a new depth_calc or raises the
existing
%      singleton*.
%
%      H = depth_calc returns the handle to a new depth_calc or the
handle to
%      the existing singleton*.
%
%      depth_calc('CALLBACK',hObject,eventData,handles,...) calls the
local
%      function named CALLBACK in depth_calc.M with the given input
arguments.
%
%      depth_calc('Property','Value',...) creates a new depth_calc or
raises the
%      existing singleton*.  Starting from the left, property value
pairs are
%      applied to the GUI before depth_calc_OpeningFcn gets called.  An
%      unrecognized property name or invalid value makes property
application
%      stop.  All inputs are passed to depth_calc_OpeningFcn via
varargin.
%
%      *See GUI Options on GUIDE's Tools menu.  Choose "GUI allows only
one
%      instance to run (singleton)".
%
% See also: GUIDE, GUIDATA, GUIHANDLES

% Edit the above text to modify the response to help depth_calc

% Last Modified by GUIDE v2.5 08-Feb-2019 21:43:56

% Begin initialization code - DO NOT EDIT
gui_Singleton = 1;
gui_State = struct('gui_Name',       mfilename, ...
                   'gui_Singleton',  gui_Singleton, ...
                   'gui_OpeningFcn', @depth_calc_OpeningFcn, ...
                   'gui_OutputFcn',  @depth_calc_OutputFcn, ...
                   'gui_LayoutFcn',  [] , ...
                   'gui_Callback',   []);
if nargin && ischar(varargin{1})
    gui_State.gui_Callback = str2func(varargin{1});
end

if nargout
```

```
    [varargout{1:nargout}] = gui_mainfcn(gui_State, varargin{:});
else
    gui_mainfcn(gui_State, varargin{:});
end
% End initialization code - DO NOT EDIT

%Global variables
Depth_of_cut = 0;
velocity_nozzle = 0;
Power = 0;

% --- Executes just before depth_calc is made visible.
function depth_calc_OpeningFcn(hObject, eventdata, handles, varargin)
% This function has no output args, see OutputFcn.
% hObject    handle to figure
% eventdata  reserved - to be defined in a future version of MATLAB
% handles    structure with handles and user data (see GUIDATA)
% varargin   command line arguments to depth_calc (see VARARGIN)

% Choose default command line output for depth_calc
handles.output = hObject;

% Update handles structure
guidata(hObject, handles);

% UIWAIT makes depth_calc wait for user response (see UIRESUME)
% uiwait(handles.figure1);


% --- Outputs from this function are returned to the command line.
function varargout = depth_calc_OutputFcn(hObject, eventdata, handles)
% varargout  cell array for returning output args (see VARARGOUT);
% hObject    handle to figure
% eventdata  reserved - to be defined in a future version of MATLAB
% handles    structure with handles and user data (see GUIDATA)

% Get default command line output from handles structure
varargout{1} = handles.output;



function edit1_Callback(hObject, eventdata, handles)
% hObject    handle to edit1 (see GCBO)
% eventdata  reserved - to be defined in a future version of MATLAB
% handles    structure with handles and user data (see GUIDATA)

% Hints: get(hObject,'String') returns contents of edit1 as text
%        str2double(get(hObject,'String')) returns contents of edit1 as
a double


% --- Executes during object creation, after setting all properties.
function edit1_CreateFcn(hObject, eventdata, handles)
% hObject    handle to edit1 (see GCBO)
% eventdata  reserved - to be defined in a future version of MATLAB
```

```
% handles    empty - handles not created until after all CreateFcns
called

% Hint: edit controls usually have a white background on Windows.
%       See ISPC and COMPUTER.
if ispc && isequal(get(hObject,'BackgroundColor'),
get(0,'defaultUicontrolBackgroundColor'))
    set(hObject,'BackgroundColor','white');
end



function edit2_Callback(hObject, eventdata, handles)
% hObject    handle to edit2 (see GCBO)
% eventdata  reserved - to be defined in a future version of MATLAB
% handles    structure with handles and user data (see GUIDATA)

% Hints: get(hObject,'String') returns contents of edit2 as text
%        str2double(get(hObject,'String')) returns contents of edit2 as
a double


% --- Executes during object creation, after setting all properties.
function edit2_CreateFcn(hObject, eventdata, handles)
% hObject    handle to edit2 (see GCBO)
% eventdata  reserved - to be defined in a future version of MATLAB
% handles    empty - handles not created until after all CreateFcns
called

% Hint: edit controls usually have a white background on Windows.
%       See ISPC and COMPUTER.
if ispc && isequal(get(hObject,'BackgroundColor'),
get(0,'defaultUicontrolBackgroundColor'))
    set(hObject,'BackgroundColor','white');
end



function edit3_Callback(hObject, eventdata, handles)
% hObject    handle to edit3 (see GCBO)
% eventdata  reserved - to be defined in a future version of MATLAB
% handles    structure with handles and user data (see GUIDATA)

% Hints: get(hObject,'String') returns contents of edit3 as text
%        str2double(get(hObject,'String')) returns contents of edit3 as
a double


% --- Executes during object creation, after setting all properties.
function edit3_CreateFcn(hObject, eventdata, handles)
% hObject    handle to edit3 (see GCBO)
% eventdata  reserved - to be defined in a future version of MATLAB
% handles    empty - handles not created until after all CreateFcns
called
```

```
% Hint: edit controls usually have a white background on Windows.
%       See ISPC and COMPUTER.
if ispc && isequal(get(hObject,'BackgroundColor'),
get(0,'defaultUicontrolBackgroundColor'))
    set(hObject,'BackgroundColor','white');
end



function edit4_Callback(hObject, eventdata, handles)
% hObject    handle to edit4 (see GCBO)
% eventdata  reserved - to be defined in a future version of MATLAB
% handles    structure with handles and user data (see GUIDATA)

% Hints: get(hObject,'String') returns contents of edit4 as text
%        str2double(get(hObject,'String')) returns contents of edit4 as
a double


% --- Executes during object creation, after setting all properties.
function edit4_CreateFcn(hObject, eventdata, handles)
% hObject    handle to edit4 (see GCBO)
% eventdata  reserved - to be defined in a future version of MATLAB
% handles    empty - handles not created until after all CreateFcns
called

% Hint: edit controls usually have a white background on Windows.
%       See ISPC and COMPUTER.
if ispc && isequal(get(hObject,'BackgroundColor'),
get(0,'defaultUicontrolBackgroundColor'))
    set(hObject,'BackgroundColor','white');
end



function edit5_Callback(hObject, eventdata, handles)
% hObject    handle to edit5 (see GCBO)
% eventdata  reserved - to be defined in a future version of MATLAB
% handles    structure with handles and user data (see GUIDATA)

% Hints: get(hObject,'String') returns contents of edit5 as text
%        str2double(get(hObject,'String')) returns contents of edit5 as
a double


% --- Executes during object creation, after setting all properties.
function edit5_CreateFcn(hObject, eventdata, handles)
% hObject    handle to edit5 (see GCBO)
% eventdata  reserved - to be defined in a future version of MATLAB
% handles    empty - handles not created until after all CreateFcns
called

% Hint: edit controls usually have a white background on Windows.
%       See ISPC and COMPUTER.
```

```
if ispc && isequal(get(hObject,'BackgroundColor'),
get(0,'defaultUicontrolBackgroundColor'))
    set(hObject,'BackgroundColor','white');
end



function edit6_Callback(hObject, eventdata, handles)
% hObject    handle to edit6 (see GCBO)
% eventdata  reserved - to be defined in a future version of MATLAB
% handles    structure with handles and user data (see GUIDATA)

% Hints: get(hObject,'String') returns contents of edit6 as text
%        str2double(get(hObject,'String')) returns contents of edit6 as
a double


% --- Executes during object creation, after setting all properties.
function edit6_CreateFcn(hObject, eventdata, handles)
% hObject    handle to edit6 (see GCBO)
% eventdata  reserved - to be defined in a future version of MATLAB
% handles    empty - handles not created until after all CreateFcns
called

% Hint: edit controls usually have a white background on Windows.
%       See ISPC and COMPUTER.
if ispc && isequal(get(hObject,'BackgroundColor'),
get(0,'defaultUicontrolBackgroundColor'))
    set(hObject,'BackgroundColor','white');
end



% --- Executes on button press in radiobutton1.
function radiobutton1_Callback(hObject, eventdata, handles)
% hObject    handle to radiobutton1 (see GCBO)
% eventdata  reserved - to be defined in a future version of MATLAB
% handles    structure with handles and user data (see GUIDATA)

% Hint: get(hObject,'Value') returns toggle state of radiobutton1


% --- Executes on button press in radiobutton2.
function radiobutton2_Callback(hObject, eventdata, handles)
% hObject    handle to radiobutton2 (see GCBO)
% eventdata  reserved - to be defined in a future version of MATLAB
% handles    structure with handles and user data (see GUIDATA)

% Hint: get(hObject,'Value') returns toggle state of radiobutton2


% --- Executes on button press in radiobutton3.
function radiobutton3_Callback(hObject, eventdata, handles)
% hObject    handle to radiobutton3 (see GCBO)
% eventdata  reserved - to be defined in a future version of MATLAB
% handles    structure with handles and user data (see GUIDATA)
```

```
% Hint: get(hObject,'Value') returns toggle state of radiobutton3


% --- Executes on button press in radiobutton4.
function radiobutton4_Callback(hObject, eventdata, handles)
% hObject    handle to radiobutton4 (see GCBO)
% eventdata  reserved - to be defined in a future version of MATLAB
% handles    structure with handles and user data (see GUIDATA)

% Hint: get(hObject,'Value') returns toggle state of radiobutton4


% --- Executes on button press in pushbutton1.
function pushbutton1_Callback(hObject, eventdata, handles)
    %Read the inputs
    water_pressue = str2num(get(handles.edit1, 'String'));
    width_of_incision = str2num(get(handles.edit2, 'String'));
    transverse_speed = str2num(get(handles.edit3, 'String'));
    E = str2num(get(handles.edit4, 'String'));
    stand_off_distance = str2num(get(handles.edit5, 'String'));
    taper_value = str2num(get(handles.edit6, 'String'));

    if(isempty(water_pressue) || isempty(width_of_incision) ||
isempty(transverse_speed) || isempty(E) || isempty(stand_off_distance)
|| isempty(taper_value))
        errordlg('Please enter values for all variables.');
    end

    if(water_pressue < 0 || width_of_incision < 0 || transverse_speed <
0 || E < 0 || stand_off_distance < 0 || taper_value < 0)
        errordlg('All values have to be non-negative.');
    end

    % Get Tube shape and adjust values
    Val_1 = get(handles.radiobutton1, 'Value');
    Val_2 = get(handles.radiobutton2, 'Value');
    Val_3 = get(handles.radiobutton3, 'Value');
    Val_4 = get(handles.radiobutton4, 'Value');

    if Val_1 %sharp-edged
        K_e=0.08;
        C_d=0.62;
    elseif Val_2 %round-edged
        K_e=0.1;
        C_d=0.98;
    elseif Val_3 %rounded-entrance
        K_e=0.15;
        C_d=0.54;
    else %square-edged
        K_e=0.50;
        C_d=0.61;
    end

    pressure=water_pressue*1000000;
    width=width_of_incision/1000;
```

```
    speed=transverse_speed/1000;
    E=E*1000000;
    distance=stand_off_distance/1000;

    %Density of water
    density=1000;

    % Orifice Diameter in m
    orifice_diameter=width/exp(taper_value*distance);
    % Orifice Diameter in mm
    Orifice_Diameter_mm=orifice_diameter*1000;


    % WJ Nozzle Velocity
    velocity_nozzle=sqrt(2*pressure/density);
    C_d
    K_e
    E
    width
    speed
    %Depth
    depth=
(pi*C_d*(orifice_diameter^2)*velocity_nozzle^3*density*K_e)/(8*width*sp
eed*E);
    Depth_of_cut=depth*1000;

    %Power

Power=sqrt(((pressure^3)*(C_d^2)*(3.14^2)*(orifice_diameter^4))/(8*dens
ity));

    %Generate Figures for results
    x_p = linspace(0, 2*pressure, 200);
    y_d_1 =
1000*(pi*C_d*2^1.5*x_p.^1.5*(orifice_diameter^2)*K_e)/(8*E*width*speed*
sqrt(density));

    x_diam = linspace(0, 2*orifice_diameter, 200);
    y_d_2 =
1000*(pi*C_d*2^1.5*pressure^1.5*(x_diam.^2)*K_e)/(8*E*width*speed*sqrt(
density));

    save('outputs.mat', 'Depth_of_cut', 'velocity_nozzle', 'Power',
'x_p', 'x_diam', 'y_d_1', 'y_d_2');
    h=open('results.fig');



% hObject    handle to pushbutton1 (see GCBO)
% eventdata  reserved - to be defined in a future version of MATLAB
% handles    structure with handles and user data (see GUIDATA)


% --- Executes during object creation, after setting all properties.
function figure1_CreateFcn(hObject, eventdata, handles)
% hObject    handle to figure1 (see GCBO)
```

```
% eventdata  reserved - to be defined in a future version of MATLAB
% handles    empty - handles not created until after all CreateFcns
called


% --- Executes on key press with focus on figure1 and none of its
controls.
function figure1_KeyPressFcn(hObject, eventdata, handles)
% hObject    handle to figure1 (see GCBO)
% eventdata  structure with the following fields (see MATLAB.UI.FIGURE)
%   Key: name of the key that was pressed, in lower case
%   Character: character interpretation of the key(s) that was pressed
%   Modifier: name(s) of the modifier key(s) (i.e., control, shift)
pressed
% handles    structure with handles and user data (see GUIDATA)
```

A.2 Minitab-Matlab Integration Code

```
% % % This function is used to import Minitab design table as input and
% it outputs the respective depth of cut values to be exported back to
% minitab % % %
%%

clc
clear all

%%% Minitab Input %%%
[file,path] = uigetfile({'*.xlsx; *.xls'});
data=xlsread([path file]);

% Pressure in MPa
pressure_input=data(:,1);
% Convert to Pa
pressure=pressure_input.*1000000;

% Width in mm
width_input=data(:,2);
% Convert to m
width=width_input./1000;

% Stand-off Distance in mm
speed_input=data(:,3);
% % Convert to m
 speed=speed_input./1000;


% Stand-off Distance in mm
distance_input=data(:,4);
% % Convert to m
 distance=distance_input./1000;



  % E user input
prompt='Please enter the Skin Specific Energy/ Elastic Modulus in MPa:
';
E_input=input(prompt);
% E_input=data(:,5);
% Convert to Pa
E=E_input.*1000000;

% Loss Coefficient
K_e=data(:,5);

% For short tube with rounded entrance

%Generate C_d column based on Loss_coeffs_column (column 5)
data(:,6) = zeros(length(data(:,5)),1);
for i = 1:length(data(:,5))
    switch(data(i,5))
```

```
        case 0.15
            data(i,6) = 0.54;
        case 0.08
            data(i,6) = 0.62;
        case 0.1
            data(i,6) = 0.98;
        case 0.5
            data(i,6) = 0.61;
        otherwise %default value
            data(i,6) = 0.54;
    end
end

% taper user input
 prompt='Please enter the taper value: ';
% % Unitless
taper=input(prompt);


% Given Data %%%
% Density of water
density=1000;


%%% Output%%%

% Orifice Diameter in m
orifice_diameter=width./exp(taper.*distance);
% Orifice Diameter in mm
Orifice_Diameter_mm=orifice_diameter.*1000;


velocity_nozzle=sqrt(2.*pressure./density);

%
depth=(C_d.*3.14.*(orifice_diameter.^2).*(velocity_nozzle.^3).*density.
*K_e)./(8.*width.*speed.*E);

depth=(data(:,6).*3.14.*(orifice_diameter.^2).*(velocity_nozzle.^3).*de
nsity.*K_e)./(8.*width.*speed.*E);

% depth=
((3.14*C_d*(orifice_diameter^2)*(pressure^(3/2))*K_e)/(4*E*width*speed)
)*sqrt(2/density);
% depth_of_cut=depth*1000

Depth_of_cut=depth.*1000;
data(:,6) = Depth_of_cut;

%Writing output to Excel sheet
col_header={'Pressure','Orifice Diamater','Traverse Speed','Stand-off
Distance', 'Loss Coefficient', 'Depth of Cut'};
xlswrite([path 'output.xls'],data,'Sheet1','A2');
xlswrite([path 'output.xls'],col_header,'Sheet1','A1');

disp('================ Excel Sheet generated ====================');
```

A.3 Calculating the Specific Energy of a Material

```
function varargout = energy_calc(varargin)
% depth_calc MATLAB code for depth_calc.fig
%      depth_calc, by itself, creates a new depth_calc or raises the
existing
%      singleton*.
%
%      H = depth_calc returns the handle to a new depth_calc or the
handle to
%      the existing singleton*.
%
%      depth_calc('CALLBACK',hObject,eventData,handles,...) calls the
local
%      function named CALLBACK in depth_calc.M with the given input
arguments.
%
%      depth_calc('Property','Value',...) creates a new depth_calc or
raises the
%      existing singleton*.  Starting from the left, property value
pairs are
%      applied to the GUI before depth_calc_OpeningFcn gets called.  An
%      unrecognized property name or invalid value makes property
application
%      stop.  All inputs are passed to depth_calc_OpeningFcn via
varargin.
%
%      *See GUI Options on GUIDE's Tools menu.  Choose "GUI allows only
one
%      instance to run (singleton)".
%
% See also: GUIDE, GUIDATA, GUIHANDLES

% Edit the above text to modify the response to help depth_calc

% Last Modified by GUIDE v2.5 08-Feb-2019 21:43:56

% Begin initialization code - DO NOT EDIT
gui_Singleton = 1;
gui_State = struct('gui_Name',       mfilename, ...
                   'gui_Singleton',  gui_Singleton, ...
                   'gui_OpeningFcn', @energy_calc_OpeningFcn, ...
                   'gui_OutputFcn',  @energy_calc_OutputFcn, ...
                   'gui_LayoutFcn',  [] , ...
                   'gui_Callback',   []);
if nargin && ischar(varargin{1})
    gui_State.gui_Callback = str2func(varargin{1});
end

if nargout
    [varargout{1:nargout}] = gui_mainfcn(gui_State, varargin{:});
else
    gui_mainfcn(gui_State, varargin{:});
end
% End initialization code - DO NOT EDIT
 %Global variables
```

```
Depth_of_cut = 0;
velocity_nozzle = 0;
Power = 0;

% --- Executes just before depth_calc is made visible.
function energy_calc_OpeningFcn(hObject, eventdata, handles, varargin)
% This function has no output args, see OutputFcn.
% hObject    handle to figure
% eventdata  reserved - to be defined in a future version of MATLAB
% handles    structure with handles and user data (see GUIDATA)
% varargin   command line arguments to depth_calc (see VARARGIN)

% Choose default command line output for depth_calc
handles.output = hObject;

% Update handles structure
guidata(hObject, handles);

% UIWAIT makes depth_calc wait for user response (see UIRESUME)
% uiwait(handles.figure1);


% --- Outputs from this function are returned to the command line.
function varargout = energy_calc_OutputFcn(hObject, eventdata, handles)
% varargout  cell array for returning output args (see VARARGOUT);
% hObject    handle to figure
% eventdata  reserved - to be defined in a future version of MATLAB
% handles    structure with handles and user data (see GUIDATA)

% Get default command line output from handles structure
varargout{1} = handles.output;



function edit1_Callback(hObject, eventdata, handles)
% hObject    handle to edit1 (see GCBO)
% eventdata  reserved - to be defined in a future version of MATLAB
% handles    structure with handles and user data (see GUIDATA)

% Hints: get(hObject,'String') returns contents of edit1 as text
%        str2double(get(hObject,'String')) returns contents of edit1 as
a double


% --- Executes during object creation, after setting all properties.
function edit1_CreateFcn(hObject, eventdata, handles)
% hObject    handle to edit1 (see GCBO)
% eventdata  reserved - to be defined in a future version of MATLAB
% handles    empty - handles not created until after all CreateFcns
called

% Hint: edit controls usually have a white background on Windows.
%       See ISPC and COMPUTER.
if ispc && isequal(get(hObject,'BackgroundColor'),
get(0,'defaultUicontrolBackgroundColor'))
```

```
    set(hObject,'BackgroundColor','white');
end



function edit2_Callback(hObject, eventdata, handles)
% hObject    handle to edit2 (see GCBO)
% eventdata  reserved - to be defined in a future version of MATLAB
% handles    structure with handles and user data (see GUIDATA)

% Hints: get(hObject,'String') returns contents of edit2 as text
%        str2double(get(hObject,'String')) returns contents of edit2 as
a double


% --- Executes during object creation, after setting all properties.
function edit2_CreateFcn(hObject, eventdata, handles)
% hObject    handle to edit2 (see GCBO)
% eventdata  reserved - to be defined in a future version of MATLAB
% handles    empty - handles not created until after all CreateFcns
called

% Hint: edit controls usually have a white background on Windows.
%       See ISPC and COMPUTER.
if ispc && isequal(get(hObject,'BackgroundColor'),
get(0,'defaultUicontrolBackgroundColor'))
    set(hObject,'BackgroundColor','white');
end



function edit3_Callback(hObject, eventdata, handles)
% hObject    handle to edit3 (see GCBO)
% eventdata  reserved - to be defined in a future version of MATLAB
% handles    structure with handles and user data (see GUIDATA)

% Hints: get(hObject,'String') returns contents of edit3 as text
%        str2double(get(hObject,'String')) returns contents of edit3 as
a double


% --- Executes during object creation, after setting all properties.
function edit3_CreateFcn(hObject, eventdata, handles)
% hObject    handle to edit3 (see GCBO)
% eventdata  reserved - to be defined in a future version of MATLAB
% handles    empty - handles not created until after all CreateFcns
called

% Hint: edit controls usually have a white background on Windows.
%       See ISPC and COMPUTER.
if ispc && isequal(get(hObject,'BackgroundColor'),
get(0,'defaultUicontrolBackgroundColor'))
    set(hObject,'BackgroundColor','white');
end
```

```
function edit4_Callback(hObject, eventdata, handles)
% hObject    handle to edit4 (see GCBO)
% eventdata  reserved - to be defined in a future version of MATLAB
% handles    structure with handles and user data (see GUIDATA)

% Hints: get(hObject,'String') returns contents of edit4 as text
%        str2double(get(hObject,'String')) returns contents of edit4 as
a double


% --- Executes during object creation, after setting all properties.
function edit4_CreateFcn(hObject, eventdata, handles)
% hObject    handle to edit4 (see GCBO)
% eventdata  reserved - to be defined in a future version of MATLAB
% handles    empty - handles not created until after all CreateFcns
called

% Hint: edit controls usually have a white background on Windows.
%       See ISPC and COMPUTER.
if ispc && isequal(get(hObject,'BackgroundColor'),
get(0,'defaultUicontrolBackgroundColor'))
    set(hObject,'BackgroundColor','white');
end



function edit5_Callback(hObject, eventdata, handles)
% hObject    handle to edit5 (see GCBO)
% eventdata  reserved - to be defined in a future version of MATLAB
% handles    structure with handles and user data (see GUIDATA)

% Hints: get(hObject,'String') returns contents of edit5 as text
%        str2double(get(hObject,'String')) returns contents of edit5 as
a double


% --- Executes during object creation, after setting all properties.
function edit5_CreateFcn(hObject, eventdata, handles)
% hObject    handle to edit5 (see GCBO)
% eventdata  reserved - to be defined in a future version of MATLAB
% handles    empty - handles not created until after all CreateFcns
called

% Hint: edit controls usually have a white background on Windows.
%       See ISPC and COMPUTER.
if ispc && isequal(get(hObject,'BackgroundColor'),
get(0,'defaultUicontrolBackgroundColor'))
    set(hObject,'BackgroundColor','white');
end



function edit6_Callback(hObject, eventdata, handles)
% hObject    handle to edit6 (see GCBO)
% eventdata  reserved - to be defined in a future version of MATLAB
```

```
% handles    structure with handles and user data (see GUIDATA)

% Hints: get(hObject,'String') returns contents of edit6 as text
%        str2double(get(hObject,'String')) returns contents of edit6 as
a double


% --- Executes during object creation, after setting all properties.
function edit6_CreateFcn(hObject, eventdata, handles)
% hObject    handle to edit6 (see GCBO)
% eventdata  reserved - to be defined in a future version of MATLAB
% handles    empty - handles not created until after all CreateFcns
called

% Hint: edit controls usually have a white background on Windows.
%       See ISPC and COMPUTER.
if ispc && isequal(get(hObject,'BackgroundColor'),
get(0,'defaultUicontrolBackgroundColor'))
    set(hObject,'BackgroundColor','white');
end


% --- Executes on button press in radiobutton1.
function radiobutton1_Callback(hObject, eventdata, handles)
% hObject    handle to radiobutton1 (see GCBO)
% eventdata  reserved - to be defined in a future version of MATLAB
% handles    structure with handles and user data (see GUIDATA)

% Hint: get(hObject,'Value') returns toggle state of radiobutton1


% --- Executes on button press in radiobutton2.
function radiobutton2_Callback(hObject, eventdata, handles)
% hObject    handle to radiobutton2 (see GCBO)
% eventdata  reserved - to be defined in a future version of MATLAB
% handles    structure with handles and user data (see GUIDATA)

% Hint: get(hObject,'Value') returns toggle state of radiobutton2


% --- Executes on button press in radiobutton3.
function radiobutton3_Callback(hObject, eventdata, handles)
% hObject    handle to radiobutton3 (see GCBO)
% eventdata  reserved - to be defined in a future version of MATLAB
% handles    structure with handles and user data (see GUIDATA)

% Hint: get(hObject,'Value') returns toggle state of radiobutton3


% --- Executes on button press in radiobutton4.
function radiobutton4_Callback(hObject, eventdata, handles)
% hObject    handle to radiobutton4 (see GCBO)
% eventdata  reserved - to be defined in a future version of MATLAB
% handles    structure with handles and user data (see GUIDATA)
```

```
% Hint: get(hObject,'Value') returns toggle state of radiobutton4


% --- Executes on button press in pushbutton1.
function pushbutton1_Callback(hObject, eventdata, handles)
    %Read the inputs
    water_pressue = str2num(get(handles.edit1, 'String'));
    width_of_incision = str2num(get(handles.edit2, 'String'));
    transverse_speed = str2num(get(handles.edit3, 'String'));
    depth_of_incision = str2num(get(handles.edit4, 'String'));
    stand_off_distance = str2num(get(handles.edit5, 'String'));
    taper_value = str2num(get(handles.edit6, 'String'));

    if(isempty(water_pressue) || isempty(width_of_incision) ||
isempty(transverse_speed) || isempty(depth_of_incision) ||
isempty(stand_off_distance) || isempty(taper_value))
        errordlg('Please enter values for all variables.');
    end

    if(water_pressue < 0 || width_of_incision < 0 || transverse_speed <
0 || depth_of_incision < 0 || stand_off_distance < 0 || taper_value <
0)
        errordlg('All values have to be non-negative.');
    end

    % Get Tube shape and adjust values
    Val_1 = get(handles.radiobutton1, 'Value');
    Val_2 = get(handles.radiobutton2, 'Value');
    Val_3 = get(handles.radiobutton3, 'Value');
    Val_4 = get(handles.radiobutton4, 'Value');

    if Val_1 %sharp-edged
        K_e=0.08;
        C_d=0.62;
    elseif Val_2 %round-edged
        K_e=0.1;
        C_d=0.98;
    elseif Val_3 %rounded-entrance
        K_e=0.15;
        C_d=0.54;
    else %square-edged
        K_e=0.50;
        C_d=0.61;
    end

    pressure=water_pressue*1000000;
    width=width_of_incision/1000;
    depth=depth_of_incision/1000;
    speed=transverse_speed/1000;
    distance=stand_off_distance/1000;

    %Density of water
    density=1000;

    % Orifice Diameter in m
    orifice_diameter=width/exp(taper_value*distance);
```

```
    % Orifice Diameter in mm
    Orifice_Diameter_mm=orifice_diameter*1000;


    % WJ Nozzle Velocity
    velocity_nozzle=sqrt(2*pressure/density);
    C_d
    K_e
    width
    speed
    %Energy

E=(C_d*pi*(orifice_diameter^2)*(velocity_nozzle^3)*density*K_e)/(8*widt
h*speed*depth);
    Energy=E/1000000;

    %Generate Figures for results
    x_p = linspace(0, 2*pressure, 200);
    y_d_1 =
(C_d*pi*(orifice_diameter^2)*(2^1.5*x_p.^1.5)*K_e)/(8*width*speed*depth
)/1000000/sqrt(density);

    x_depth = linspace(0, 2*depth, 200);
    y_d_2 =
(C_d*pi*(orifice_diameter^2)*(velocity_nozzle^3)*density*K_e)./(8*width
*speed*x_depth)/1000000;

    save('outputs.mat', 'Energy', 'velocity_nozzle', 'x_p', 'x_depth',
'y_d_1', 'y_d_2');
    h=open('results.fig');



% hObject    handle to pushbutton1 (see GCBO)
% eventdata  reserved - to be defined in a future version of MATLAB
% handles    structure with handles and user data (see GUIDATA)


% --- Executes during object creation, after setting all properties.
function figure1_CreateFcn(hObject, eventdata, handles)
% hObject    handle to figure1 (see GCBO)
% eventdata  reserved - to be defined in a future version of MATLAB
% handles    empty - handles not created until after all CreateFcns
called


% --- Executes on key press with focus on figure1 and none of its
controls.
function figure1_KeyPressFcn(hObject, eventdata, handles)
% hObject    handle to figure1 (see GCBO)
% eventdata  structure with the following fields (see MATLAB.UI.FIGURE)
%   Key: name of the key that was pressed, in lower case
%   Character: character interpretation of the key(s) that was pressed
%   Modifier: name(s) of the modifier key(s) (i.e., control, shift)
pressed
% handles    structure with handles and user data (see GUIDATA)
```

APPENDIX B

MINITAB DOE

B.1 Taguchi Design

Taguchi Design

Design Summary

Taguchi Array	L32(2^5)
Factors:	5
Runs:	32

Columns of L32(2^31) array: 1 2 4 8 16

Taguchi Analysis: 0.75 GPa, 1 GPa, 1.25 GPa versus ... e, Loss Coefficient

Linear Model Analysis: SN ratios versus Pressure, Orifice Diameter, Traverse Speed, Stand-off Distance, Loss Coefficient

Estimated Model Coefficients for SN ratios

Term	Coef	SE Coef	T	P
Constant	5.31347	0.000000	*	*
Pressure 10	-2.64137	0.000000	*	*
Orifice 0.2	-3.01030	0.000000	*	*
Traverse 12	1.51268	0.000000	*	*
Stand-of 5	0.01086	0.000000	*	*
Loss Coe 0.08	-2.13003	0.000000	*	*
Pressure*Orifice 10 0.2	0.00000	0.000000	*	*
Pressure*Traverse 10 12	-0.00000	0.000000	*	*
Pressure*Stand-of 10 5	0.00000	0.000000	*	*
Pressure*Loss Coe 10 0.08	0.00000	0.000000	*	*
Orifice *Traverse 0.2 12	-0.00000	0.000000	*	*
Orifice *Stand-of 0.2 5	0.00000	0.000000	*	*
Orifice *Loss Coe 0.2 0.08	-0.00000	0.000000	*	*
Traverse*Stand-of 12 5	0.00000	0.000000	*	*
Traverse*Loss Coe 12 0.08	-0.00000	0.000000	*	*

Stand-of*Loss Coe 5 0.08	-0.00000	0.000000	*	*	

Model Summary

S	R-Sq	R-Sq(adj)
0.0000	100.00%	100.00%

Analysis of Variance for SN ratios

Source	DF	Seq SS	Adj SS	Adj MS	F	P
Pressure	1	223.259	223.259	223.259	*	*
Orifice Diameter	1	289.981	289.981	289.981	*	*
Traverse Speed	1	73.222	73.222	73.222	*	*
Stand-off Distance	1	0.004	0.004	0.004	*	*
Loss Coefficient	1	145.185	145.185	145.185	*	*
Pressure*Orifice Diameter	1	0.000	0.000	0.000	*	*
Pressure*Traverse Speed	1	0.000	0.000	0.000	*	*
Pressure*Stand-off Distance	1	0.000	0.000	0.000	*	*
Pressure*Loss Coefficient	1	0.000	0.000	0.000	*	*
Orifice Diameter*Traverse Speed	1	0.000	0.000	0.000	*	*
Orifice Diameter*Stand-off Distance	1	0.000	0.000	0.000	*	*
Orifice Diameter*Loss Coefficient	1	0.000	0.000	0.000	*	*
Traverse Speed*Stand-off Distance	1	0.000	0.000	0.000	*	*
Traverse Speed*Loss Coefficient	1	0.000	0.000	0.000	*	*
Stand-off Distance*Loss Coefficient	1	0.000	0.000	0.000	*	*
Residual Error	16	0.000	0.000	0.000		
Total	31	731.651				

Linear Model Analysis: Means versus Pressure, Orifice Diameter, Traverse Speed, Stand-off Distance, Loss Coefficient

Estimated Model Coefficients for Means

Term	Coef	SE Coef	T	P
Constant	2.28171	0.01979	115.281	0.000
Pressure 10	-0.67324	0.01979	-34.015	0.000
Orifice 0.2	-0.76057	0.01979	-38.427	0.000
Traverse 12	0.39340	0.01979	19.876	0.000
Stand-of 5	0.00285	0.01979	0.144	0.887
Loss Coe 0.08	-0.54859	0.01979	-27.717	0.000
Pressure*Orifice 10 0.2	0.22441	0.01979	11.338	0.000

Pressure*Traverse 10 12	-0.11608	0.01979	-5.865	0.000
Pressure*Stand-of 10 5	-0.00084	0.01979	-0.043	0.967
Pressure*Loss Coe 10 0.08	0.16187	0.01979	8.178	0.000
Orifice *Traverse 0.2 12	-0.13113	0.01979	-6.625	0.000
Orifice *Stand-of 0.2 5	-0.00095	0.01979	-0.048	0.962
Orifice *Loss Coe 0.2 0.08	0.18286	0.01979	9.239	0.000
Traverse*Stand-of 12 5	0.00049	0.01979	0.025	0.980
Traverse*Loss Coe 12 0.08	-0.09458	0.01979	-4.779	0.000
Stand-of*Loss Coe 5 0.08	-0.00069	0.01979	-0.035	0.973

Model Summary

S	R-Sq	R-Sq(adj)
0.1120	99.62%	99.26%

Analysis of Variance for Means

Source	DF	Seq SS	Adj SS	Adj MS	F	P
Pressure	1	14.5041	14.5041	14.5041	1157.01	0.000
Orifice Diameter	1	18.5110	18.5110	18.5110	1476.64	0.000
Traverse Speed	1	4.9524	4.9524	4.9524	395.06	0.000
Stand-off Distance	1	0.0003	0.0003	0.0003	0.02	0.887
Loss Coefficient	1	9.6304	9.6304	9.6304	768.23	0.000
Pressure*Orifice Diameter	1	1.6116	1.6116	1.6116	128.56	0.000
Pressure*Traverse Speed	1	0.4312	0.4312	0.4312	34.39	0.000
Pressure*Stand-off Distance	1	0.0000	0.0000	0.0000	0.00	0.967
Pressure*Loss Coefficient	1	0.8384	0.8384	0.8384	66.88	0.000
Orifice Diameter*Traverse Speed	1	0.5503	0.5503	0.5503	43.90	0.000
Orifice Diameter*Stand-off Distance	1	0.0000	0.0000	0.0000	0.00	0.962
Orifice Diameter*Loss Coefficient	1	1.0700	1.0700	1.0700	85.36	0.000
Traverse Speed*Stand-off Distance	1	0.0000	0.0000	0.0000	0.00	0.980
Traverse Speed*Loss Coefficient	1	0.2863	0.2863	0.2863	22.84	0.000
Stand-off Distance*Loss Coefficient	1	0.0000	0.0000	0.0000	0.00	0.973
Residual Error	16	0.2006	0.2006	0.0125		
Total	31	52.5866				

Unusual Observations for Means

Observation	Means	Fit	SE Fit	Residual	St Resid	
26	5.737	5.574	0.079	0.163	2.06	R

28	5.723	5.563	0.079	0.160	2.02	R

R denotes an observation with a large standardized residual.

Linear Model Analysis: StDevs versus Pressure, Orifice Diameter, Traverse Speed, Stand-off Distance, Loss Coefficient

Estimated Model Coefficients for StDevs

Term	Coef	SE Coef	T	P
Constant	0.588603	0.005106	115.281	0.000
Pressure 10	-0.173673	0.005106	-34.015	0.000
Orifice 0.2	-0.196201	0.005106	-38.427	0.000
Traverse 12	0.101483	0.005106	19.876	0.000
Stand-of 5	0.000736	0.005106	0.144	0.887
Loss Coe 0.08	-0.141517	0.005106	-27.717	0.000
Pressure*Orifice 10 0.2	0.057891	0.005106	11.338	0.000
Pressure*Traverse 10 12	-0.029944	0.005106	-5.865	0.000
Pressure*Stand-of 10 5	-0.000217	0.005106	-0.043	0.967
Pressure*Loss Coe 10 0.08	0.041756	0.005106	8.178	0.000
Orifice *Traverse 0.2 12	-0.033828	0.005106	-6.625	0.000
Orifice *Stand-of 0.2 5	-0.000245	0.005106	-0.048	0.962
Orifice *Loss Coe 0.2 0.08	0.047172	0.005106	9.239	0.000
Traverse*Stand-of 12 5	0.000127	0.005106	0.025	0.980
Traverse*Loss Coe 12 0.08	-0.024399	0.005106	-4.779	0.000
Stand-of*Loss Coe 5 0.08	-0.000177	0.005106	-0.035	0.973

Model Summary

S	R-Sq	R-Sq(adj)
0.0289	99.62%	99.26%

Analysis of Variance for StDevs

Source	DF	Seq SS	Adj SS	Adj MS	F	P
Pressure	1	0.96519	0.96519	0.96519	1157.01	0.000
Orifice Diameter	1	1.23183	1.23183	1.23183	1476.64	0.000
Traverse Speed	1	0.32956	0.32956	0.32956	395.06	0.000
Stand-off Distance	1	0.00002	0.00002	0.00002	0.02	0.887
Loss Coefficient	1	0.64087	0.64087	0.64087	768.23	0.000
Pressure*Orifice Diameter	1	0.10724	0.10724	0.10724	128.56	0.000
Pressure*Traverse Speed	1	0.02869	0.02869	0.02869	34.39	0.000

Pressure*Stand-off Distance	1	0.00000	0.00000	0.00000	0.00	0.967
Pressure*Loss Coefficient	1	0.05579	0.05579	0.05579	66.88	0.000
Orifice Diameter*Traverse Speed	1	0.03662	0.03662	0.03662	43.90	0.000
Orifice Diameter*Stand-off Distance	1	0.00000	0.00000	0.00000	0.00	0.962
Orifice Diameter*Loss Coefficient	1	0.07121	0.07121	0.07121	85.36	0.000
Traverse Speed*Stand-off Distance	1	0.00000	0.00000	0.00000	0.00	0.980
Traverse Speed*Loss Coefficient	1	0.01905	0.01905	0.01905	22.84	0.000
Stand-off Distance*Loss Coefficient	1	0.00000	0.00000	0.00000	0.00	0.973
Residual Error	16	0.01335	0.01335	0.00083		
Total	31	3.49942				

Unusual Observations for StDevs

Observation	StDevs	Fit	SE Fit	Residual	St Resid	
26	1.480	1.438	0.020	0.042	2.06	R
28	1.476	1.435	0.020	0.041	2.02	R

Response Table for Signal to Noise Ratios

Larger is better

Level	Pressure	Orifice Diameter	Traverse Speed	Stand-off Distance	Loss Coefficient
1	2.672	2.303	6.826	5.324	3.183
2	7.955	8.324	3.801	5.303	7.444
Delta	5.283	6.021	3.025	0.022	4.260
Rank	2	1	4	5	3

Response Table for Means

Level	Pressure	Orifice Diameter	Traverse Speed	Stand-off Distance	Loss Coefficient
1	1.608	1.521	2.675	2.285	1.733
2	2.955	3.042	1.888	2.279	2.830
Delta	1.346	1.521	0.787	0.006	1.097
Rank	2	1	4	5	3

Response Table for Standard Deviations

Level	Pressure	Orifice Diameter	Traverse Speed	Stand-off Distance	Loss Coefficient
1	0.4149	0.3924	0.6901	0.5893	0.4471
2	0.7623	0.7848	0.4871	0.5879	0.7301
Delta	0.3473	0.3924	0.2030	0.0015	0.2830

Rank	2	1	4	5	3

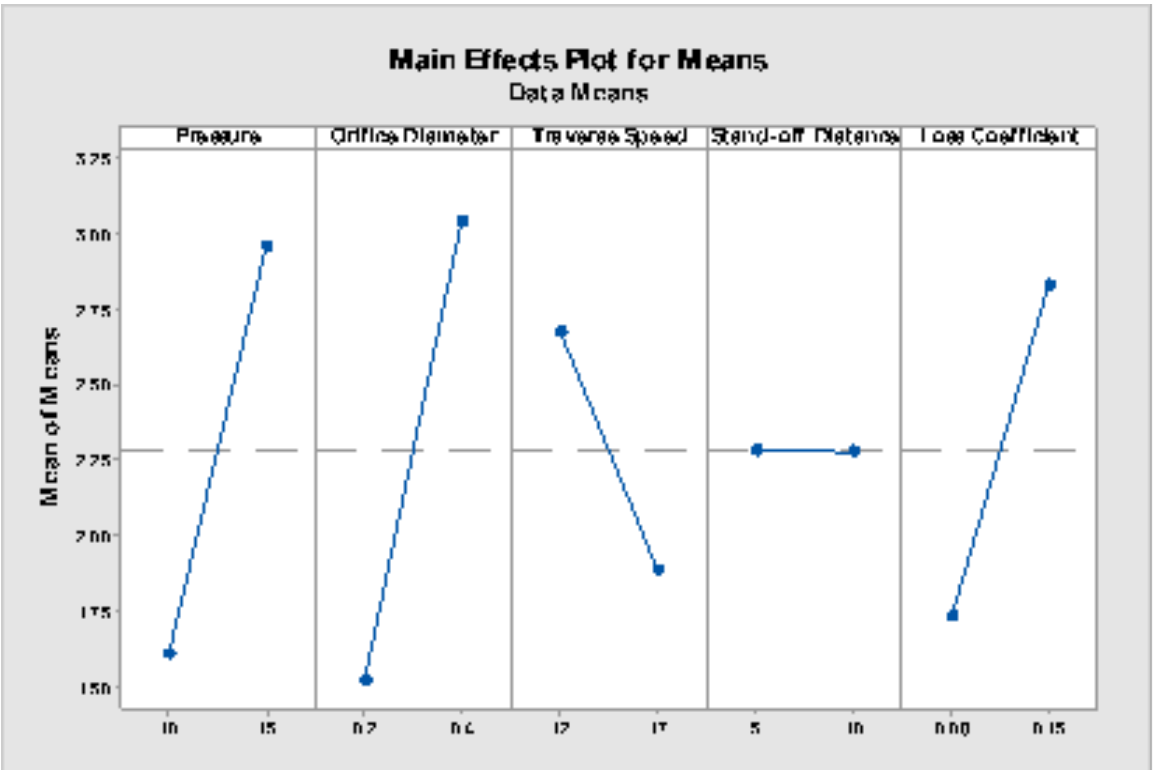
Main Effects Plot for Means
Data Means
Pressure
Orifice Diameter
Traverse Speed
Stand-off Distance
Loss Coefficient
Mean of Means
325
300
275
250
225
200
175
150
10
15
0.2
0.4
12
17
5
10
0.00
0.15

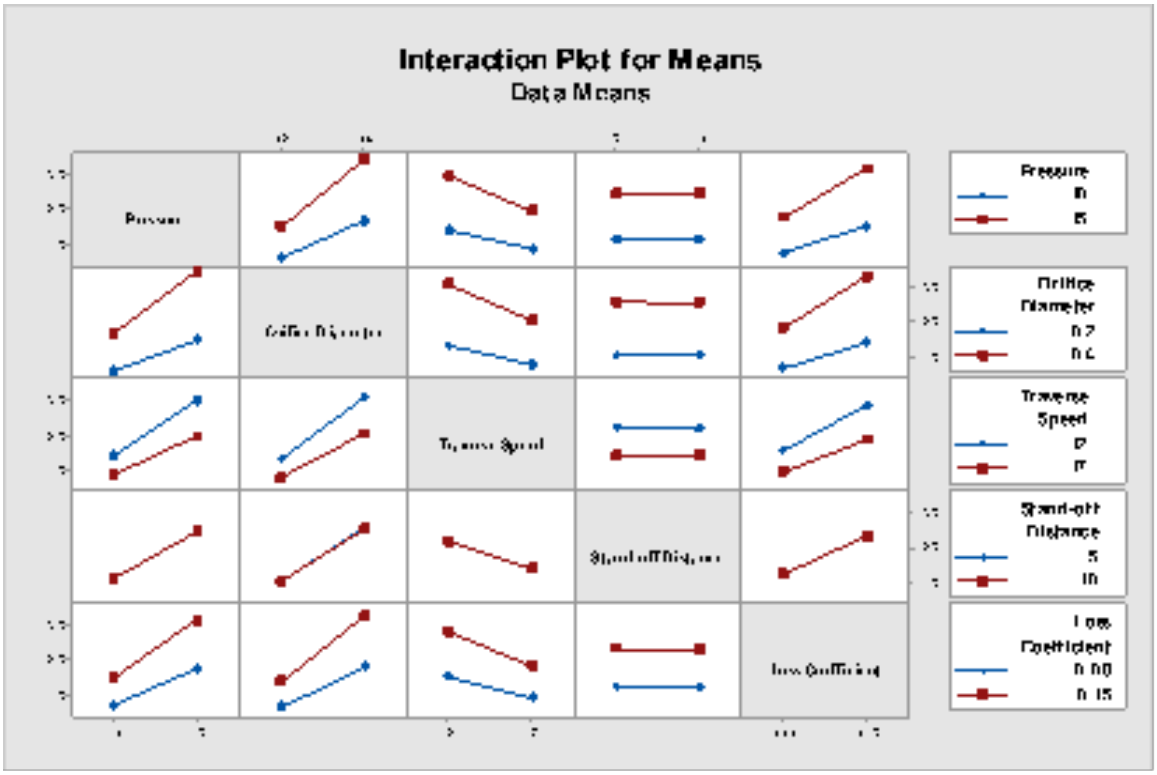
Interaction Plot for Means
Data Means
Pressure
10
15
Orifice Diameter
0.2
0.4
Traverse Speed
12
17
Stand-off Distance
5
10
Loss Coefficient
0.00
0.15

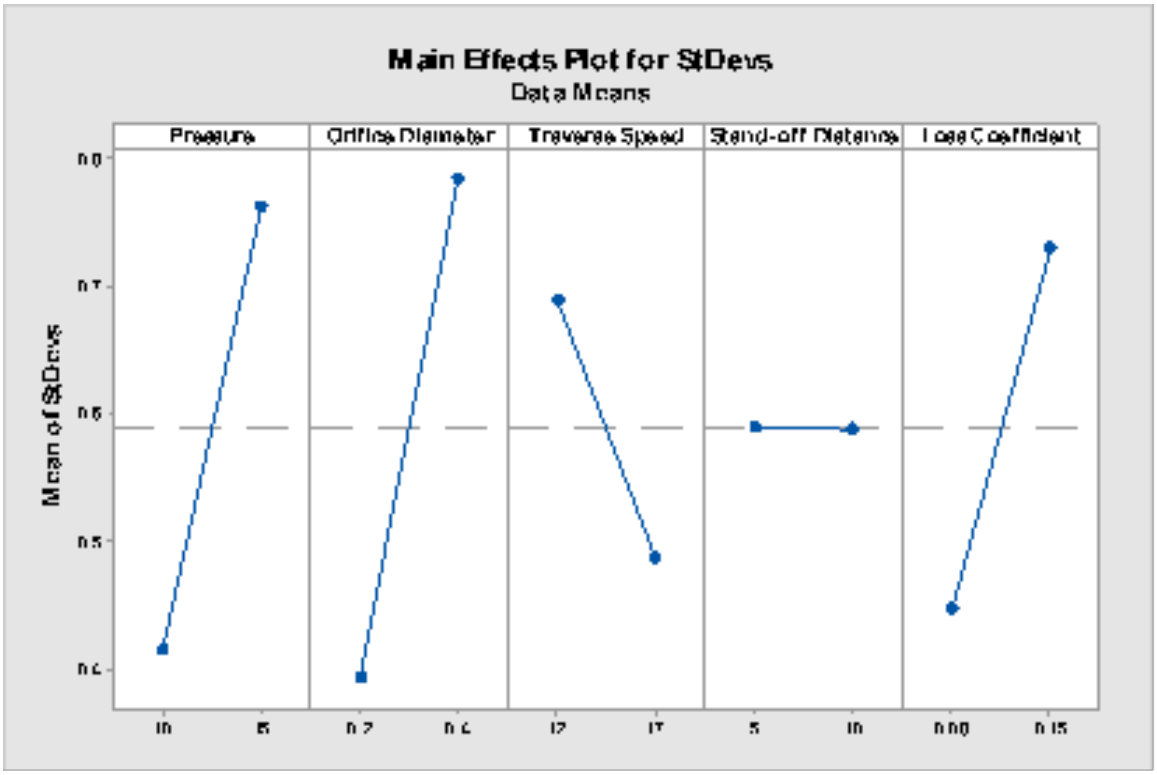
Main Effects Plot for StDevs
Data Means
Pressure
Orifice Diameter
Traverse Speed
Stand-off Distance
Loss Coefficient
Mean of StDevs

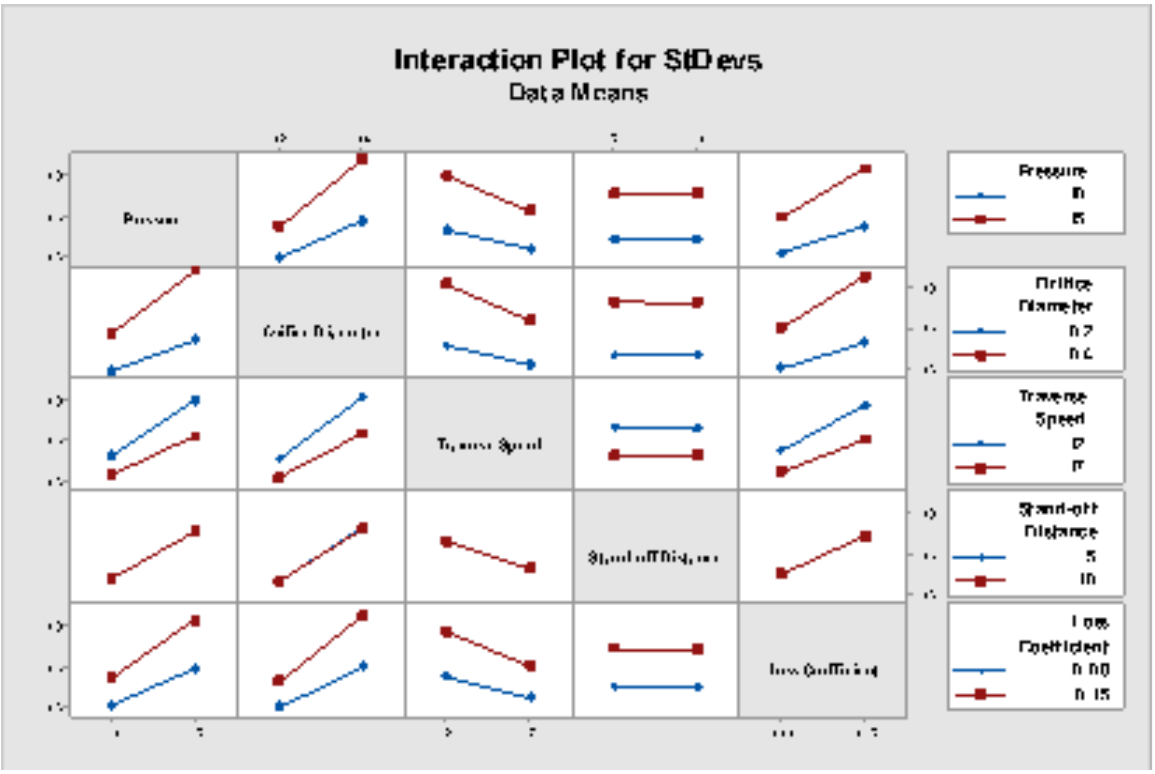
Interaction Plot for StDevs
Data Means
Pressure
Orifice Diameter
Traverse Speed
Stand-off Distance
Loss Coefficient

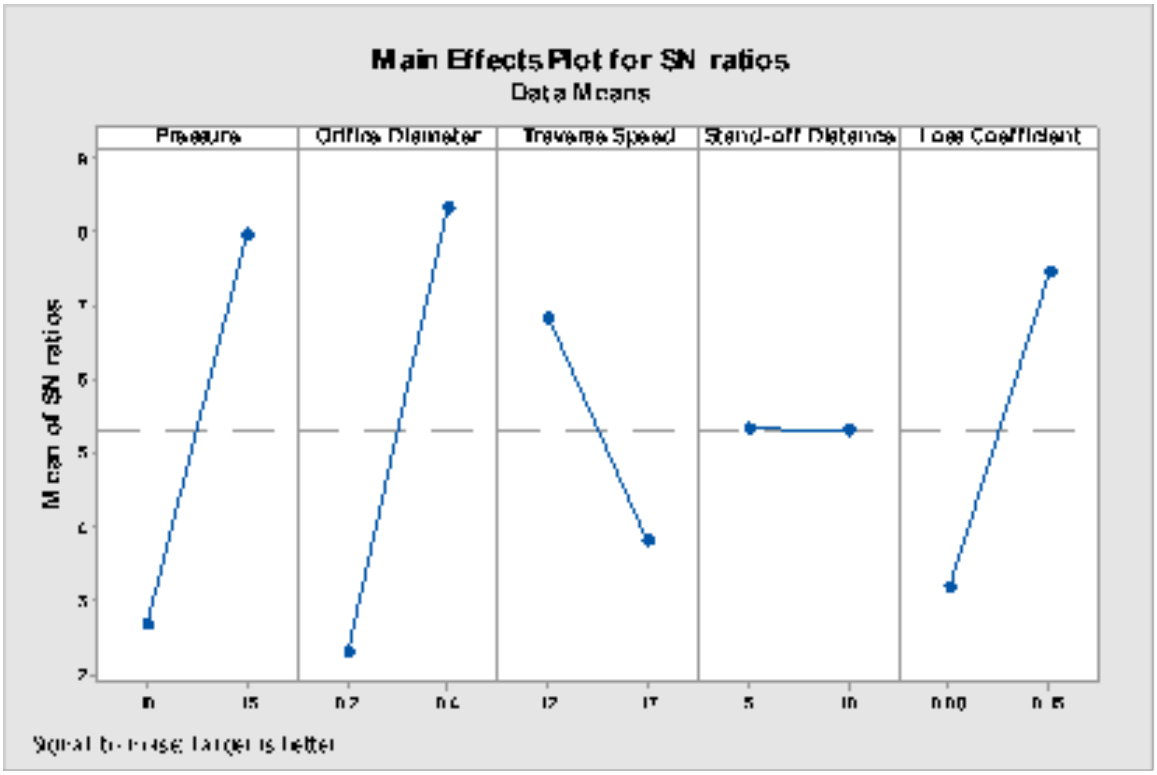
Main Effects Plot for SN ratios
Data Means
Pressure
Orifice Diameter
Traverse Speed
Stand-off Distance
Loss Coefficient
Mean of SN ratios
Signal-to-noise: Larger is better

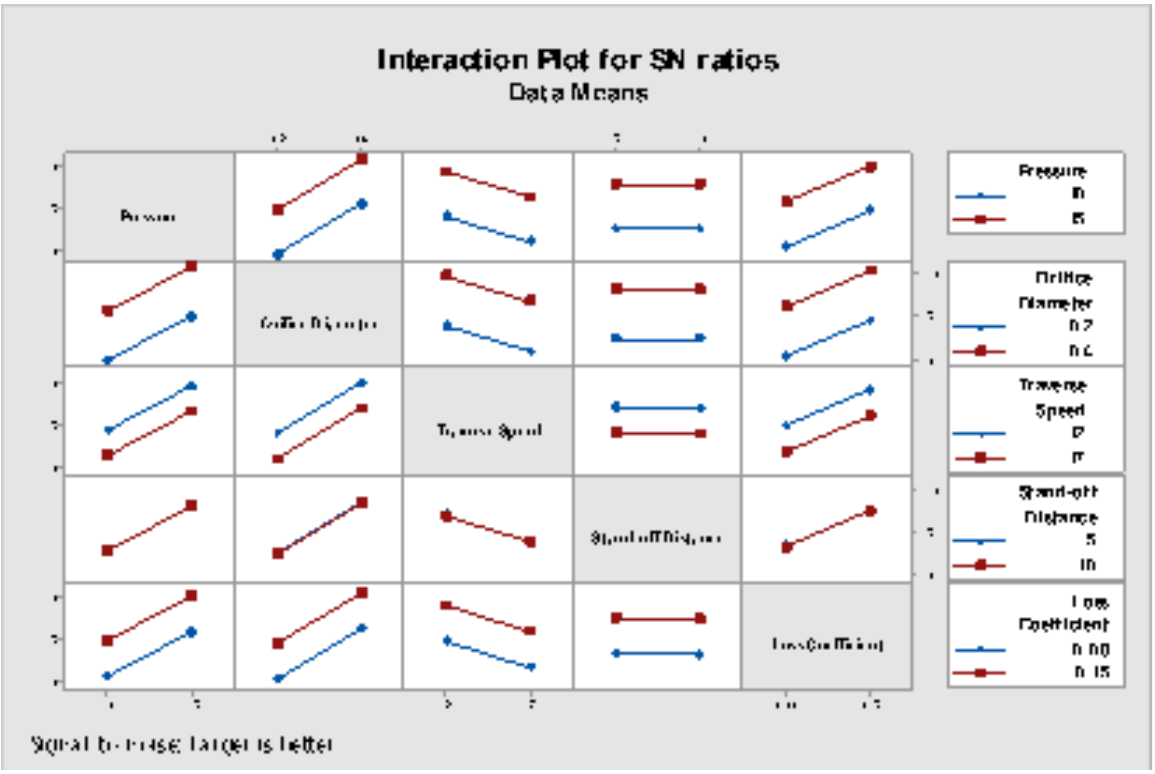
Interaction Plot for SN ratios
Data Means
Pressure
Orifice Diameter
Traverse Speed
Stand-off Distance
Loss Coefficient
Signal-to-noise: Larger is better

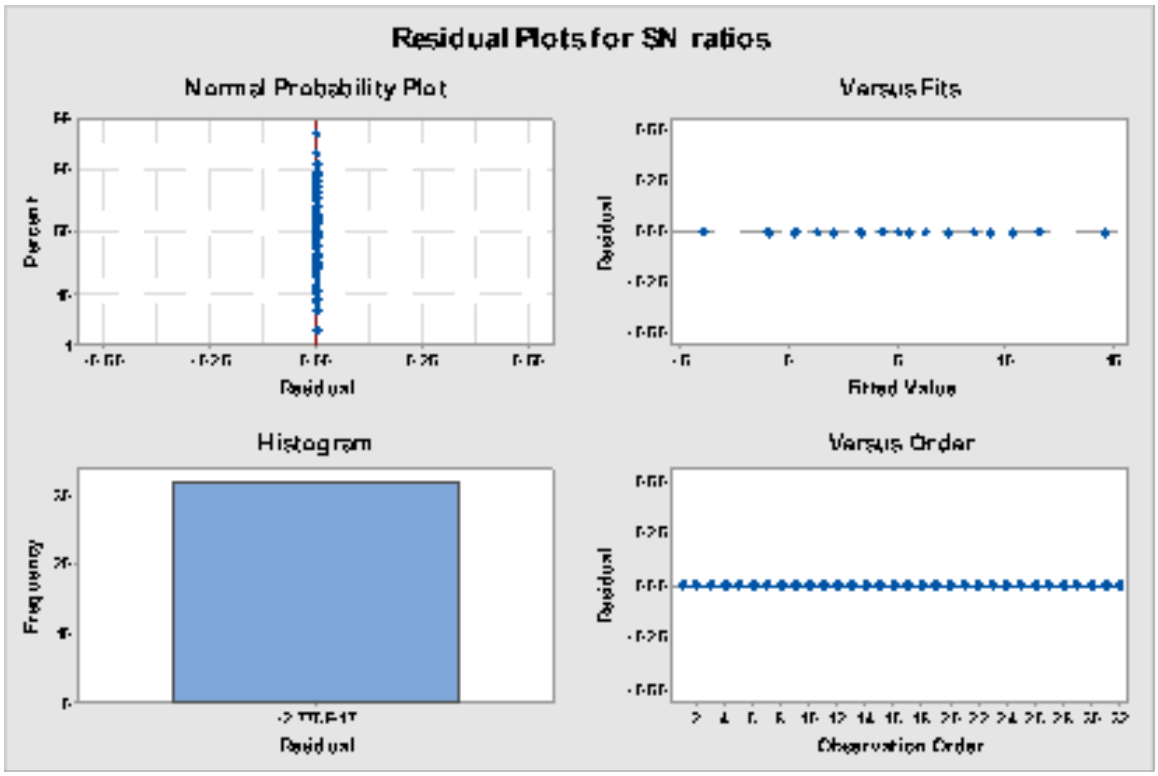
Residual Plots for SN ratios
Normal Probability Plot
Versus Fits
Histogram
Versus Order
Percent
Residual
Fitted Value
Frequency
Observation Order

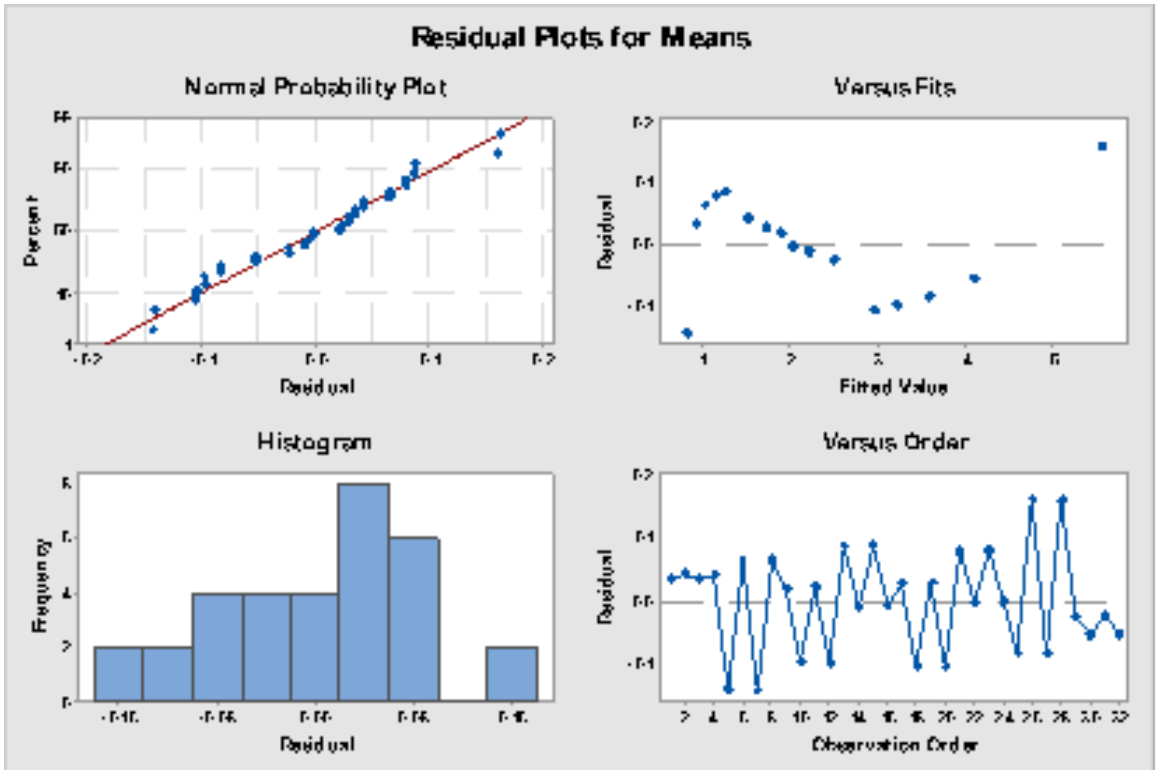
Residual Plots for Means
Normal Probability Plot
Versus Fits
Histogram
Versus Order
Percent
Residual
Fitted Value
Frequency
Observation Order

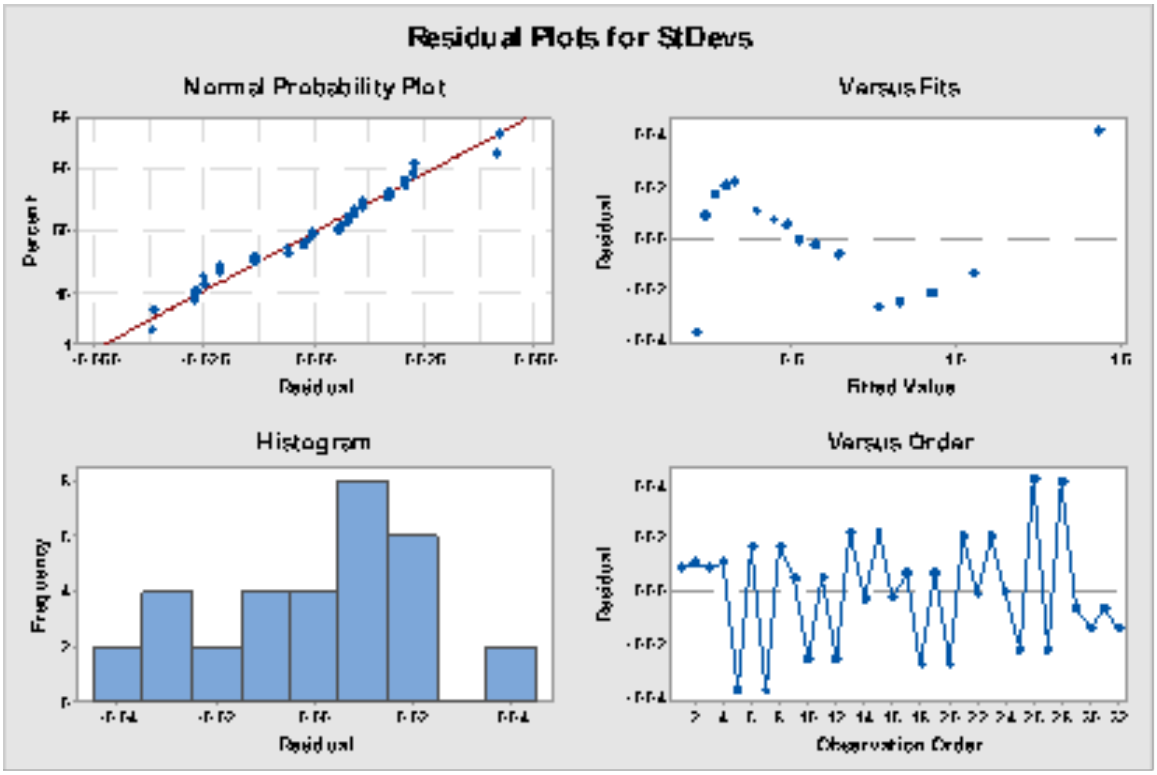

Taguchi Analysis: 0.75 GPa, 1 GPa, 1.25 GPa versus ... e, Loss Coefficient

Predicted values

Prediction

S/N Ratio	Mean	StDev	Ln(StDev)
-0.9556	0.92006	0.23734	-1.40105
3.3045	1.51695	0.39132	-0.91059
-0.9556	0.92006	0.23734	-1.40105
3.3045	1.51695	0.39132	-0.91059
-3.9809	0.81685	0.21072	-1.74935
0.2792	1.03540	0.26710	-1.25890
-3.9809	0.81685	0.21072	-1.74935
0.2792	1.03540	0.26710	-1.25890
5.0650	1.88892	0.48727	-0.70790
9.3251	3.21726	0.82994	-0.21744
5.0650	1.88892	0.48727	-0.70790
9.3251	3.21726	0.82994	-0.21744

2.0397	1.26117	0.32534	-1.05621
6.2998	2.21118	0.57041	-0.56575
2.0397	1.26117	0.32534	-1.05621
6.2998	2.21118	0.57041	-0.56575
4.3272	1.72613	0.44528	-0.79285
8.5872	2.97049	0.76628	-0.30239
4.3272	1.72613	0.44528	-0.79285
8.5872	2.97049	0.76628	-0.30239
1.3018	1.15862	0.29888	-1.14116
5.5619	2.02464	0.52229	-0.65070
1.3018	1.15862	0.29888	-1.14116
5.5619	2.02464	0.52229	-0.65070
10.3478	3.59264	0.92678	-0.09970
14.6078	5.56845	1.43647	0.39076
10.3478	3.59264	0.92678	-0.09970
14.6078	5.56845	1.43647	0.39076
7.3224	2.50060	0.64507	-0.44801
11.5825	4.09807	1.05716	0.04245
7.3224	2.50060	0.64507	-0.44801
11.5825	4.09807	1.05716	0.04245

Settings

Pressure	Orifice Diameter	Traverse Speed	Loss Coefficient
10	0.2	12	0.08
10	0.2	12	0.15
10	0.2	12	0.08
10	0.2	12	0.15
10	0.2	17	0.08
10	0.2	17	0.15
10	0.2	17	0.08
10	0.2	17	0.15
10	0.4	12	0.08
10	0.4	12	0.15
10	0.4	12	0.08

10	0.4	12	0.15
10	0.4	17	0.08
10	0.4	17	0.15
10	0.4	17	0.08
10	0.4	17	0.15
15	0.2	12	0.08
15	0.2	12	0.15
15	0.2	12	0.08
15	0.2	12	0.15
15	0.2	17	0.08
15	0.2	17	0.15
15	0.2	17	0.08
15	0.2	17	0.15
15	0.4	12	0.08
15	0.4	12	0.15
15	0.4	12	0.08
15	0.4	12	0.15
15	0.4	17	0.08
15	0.4	17	0.15
15	0.4	17	0.08
15	0.4	17	0.15

Full Factorial Design

Design Summary

Factors:	5	Base Design:	5, 32
Runs:	96	Replicates:	3
Blocks:	1	Center pts (total):	0

All terms are free from aliasing.

Design Table

Run	Blk	A	B	C	D	E
1	1	-	-	-	-	-
2	1	+	-	-	-	-
3	1	-	+	-	-	-
4	1	+	+	-	-	-
5	1	-	-	+	-	-
6	1	+	-	+	-	-
7	1	-	+	+	-	-
8	1	+	+	+	-	-
9	1	-	-	-	+	-
10	1	+	-	-	+	-
11	1	-	+	-	+	-
12	1	+	+	-	+	-
13	1	-	-	+	+	-
14	1	+	-	+	+	-
15	1	-	+	+	+	-
16	1	+	+	+	+	-
17	1	-	-	-	-	+
18	1	+	-	-	-	+
19	1	-	+	-	-	+
20	1	+	+	-	-	+
21	1	-	-	+	-	+
22	1	+	-	+	-	+
23	1	-	+	+	-	+
24	1	+	+	+	-	+

25	1	-	-	-	+	+
26	1	+	-	-	+	+
27	1	-	+	-	+	+
28	1	+	+	-	+	+
29	1	-	-	+	+	+
30	1	+	-	+	+	+
31	1	-	+	+	+	+
32	1	+	+	+	+	+
33	1	-	-	-	-	-
34	1	+	-	-	-	-
35	1	-	+	-	-	-
36	1	+	+	-	-	-
37	1	-	-	+	-	-
38	1	+	-	+	-	-
39	1	-	+	+	-	-
40	1	+	+	+	-	-
41	1	-	-	-	+	-
42	1	+	-	-	+	-
43	1	-	+	-	+	-
44	1	+	+	-	+	-
45	1	-	-	+	+	-
46	1	+	-	+	+	-
47	1	-	+	+	+	-
48	1	+	+	+	+	-
49	1	-	-	-	-	+
50	1	+	-	-	-	+
51	1	-	+	-	-	+
52	1	+	+	-	-	+
53	1	-	-	+	-	+
54	1	+	-	+	-	+
55	1	-	+	+	-	+
56	1	+	+	+	-	+
57	1	-	-	-	+	+

58	1	+	-	-	+	+
59	1	-	+	-	+	+
60	1	+	+	-	+	+
61	1	-	-	+	+	+
62	1	+	-	+	+	+
63	1	-	+	+	+	+
64	1	+	+	+	+	+
65	1	-	-	-	-	-
66	1	+	-	-	-	-
67	1	-	+	-	-	-
68	1	+	+	-	-	-
69	1	-	-	+	-	-
70	1	+	-	+	-	-
71	1	-	+	+	-	-
72	1	+	+	+	-	-
73	1	-	-	-	+	-
74	1	+	-	-	+	-
75	1	-	+	-	+	-
76	1	+	+	-	+	-
77	1	-	-	+	+	-
78	1	+	-	+	+	-
79	1	-	+	+	+	-
80	1	+	+	+	+	-
81	1	-	-	-	-	+
82	1	+	-	-	-	+
83	1	-	+	-	-	+
84	1	+	+	-	-	+
85	1	-	-	+	-	+
86	1	+	-	+	-	+
87	1	-	+	+	-	+
88	1	+	+	+	-	+
89	1	-	-	-	+	+
90	1	+	-	-	+	+

91	1	-	+	-	+	+
92	1	+	+	-	+	+
93	1	-	-	+	+	+
94	1	+	-	+	+	+
95	1	-	+	+	+	+
96	1	+	+	+	+	+

Factorial Regression: Depth of Cut versus Elastic ... ce, Loss Coefficient

Analysis of Variance

Source	DF	Adj SS
Model	32	179.480
Covariates	1	21.720
Elastic Modulus	1	21.720
Linear	5	142.795
Pressure	1	43.512
Orifice Diameter	1	55.533
Traverse Speed	1	14.857
Stand-off Distance	1	0.001
Loss Coefficient	1	28.891
2-Way Interactions	10	14.363
Pressure*Orifice Diameter	1	4.835
Pressure*Traverse Speed	1	1.293
Pressure*Stand-off Distance	1	0.000
Pressure*Loss Coefficient	1	2.515
Orifice Diameter*Traverse Speed	1	1.651
Orifice Diameter*Stand-off Distance	1	0.000
Orifice Diameter*Loss Coefficient	1	3.210
Traverse Speed*Stand-off Distance	1	0.000
Traverse Speed*Loss Coefficient	1	0.859
Stand-off Distance*Loss Coefficient	1	0.000
3-Way Interactions	10	0.593
Pressure*Orifice Diameter*Traverse Speed	1	0.144

Pressure*Orifice Diameter*Stand-off Distance	1	0.000
Pressure*Orifice Diameter*Loss Coefficient	1	0.279
Pressure*Traverse Speed*Stand-off Distance	1	0.000
Pressure*Traverse Speed*Loss Coefficient	1	0.075
Pressure*Stand-off Distance*Loss Coefficient	1	0.000
Orifice Diameter*Traverse Speed*Stand-off Distance	1	0.000
Orifice Diameter*Traverse Speed*Loss Coefficient	1	0.095
Orifice Diameter*Stand-off Distance*Loss Coefficient	1	0.000
Traverse Speed*Stand-off Distance*Loss Coefficient	1	0.000
4-Way Interactions	5	0.008
Pressure*Orifice Diameter*Traverse Speed*Stand-off Distance	1	0.000
Pressure*Orifice Diameter*Traverse Speed*Loss Coefficient	1	0.008
Pressure*Orifice Diameter*Stand-off Distance*Loss Coefficient	1	0.000
Pressure*Traverse Speed*Stand-off Distance*Loss Coefficient	1	0.000
Orifice Diameter*Traverse Speed*Stand-off Distance*Loss Coefficient	1	0.000
5-Way Interactions	1	0.000
Pressure*Orifice Diameter*Traverse Speed*Stand-off Distance*Loss Coefficient	1	0.000
Error	63	7.451
Total	95	186.932

Source	Adj MS
Model	5.6088
Covariates	21.7205
Elastic Modulus	21.7205
Linear	28.5589
Pressure	43.5123
Orifice Diameter	55.5330
Traverse Speed	14.8572
Stand-off Distance	0.0008
Loss Coefficient	28.8913
2-Way Interactions	1.4363
Pressure*Orifice Diameter	4.8347
Pressure*Traverse Speed	1.2935
Pressure*Stand-off Distance	0.0001

Pressure*Loss Coefficient	2.5153
Orifice Diameter*Traverse Speed	1.6508
Orifice Diameter*Stand-off Distance	0.0001
Orifice Diameter*Loss Coefficient	3.2101
Traverse Speed*Stand-off Distance	0.0000
Traverse Speed*Loss Coefficient	0.8588
Stand-off Distance*Loss Coefficient	0.0000
3-Way Interactions	0.0593
Pressure*Orifice Diameter*Traverse Speed	0.1437
Pressure*Orifice Diameter*Stand-off Distance	0.0000
Pressure*Orifice Diameter*Loss Coefficient	0.2795
Pressure*Traverse Speed*Stand-off Distance	0.0000
Pressure*Traverse Speed*Loss Coefficient	0.0748
Pressure*Stand-off Distance*Loss Coefficient	0.0000
Orifice Diameter*Traverse Speed*Stand-off Distance	0.0000
Orifice Diameter*Traverse Speed*Loss Coefficient	0.0954
Orifice Diameter*Stand-off Distance*Loss Coefficient	0.0000
Traverse Speed*Stand-off Distance*Loss Coefficient	0.0000
4-Way Interactions	0.0017
Pressure*Orifice Diameter*Traverse Speed*Stand-off Distance	0.0000
Pressure*Orifice Diameter*Traverse Speed*Loss Coefficient	0.0083
Pressure*Orifice Diameter*Stand-off Distance*Loss Coefficient	0.0000
Pressure*Traverse Speed*Stand-off Distance*Loss Coefficient	0.0000
Orifice Diameter*Traverse Speed*Stand-off Distance*Loss Coefficient	0.0000
5-Way Interactions	0.0000
Pressure*Orifice Diameter*Traverse Speed*Stand-off Distance*Loss Coefficient	0.0000
Error	0.1183
Total	

Source	F-Value
Model	47.42
Covariates	183.64
Elastic Modulus	183.64
Linear	241.46

Pressure	367.89
Orifice Diameter	469.52
Traverse Speed	125.62
Stand-off Distance	0.01
Loss Coefficient	244.27
2-Way Interactions	12.14
Pressure*Orifice Diameter	40.88
Pressure*Traverse Speed	10.94
Pressure*Stand-off Distance	0.00
Pressure*Loss Coefficient	21.27
Orifice Diameter*Traverse Speed	13.96
Orifice Diameter*Stand-off Distance	0.00
Orifice Diameter*Loss Coefficient	27.14
Traverse Speed*Stand-off Distance	0.00
Traverse Speed*Loss Coefficient	7.26
Stand-off Distance*Loss Coefficient	0.00
3-Way Interactions	0.50
Pressure*Orifice Diameter*Traverse Speed	1.22
Pressure*Orifice Diameter*Stand-off Distance	0.00
Pressure*Orifice Diameter*Loss Coefficient	2.36
Pressure*Traverse Speed*Stand-off Distance	0.00
Pressure*Traverse Speed*Loss Coefficient	0.63
Pressure*Stand-off Distance*Loss Coefficient	0.00
Orifice Diameter*Traverse Speed*Stand-off Distance	0.00
Orifice Diameter*Traverse Speed*Loss Coefficient	0.81
Orifice Diameter*Stand-off Distance*Loss Coefficient	0.00
Traverse Speed*Stand-off Distance*Loss Coefficient	0.00
4-Way Interactions	0.01
Pressure*Orifice Diameter*Traverse Speed*Stand-off Distance	0.00
Pressure*Orifice Diameter*Traverse Speed*Loss Coefficient	0.07
Pressure*Orifice Diameter*Stand-off Distance*Loss Coefficient	0.00
Pressure*Traverse Speed*Stand-off Distance*Loss Coefficient	0.00
Orifice Diameter*Traverse Speed*Stand-off Distance*Loss Coefficient	0.00

5-Way Interactions	0.00
Pressure*Orifice Diameter*Traverse Speed*Stand-off Distance*Loss Coefficient	0.00
Error	
Total	

Source	P-Value
Model	0.000
Covariates	0.000
Elastic Modulus	0.000
Linear	0.000
Pressure	0.000
Orifice Diameter	0.000
Traverse Speed	0.000
Stand-off Distance	0.935
Loss Coefficient	0.000
2-Way Interactions	0.000
Pressure*Orifice Diameter	0.000
Pressure*Traverse Speed	0.002
Pressure*Stand-off Distance	0.981
Pressure*Loss Coefficient	0.000
Orifice Diameter*Traverse Speed	0.000
Orifice Diameter*Stand-off Distance	0.978
Orifice Diameter*Loss Coefficient	0.000
Traverse Speed*Stand-off Distance	0.989
Traverse Speed*Loss Coefficient	0.009
Stand-off Distance*Loss Coefficient	0.984
3-Way Interactions	0.883
Pressure*Orifice Diameter*Traverse Speed	0.275
Pressure*Orifice Diameter*Stand-off Distance	0.994
Pressure*Orifice Diameter*Loss Coefficient	0.129
Pressure*Traverse Speed*Stand-off Distance	0.997
Pressure*Traverse Speed*Loss Coefficient	0.430
Pressure*Stand-off Distance*Loss Coefficient	0.995
Orifice Diameter*Traverse Speed*Stand-off Distance	0.996

Orifice Diameter*Traverse Speed*Loss Coefficient	0.372
Orifice Diameter*Stand-off Distance*Loss Coefficient	0.995
Traverse Speed*Stand-off Distance*Loss Coefficient	0.997
4-Way Interactions	1.000
Pressure*Orifice Diameter*Traverse Speed*Stand-off Distance	0.999
Pressure*Orifice Diameter*Traverse Speed*Loss Coefficient	0.792
Pressure*Orifice Diameter*Stand-off Distance*Loss Coefficient	0.998
Pressure*Traverse Speed*Stand-off Distance*Loss Coefficient	0.999
Orifice Diameter*Traverse Speed*Stand-off Distance*Loss Coefficient	0.999
5-Way Interactions	1.000
Pressure*Orifice Diameter*Traverse Speed*Stand-off Distance*Loss Coefficient	1.000
Error	
Total	

Model Summary

S	R-sq	R-sq(adj)	R-sq(pred)
0.343912	96.01%	93.99%	90.62%

Coded Coefficients

Term	Effect
Constant	
Elastic Modulus	
Pressure	1.3465
Orifice Diameter	1.5211
Traverse Speed	-0.7868
Stand-off Distance	-0.0057
Loss Coefficient	1.0972
Pressure*Orifice Diameter	0.4488
Pressure*Traverse Speed	-0.2322
Pressure*Stand-off Distance	-0.0017
Pressure*Loss Coefficient	0.3237
Orifice Diameter*Traverse Speed	-0.2623
Orifice Diameter*Stand-off Distance	-0.0019
Orifice Diameter*Loss Coefficient	0.3657
Traverse Speed*Stand-off Distance	0.0010
Traverse Speed*Loss Coefficient	-0.1892

Stand-off Distance*Loss Coefficient	-0.0014
Pressure*Orifice Diameter*Traverse Speed	-0.0774
Pressure*Orifice Diameter*Stand-off Distance	-0.0006
Pressure*Orifice Diameter*Loss Coefficient	0.1079
Pressure*Traverse Speed*Stand-off Distance	0.0003
Pressure*Traverse Speed*Loss Coefficient	-0.0558
Pressure*Stand-off Distance*Loss Coefficient	-0.0004
Orifice Diameter*Traverse Speed*Stand-off Distance	0.0003
Orifice Diameter*Traverse Speed*Loss Coefficient	-0.0631
Orifice Diameter*Stand-off Distance*Loss Coefficient	-0.0005
Traverse Speed*Stand-off Distance*Loss Coefficient	0.0002
Pressure*Orifice Diameter*Traverse Speed*Stand-off Distance	0.0001
Pressure*Orifice Diameter*Traverse Speed*Loss Coefficient	-0.0186
Pressure*Orifice Diameter*Stand-off Distance*Loss Coefficient	-0.0001
Pressure*Traverse Speed*Stand-off Distance*Loss Coefficient	0.0001
Orifice Diameter*Traverse Speed*Stand-off Distance*Loss Coefficient	0.0001
Pressure*Orifice Diameter*Traverse Speed*Stand-off Distance*Loss Coefficient	0.0000

Term	Coef
Constant	4.612
Elastic Modulus	-2.330
Pressure	0.6732
Orifice Diameter	0.7606
Traverse Speed	-0.3934
Stand-off Distance	-0.0029
Loss Coefficient	0.5486
Pressure*Orifice Diameter	0.2244
Pressure*Traverse Speed	-0.1161
Pressure*Stand-off Distance	-0.0008
Pressure*Loss Coefficient	0.1619
Orifice Diameter*Traverse Speed	-0.1311
Orifice Diameter*Stand-off Distance	-0.0010
Orifice Diameter*Loss Coefficient	0.1829
Traverse Speed*Stand-off Distance	0.0005

Traverse Speed*Loss Coefficient	-0.0946
Stand-off Distance*Loss Coefficient	-0.0007
Pressure*Orifice Diameter*Traverse Speed	-0.0387
Pressure*Orifice Diameter*Stand-off Distance	-0.0003
Pressure*Orifice Diameter*Loss Coefficient	0.0540
Pressure*Traverse Speed*Stand-off Distance	0.0001
Pressure*Traverse Speed*Loss Coefficient	-0.0279
Pressure*Stand-off Distance*Loss Coefficient	-0.0002
Orifice Diameter*Traverse Speed*Stand-off Distance	0.0002
Orifice Diameter*Traverse Speed*Loss Coefficient	-0.0315
Orifice Diameter*Stand-off Distance*Loss Coefficient	-0.0002
Traverse Speed*Stand-off Distance*Loss Coefficient	0.0001
Pressure*Orifice Diameter*Traverse Speed*Stand-off Distance	0.0000
Pressure*Orifice Diameter*Traverse Speed*Loss Coefficient	-0.0093
Pressure*Orifice Diameter*Stand-off Distance*Loss Coefficient	-0.0001
Pressure*Traverse Speed*Stand-off Distance*Loss Coefficient	0.0000
Orifice Diameter*Traverse Speed*Stand-off Distance*Loss Coefficient	0.0000
Pressure*Orifice Diameter*Traverse Speed*Stand-off Distance*Loss Coefficient	0.0000

Term	SE Coef
Constant	0.176
Elastic Modulus	0.172
Pressure	0.0351
Orifice Diameter	0.0351
Traverse Speed	0.0351
Stand-off Distance	0.0351
Loss Coefficient	0.0351
Pressure*Orifice Diameter	0.0351
Pressure*Traverse Speed	0.0351
Pressure*Stand-off Distance	0.0351
Pressure*Loss Coefficient	0.0351
Orifice Diameter*Traverse Speed	0.0351
Orifice Diameter*Stand-off Distance	0.0351
Orifice Diameter*Loss Coefficient	0.0351

Traverse Speed*Stand-off Distance	0.0351
Traverse Speed*Loss Coefficient	0.0351
Stand-off Distance*Loss Coefficient	0.0351
Pressure*Orifice Diameter*Traverse Speed	0.0351
Pressure*Orifice Diameter*Stand-off Distance	0.0351
Pressure*Orifice Diameter*Loss Coefficient	0.0351
Pressure*Traverse Speed*Stand-off Distance	0.0351
Pressure*Traverse Speed*Loss Coefficient	0.0351
Pressure*Stand-off Distance*Loss Coefficient	0.0351
Orifice Diameter*Traverse Speed*Stand-off Distance	0.0351
Orifice Diameter*Traverse Speed*Loss Coefficient	0.0351
Orifice Diameter*Stand-off Distance*Loss Coefficient	0.0351
Traverse Speed*Stand-off Distance*Loss Coefficient	0.0351
Pressure*Orifice Diameter*Traverse Speed*Stand-off Distance	0.0351
Pressure*Orifice Diameter*Traverse Speed*Loss Coefficient	0.0351
Pressure*Orifice Diameter*Stand-off Distance*Loss Coefficient	0.0351
Pressure*Traverse Speed*Stand-off Distance*Loss Coefficient	0.0351
Orifice Diameter*Traverse Speed*Stand-off Distance*Loss Coefficient	0.0351
Pressure*Orifice Diameter*Traverse Speed*Stand-off Distance*Loss Coefficient	0.0351

Term	T-Value
Constant	26.28
Elastic Modulus	-13.55
Pressure	19.18
Orifice Diameter	21.67
Traverse Speed	-11.21
Stand-off Distance	-0.08
Loss Coefficient	15.63
Pressure*Orifice Diameter	6.39
Pressure*Traverse Speed	-3.31
Pressure*Stand-off Distance	-0.02
Pressure*Loss Coefficient	4.61
Orifice Diameter*Traverse Speed	-3.74
Orifice Diameter*Stand-off Distance	-0.03

Orifice Diameter*Loss Coefficient	5.21	
Traverse Speed*Stand-off Distance	0.01	
Traverse Speed*Loss Coefficient	-2.69	
Stand-off Distance*Loss Coefficient	-0.02	
Pressure*Orifice Diameter*Traverse Speed	-1.10	
Pressure*Orifice Diameter*Stand-off Distance	-0.01	
Pressure*Orifice Diameter*Loss Coefficient	1.54	
Pressure*Traverse Speed*Stand-off Distance	0.00	
Pressure*Traverse Speed*Loss Coefficient	-0.80	
Pressure*Stand-off Distance*Loss Coefficient	-0.01	
Orifice Diameter*Traverse Speed*Stand-off Distance	0.00	
Orifice Diameter*Traverse Speed*Loss Coefficient	-0.90	
Orifice Diameter*Stand-off Distance*Loss Coefficient	-0.01	
Traverse Speed*Stand-off Distance*Loss Coefficient	0.00	
Pressure*Orifice Diameter*Traverse Speed*Stand-off Distance	0.00	
Pressure*Orifice Diameter*Traverse Speed*Loss Coefficient	-0.27	
Pressure*Orifice Diameter*Stand-off Distance*Loss Coefficient	-0.00	
Pressure*Traverse Speed*Stand-off Distance*Loss Coefficient	0.00	
Orifice Diameter*Traverse Speed*Stand-off Distance*Loss Coefficient	0.00	
Pressure*Orifice Diameter*Traverse Speed*Stand-off Distance*Loss Coefficient	0.00	

Term	P-Value	VIF
Constant	0.000	
Elastic Modulus	0.000	1.00
Pressure	0.000	1.00
Orifice Diameter	0.000	1.00
Traverse Speed	0.000	1.00
Stand-off Distance	0.935	1.00
Loss Coefficient	0.000	1.00
Pressure*Orifice Diameter	0.000	1.00
Pressure*Traverse Speed	0.002	1.00
Pressure*Stand-off Distance	0.981	1.00
Pressure*Loss Coefficient	0.000	1.00
Orifice Diameter*Traverse Speed	0.000	1.00

Orifice Diameter*Stand-off Distance	0.978	1.00
Orifice Diameter*Loss Coefficient	0.000	1.00
Traverse Speed*Stand-off Distance	0.989	1.00
Traverse Speed*Loss Coefficient	0.009	1.00
Stand-off Distance*Loss Coefficient	0.984	1.00
Pressure*Orifice Diameter*Traverse Speed	0.275	1.00
Pressure*Orifice Diameter*Stand-off Distance	0.994	1.00
Pressure*Orifice Diameter*Loss Coefficient	0.129	1.00
Pressure*Traverse Speed*Stand-off Distance	0.997	1.00
Pressure*Traverse Speed*Loss Coefficient	0.430	1.00
Pressure*Stand-off Distance*Loss Coefficient	0.995	1.00
Orifice Diameter*Traverse Speed*Stand-off Distance	0.996	1.00
Orifice Diameter*Traverse Speed*Loss Coefficient	0.372	1.00
Orifice Diameter*Stand-off Distance*Loss Coefficient	0.995	1.00
Traverse Speed*Stand-off Distance*Loss Coefficient	0.997	1.00
Pressure*Orifice Diameter*Traverse Speed*Stand-off Distance	0.999	1.00
Pressure*Orifice Diameter*Traverse Speed*Loss Coefficient	0.792	1.00
Pressure*Orifice Diameter*Stand-off Distance*Loss Coefficient	0.998	1.00
Pressure*Traverse Speed*Stand-off Distance*Loss Coefficient	0.999	1.00
Orifice Diameter*Traverse Speed*Stand-off Distance*Loss Coefficient	0.999	1.00
Pressure*Orifice Diameter*Traverse Speed*Stand-off Distance*Loss Coefficient	1.000	1.00

Regression Equation in Uncoded Units

Depth of Cut = 2.3 - 2.330 Elastic Modulus + 0.000 Pressure - 7.3 Orifice Diameter
+ 0.000 Traverse Speed + 0.00 Stand-off Distance + 0.0 Loss Coefficient
+ 1.80 Pressure*Orifice Diameter - 0.0000 Pressure*Traverse Speed
- 0.000 Pressure*Stand-off Distance - 0.000 Pressure*Loss Coefficient
+ 0.25 Orifice Diameter*Traverse Speed
+ 0.00 Orifice Diameter*Stand-off Distance
- 1.7 Orifice Diameter*Loss Coefficient
- 0.0000 Traverse Speed*Stand-off Distance
- 0.000 Traverse Speed*Loss Coefficient
- 0.00 Stand-off Distance*Loss Coefficient
- 0.062 Pressure*Orifice Diameter*Traverse Speed
- 0.001 Pressure*Orifice Diameter*Stand-off Distance
+ 0.43 Pressure*Orifice Diameter*Loss Coefficient
+ 0.00000 Pressure*Traverse Speed*Stand-off Distance
+ 0.0000 Pressure*Traverse Speed*Loss Coefficient
+ 0.000 Pressure*Stand-off Distance*Loss Coefficient

- 0.000 Orifice Diameter*Traverse Speed*Stand-off Distance
+ 0.06 Orifice Diameter*Traverse Speed*Loss Coefficient
+ 0.00 Orifice Diameter*Stand-off Distance*Loss Coefficient
+ 0.0000 Traverse Speed*Stand-off Distance*Loss Coefficient
+ 0.0000 Pressure*Orifice Diameter*Traverse Speed*Stand-off Distance
- 0.015 Pressure*Orifice Diameter*Traverse Speed*Loss Coefficient
- 0.000 Pressure*Orifice Diameter*Stand-off Distance*Loss Coefficient
- 0.00000 Pressure*Traverse Speed*Stand-off Distance*Loss Coefficient
- 0.000 Orifice Diameter*Traverse Speed*Stand-off Distance*Loss Coefficient
+ 0.0000 Pressure*Orifice Diameter*Traverse Speed*Stand-off Distance*Loss Coef
ficient

Alias Structure

Factor	Name
A	Pressure
B	Orifice Diameter
C	Traverse Speed
D	Stand-off Distance
E	Loss Coefficient

Aliases
I
A
B
C
D
E
AB
AC
AD
AE
BC
BD
BE
CD
CE
DE
ABC
ABD

ABE

ACD

ACE

ADE

BCD

BCE

BDE

CDE

ABCD

ABCE

ABDE

ACDE

BCDE

ABCDE

Fits and Diagnostics for Unusual Observations

Obs	Depth of Cut	Fit	Resid	Std Resid	
20	7.324	6.320	1.004	3.62	R
28	7.306	6.305	1.000	3.60	R
84	4.394	5.154	-0.760	-2.74	R
92	4.383	5.140	-0.757	-2.73	R

R Large residual

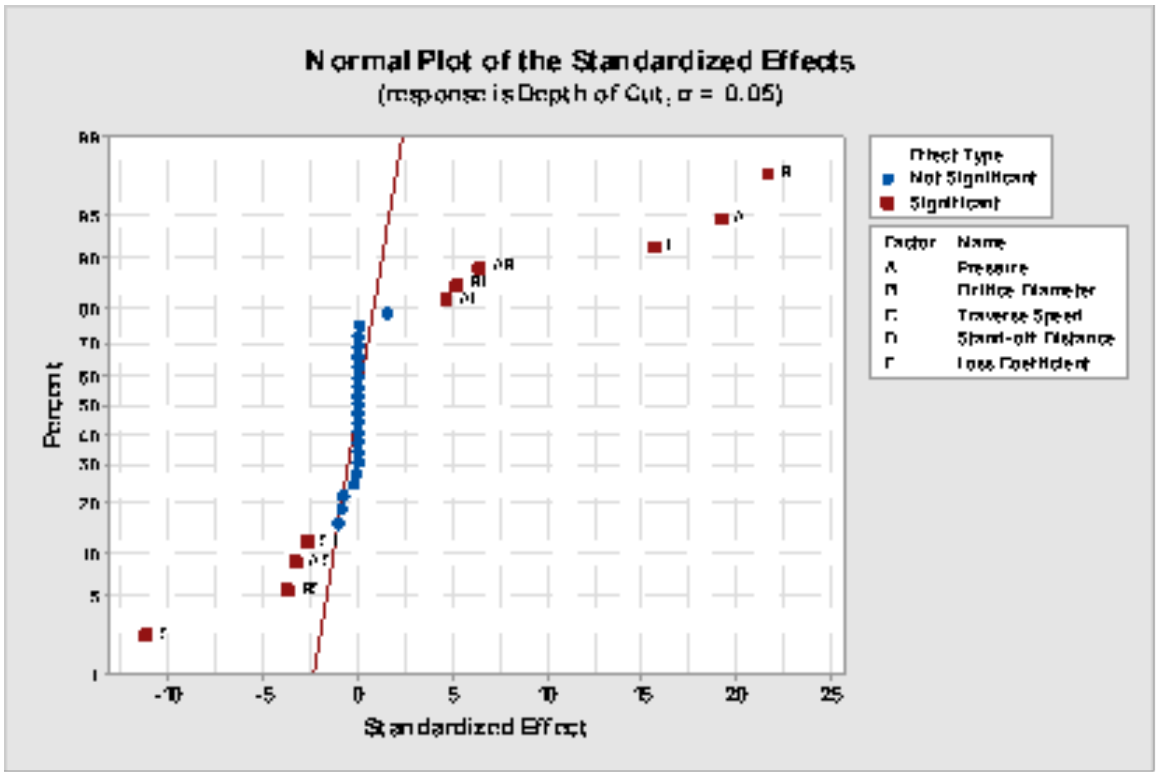
Normal Plot of the Standardized Effects
(response is Depth of Cut, α = 0.05)
Percent
Standardized Effect
Effect Type
Not Significant
Significant
Factor Name
A Pressure
B Orifice Diameter
C Traverse Speed
D Stand-off Distance
E Loss Coefficient

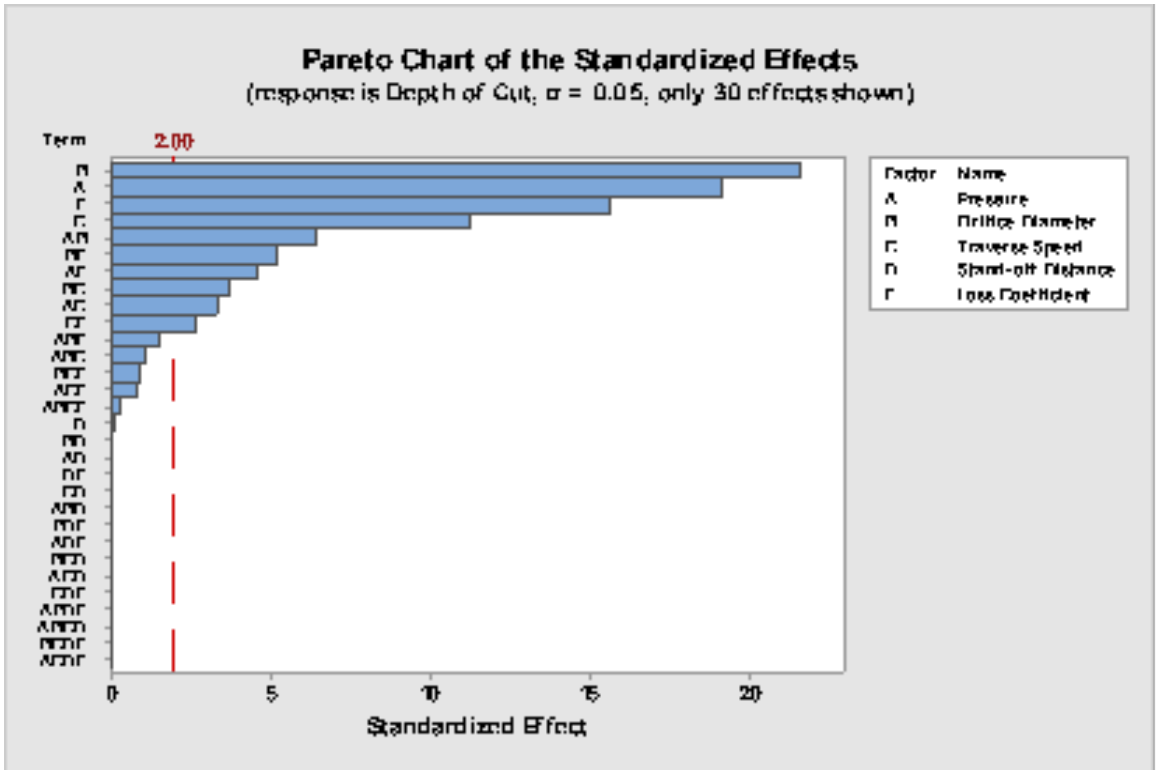
Pareto Chart of the Standardized Effects
(response is Depth of Cut, α = 0.05, only 30 effects shown)
Term
2.00
Standardized Effect
Factor Name
A Pressure
B Orifice Diameter
C Traverse Speed
D Stand-off Distance
E Loss Coefficient

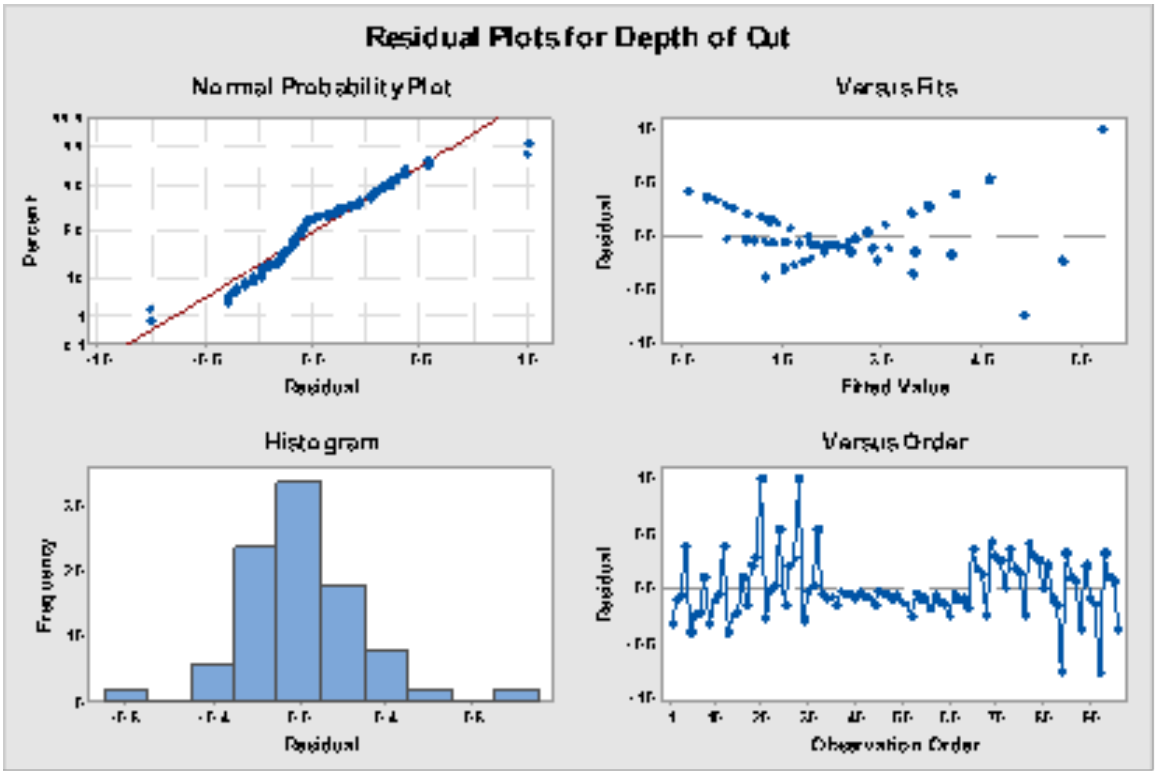

Factorial Plots for Depth of Cut

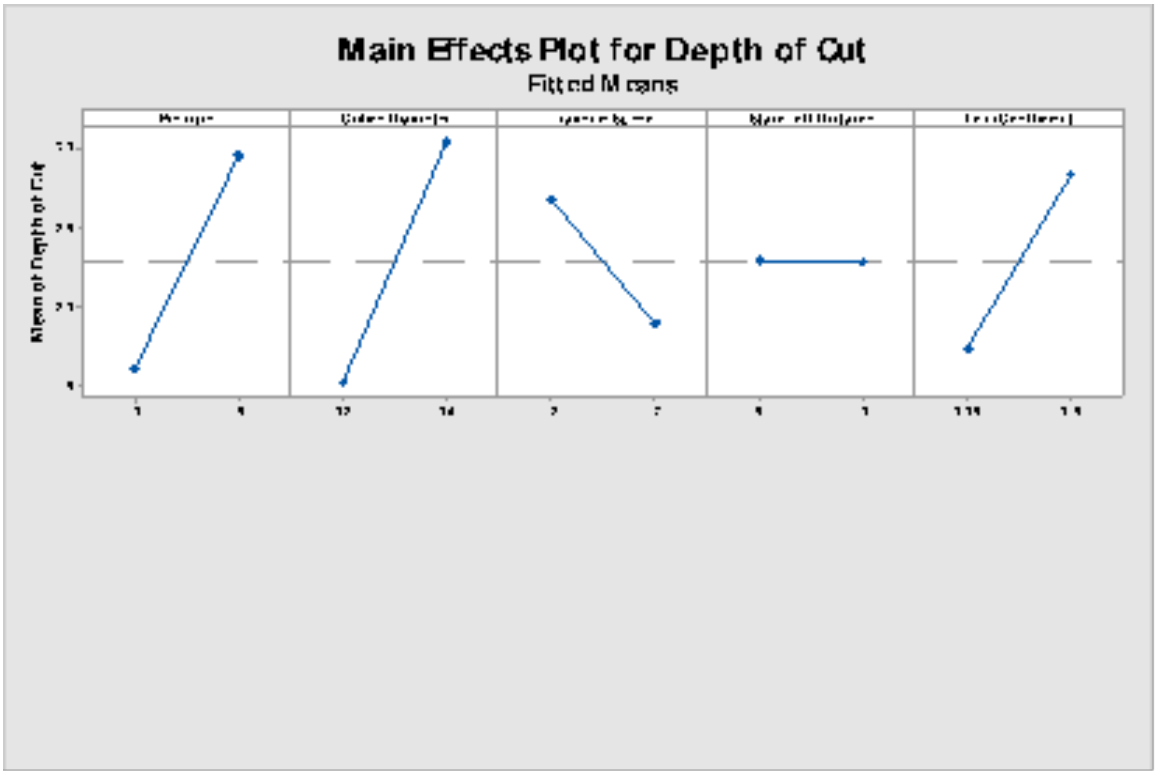

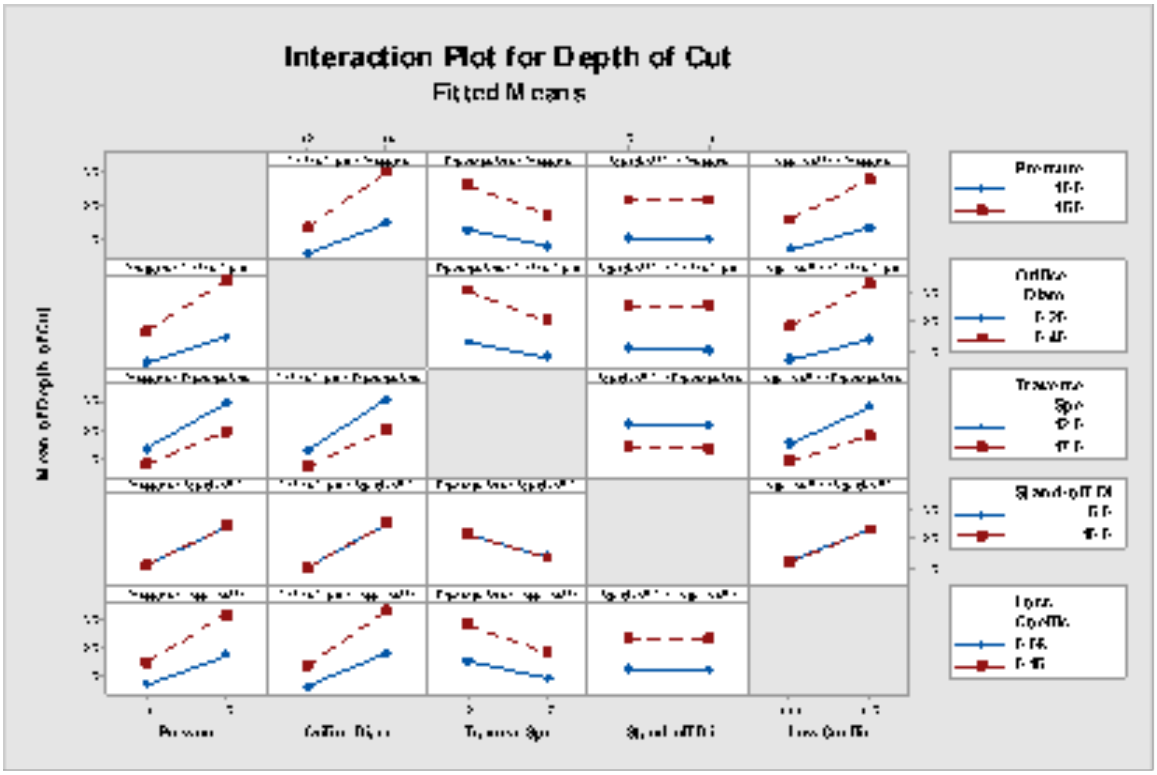

Factorial Regression: Depth of Cut versus Elastic ... ce, Loss Coefficient

Stepwise Selection of Terms

α to enter = 0.15, α to remove = 0.15

Analysis of Variance

Source	DF	Adj SS	Adj MS	F-Value	P-Value
Model	12	179.157	14.9297	159.39	0.000
Covariates	1	21.720	21.7205	231.88	0.000
Elastic Modulus	1	21.720	21.7205	231.88	0.000
Linear	4	142.794	35.6985	381.11	0.000
Pressure	1	43.512	43.5123	464.53	0.000
Orifice Diameter	1	55.533	55.5330	592.86	0.000
Traverse Speed	1	14.857	14.8572	158.61	0.000
Loss Coefficient	1	28.891	28.8913	308.44	0.000
2-Way Interactions	6	14.363	2.3939	25.56	0.000
Pressure*Orifice Diameter	1	4.835	4.8347	51.61	0.000
Pressure*Traverse Speed	1	1.293	1.2935	13.81	0.000
Pressure*Loss Coefficient	1	2.515	2.5153	26.85	0.000

Orifice Diameter*Traverse Speed	1	1.651	1.6508	17.62	0.000
Orifice Diameter*Loss Coefficient	1	3.210	3.2101	34.27	0.000
Traverse Speed*Loss Coefficient	1	0.859	0.8588	9.17	0.003
3-Way Interactions	1	0.279	0.2795	2.98	0.088
Pressure*Orifice Diameter*Loss Coefficient	1	0.279	0.2795	2.98	0.088
Error	83	7.775	0.0937		
Total	95	186.932			

Model Summary

S	R-sq	R-sq(adj)	R-sq(pred)
0.306056	95.84%	95.24%	94.38%

Coded Coefficients

Term	Effect	Coef	SE Coef	T-Value	P-Value	VIF
Constant		4.612	0.156	29.53	0.000	
Elastic Modulus		-2.330	0.153	-15.23	0.000	1.00
Pressure	1.3465	0.6732	0.0312	21.55	0.000	1.00
Orifice Diameter	1.5211	0.7606	0.0312	24.35	0.000	1.00
Traverse Speed	-0.7868	-0.3934	0.0312	-12.59	0.000	1.00
Loss Coefficient	1.0972	0.5486	0.0312	17.56	0.000	1.00
Pressure*Orifice Diameter	0.4488	0.2244	0.0312	7.18	0.000	1.00
Pressure*Traverse Speed	-0.2322	-0.1161	0.0312	-3.72	0.000	1.00
Pressure*Loss Coefficient	0.3237	0.1619	0.0312	5.18	0.000	1.00
Orifice Diameter*Traverse Speed	-0.2623	-0.1311	0.0312	-4.20	0.000	1.00
Orifice Diameter*Loss Coefficient	0.3657	0.1829	0.0312	5.85	0.000	1.00
Traverse Speed*Loss Coefficient	-0.1892	-0.0946	0.0312	-3.03	0.003	1.00
Pressure*Orifice Diameter*Loss Coefficient	0.1079	0.0540	0.0312	1.73	0.088	1.00

Regression Equation in Uncoded Units

Depth of Cut = -1.04 - 2.330 Elastic Modulus + 0.2693 Pressure + 3.99 Orifice Diameter
+ 0.2322 Traverse Speed + 0.549 Loss Coefficient
+ 0.898 Pressure*Orifice Diameter - 0.01857 Pressure*Traverse Speed
+ 0.0000 Pressure*Loss Coefficient - 0.525 Orifice Diameter*Traverse Speed
- 0.87 Orifice Diameter*Loss Coefficient
- 0.0378 Traverse Speed*Loss Coefficient
+ 0.216 Pressure*Orifice Diameter*Loss Coefficient

Alias Structure

Factor	Name
A	Pressure
B	Orifice Diameter
C	Traverse Speed
D	Stand-off Distance
E	Loss Coefficient

Aliases
I
A
B
C
E
AB
AC
AE
BC
BE
CE
ABE

Fits and Diagnostics for Unusual Observations

Obs	Depth of Cut	Fit	Resid	Std Resid	
20	7.324	6.205	1.119	3.94	R
28	7.306	6.205	1.101	3.88	R
84	4.394	5.040	-0.646	-2.28	R
92	4.383	5.040	-0.657	-2.31	R

R Large residual

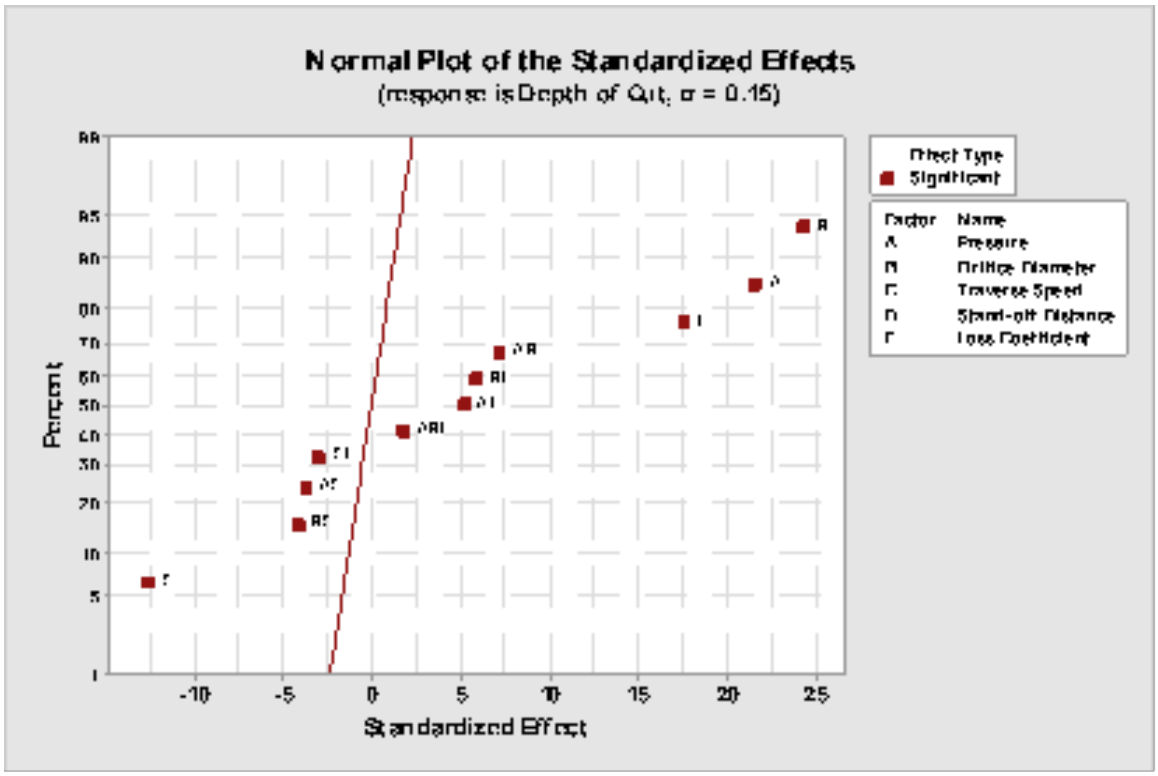
Normal Plot of the Standardized Effects
(response is Depth of Cut, α = 0.15)
Percent
Standardized Effect
Effect Type
Significant
Factor Name
A Pressure
B Orifice Diameter
C Traverse Speed
D Stand-off Distance
F Loss Coefficient

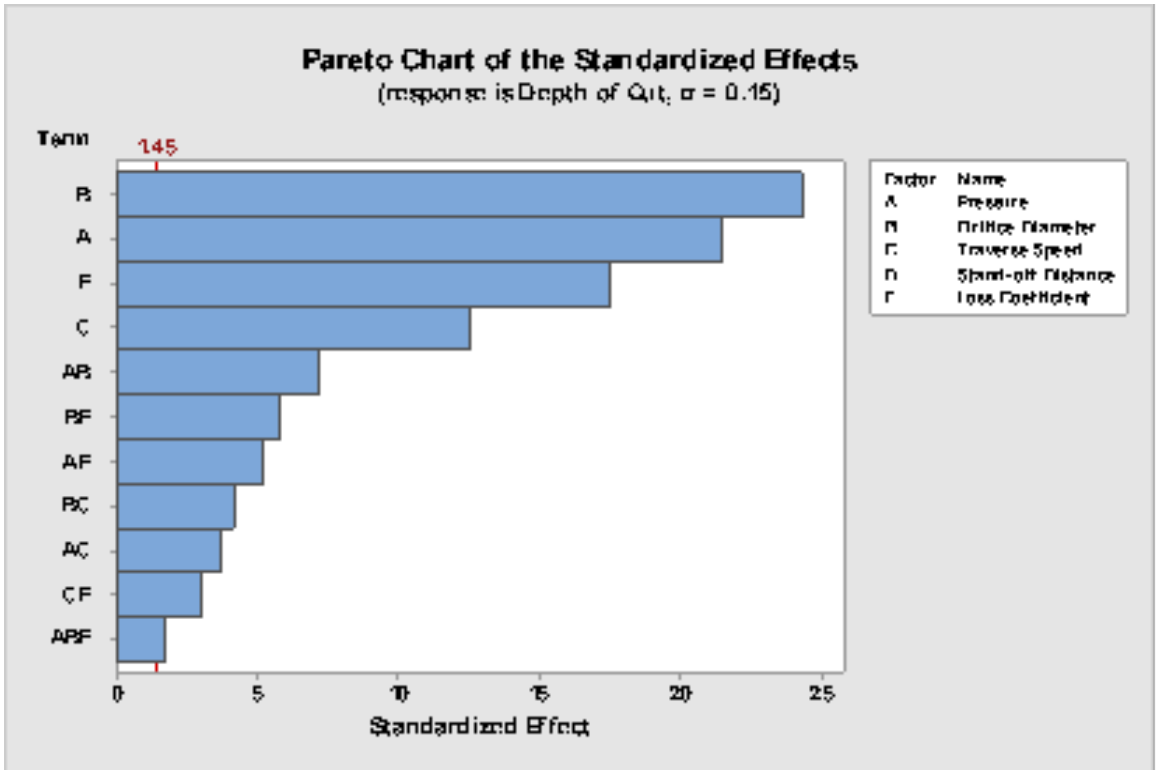
Pareto Chart of the Standardized Effects
(response is Depth of Cut, α = 0.15)
Term
145
B
A
F
C
AB
BF
AF
BC
AC
CF
ABF
Standardized Effect
Factor Name
A Pressure
B Orifice Diameter
C Traverse Speed
D Stand-off Distance
F Loss Coefficient

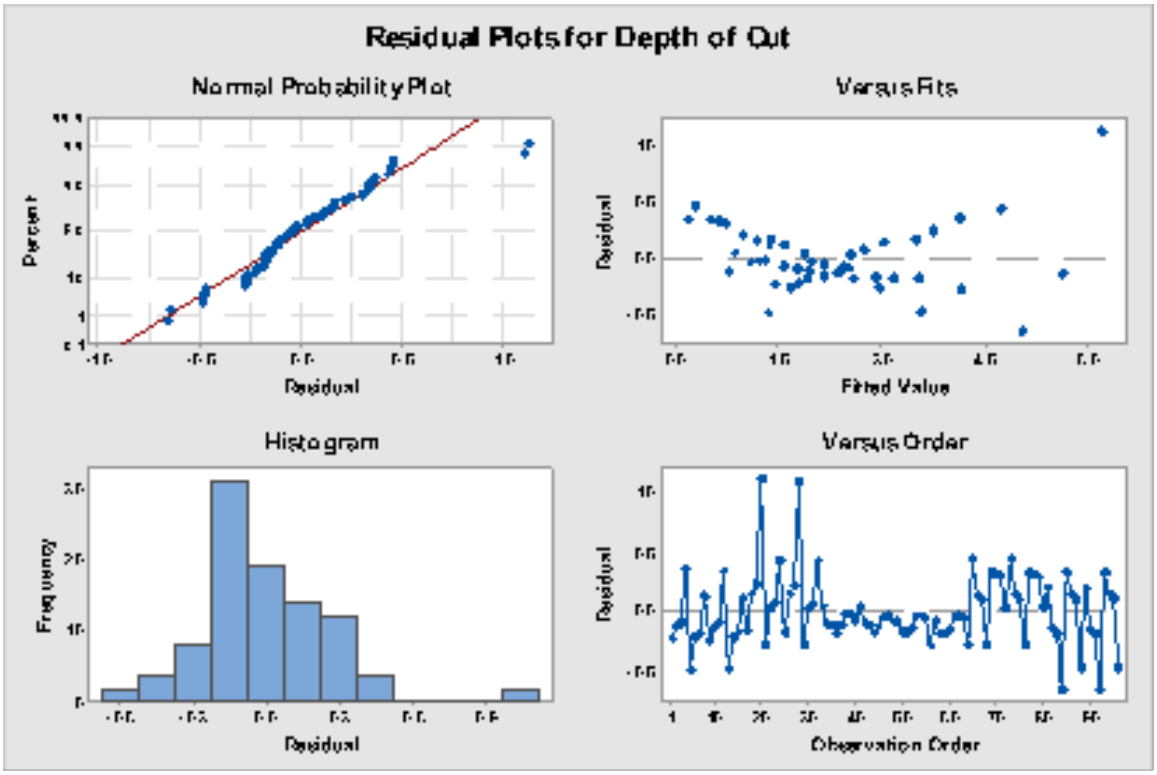

Factorial Plots for Depth of Cut

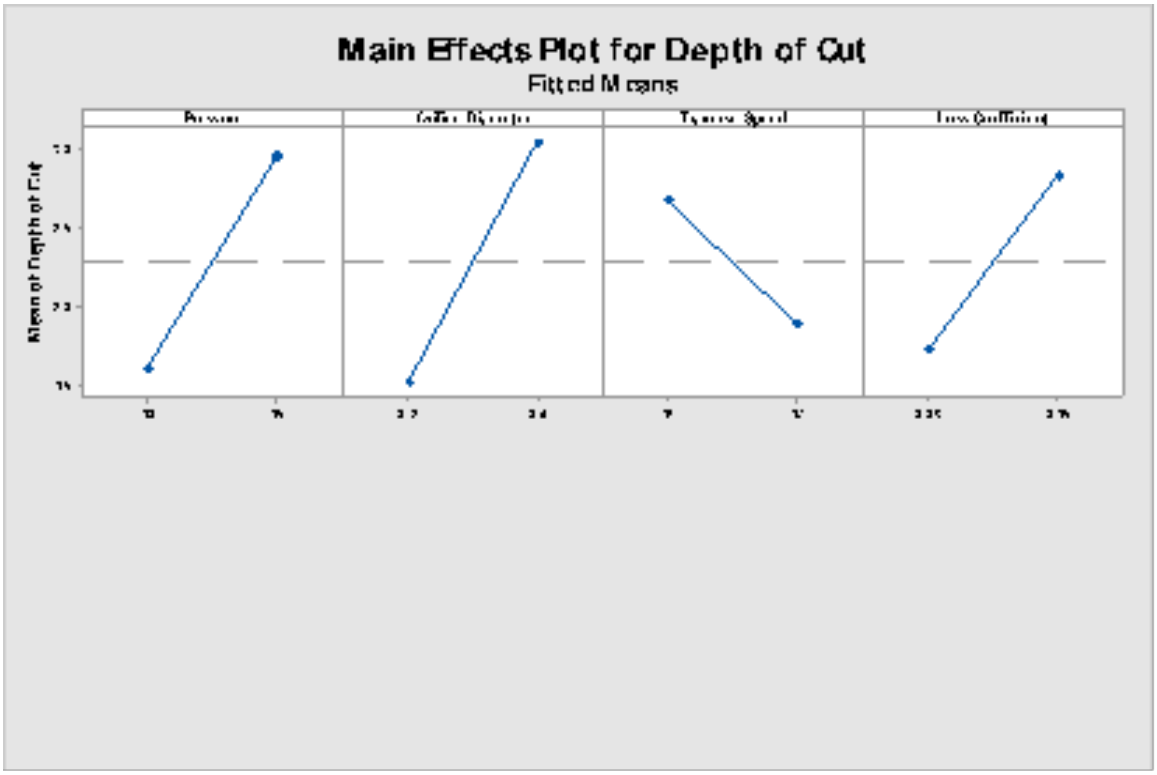

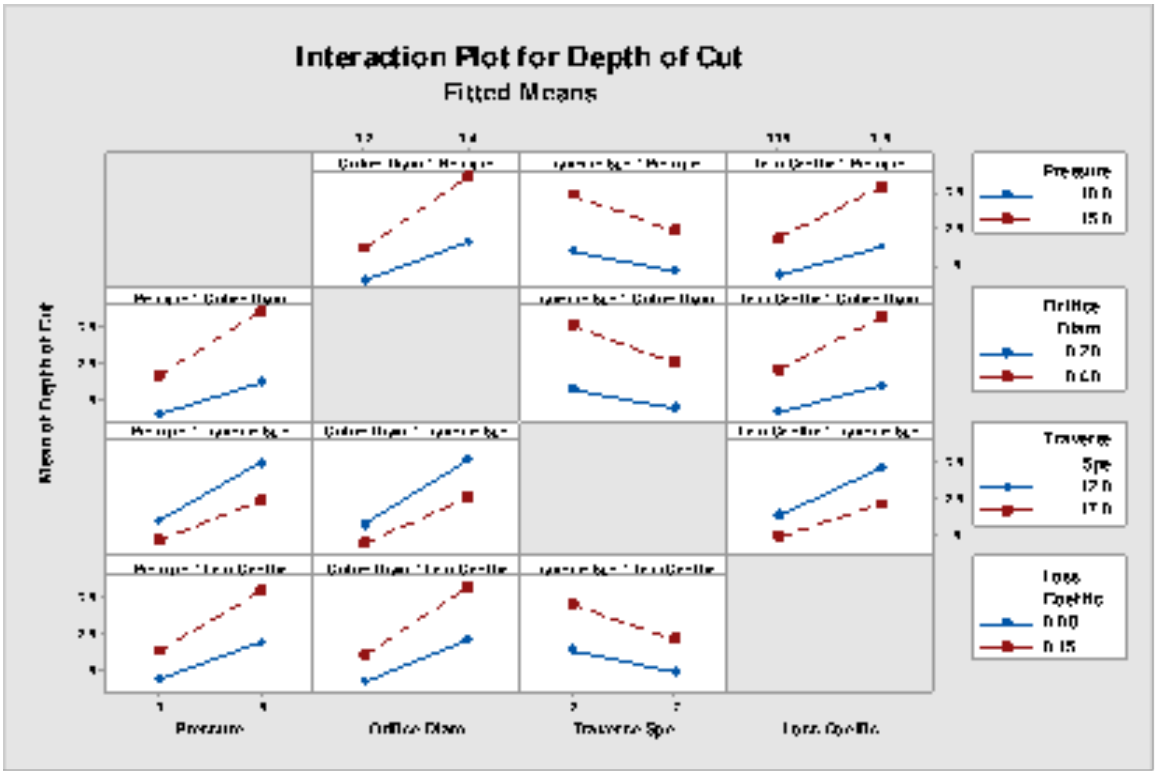

Prediction for Depth of Cut

Regression Equation in Uncoded Units

Depth of Cut = -1.04 - 2.330 Elastic Modulus + 0.2693 Pressure + 3.99 Orifice Diameter + 0.2322 Traverse Speed + 0.549 Loss Coefficient + 0.898 Pressure*Orifice Diameter - 0.01857 Pressure*Traverse Speed + 0.0000 Pressure*Loss Coefficient - 0.525 Orifice Diameter*Traverse Speed - 0.87 Orifice Diameter*Loss Coefficient - 0.0378 Traverse Speed*Loss Coefficient + 0.216 Pressure*Orifice Diameter*Loss Coefficient

Settings

Variable	Setting
Elastic Modulus	1
Pressure	5
Orifice Diameter	0.4
Traverse Speed	12
Loss Coefficient	0.08

Prediction

Fit	SE Fit	95% CI	95% PI	
0.347056	0.225251	(-0.100959, 0.795070)	(-0.408770, 1.10288)	X

X denotes an unusual point relative to predictor levels used to fit the model.

Settings

Variable	Setting
Elastic Modulus	1
Pressure	10
Orifice Diameter	0.4
Traverse Speed	12
Loss Coefficient	0.08

Prediction

Fit	SE Fit	95% CI	95% PI
1.94287	0.108207	(1.72765, 2.15809)	(1.29721, 2.58853)

Settings

Variable	Setting
Elastic Modulus	1
Pressure	15
Orifice Diameter	0.4
Traverse Speed	12
Loss Coefficient	0.08

Prediction

Fit	SE Fit	95% CI	95% PI
3.53869	0.108207	(3.32347, 3.75391)	(2.89303, 4.18435)

Settings

Variable	Setting
Elastic Modulus	1
Pressure	20
Orifice Diameter	0.4
Traverse Speed	12
Loss Coefficient	0.08

Prediction

Fit	SE Fit	95% CI	95% PI	
5.13451	0.225251	(4.68649, 5.58252)	(4.37868, 5.89033)	X

X denotes an unusual point relative to predictor levels used to fit the model.

Response Optimization: Depth of Cut

Parameters

Response	Goal	Lower	Target	Upper	Weight	Importance
Depth of Cut	Target	0.515663	2.3	7.32383	1	1

Variable Ranges

Variable	Values
Pressure	(10, 15)
Orifice Diameter	(0.2, 0.4)
Traverse Speed	(12, 17)
Loss Coefficient	0.08, 0.15
Elastic Modulus	1

Solution

Solution	Pressure	Orifice Diameter	Traverse Speed	Loss Coefficient	Elastic Modulus	Depth of Cut Fit	Composite Desirability
1	12.5	0.294790	17	0.15	1	2.3	1

Multiple Response Prediction

Variable	Setting
Pressure	12.5
Orifice Diameter	0.29479
Traverse Speed	17
Loss Coefficient	0.15
Elastic Modulus	1

Response	Fit	SE Fit	95% CI	95% PI
Depth of Cut	2.3000	0.0625	(2.1756, 2.4244)	(1.6787, 2.9213)

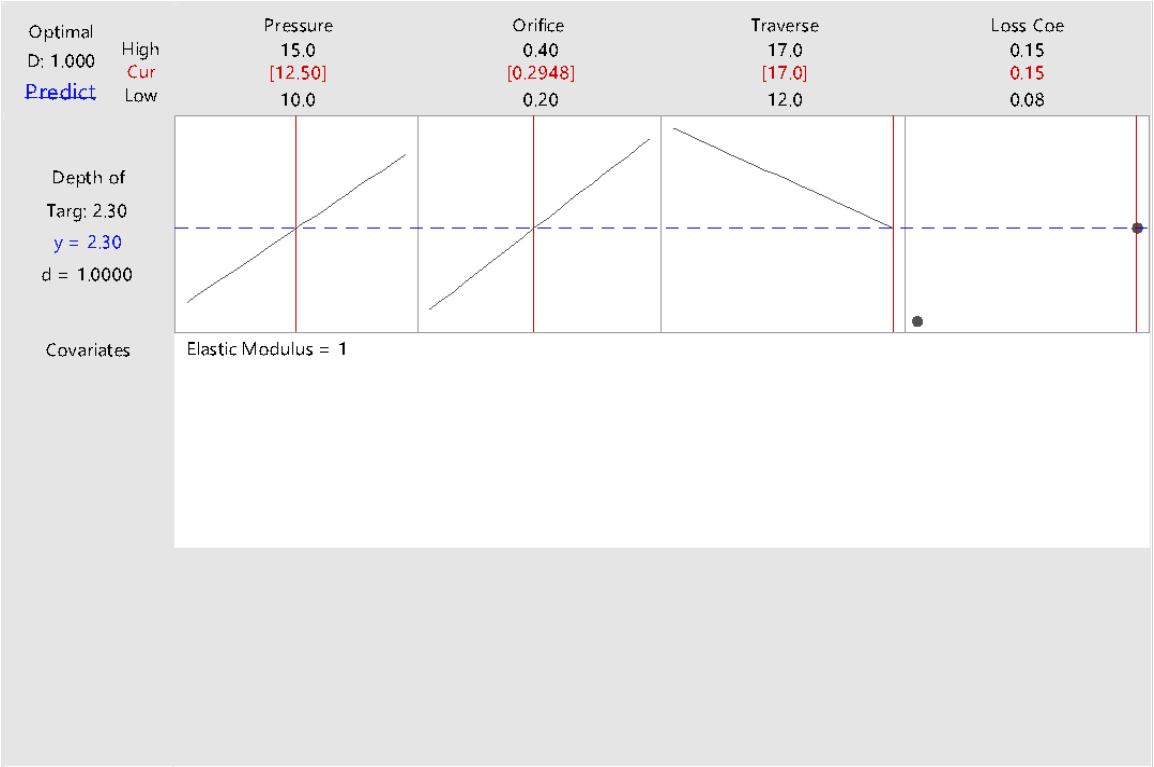

Response Optimization: Depth of Cut

Parameters

Response	Goal	Lower	Target	Upper	Weight	Importance
Depth of Cut	Maximum	0.515663	7.32383		1	1

Variable Ranges

Variable	Values
Pressure	(10, 15)
Orifice Diameter	(0.2, 0.4)
Traverse Speed	(12, 17)
Loss Coefficient	0.08, 0.15
Elastic Modulus	1

Solution

Solution	Pressure	Orifice Diameter	Traverse Speed	Loss Coefficient	Elastic Modulus	Depth of Cut Fit	Composite Desirability
1	15	0.4	12	0.15	1	5.62241	0.750091

Multiple Response Prediction

Variable	Setting
Pressure	15

Orifice Diameter	0.4
Traverse Speed	12
Loss Coefficient	0.15
Elastic Modulus	1

Response	Fit	SE Fit	95% CI	95% PI
Depth of Cut	5.622	0.108	(5.407, 5.838)	(4.977, 6.268)

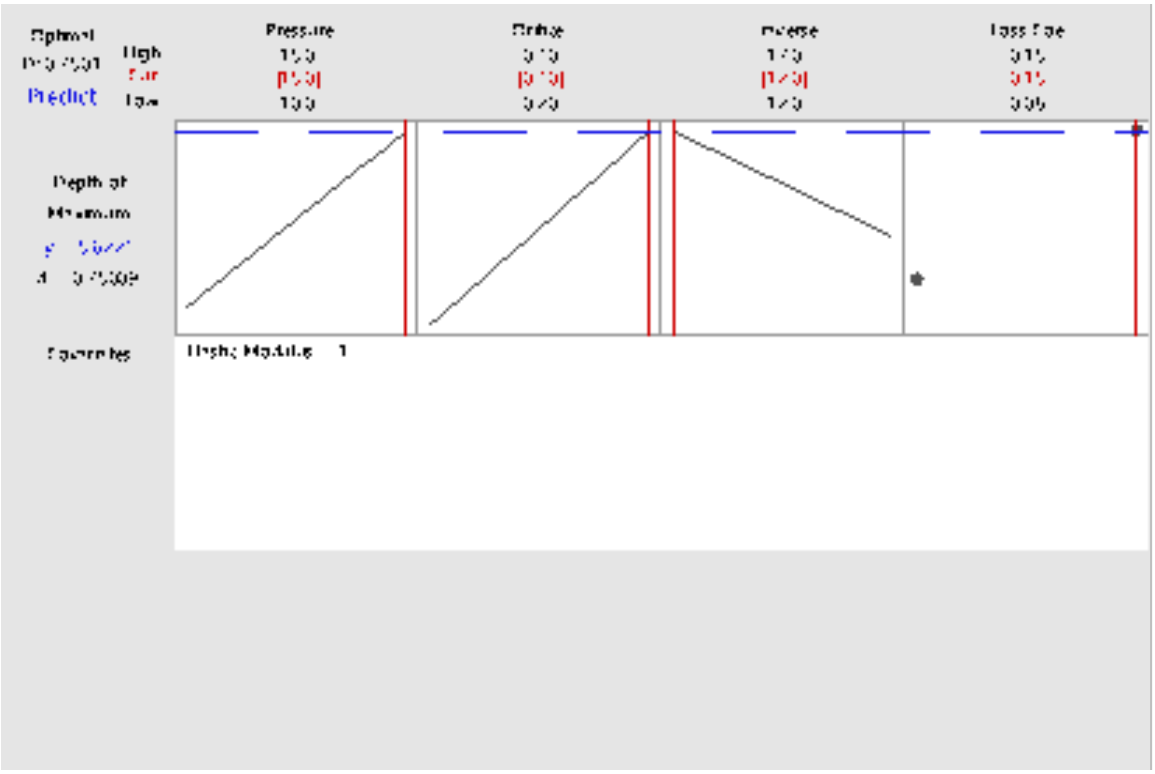

APPENDIX C

EXPERIMENTS VIDEOS

Cow bone WJ incision and measurement:

https://youtu.be/7m_PyZEFSSs

Cow skin WJ incision:

https://youtu.be/Ev1TfsQrHGE

Cow skin WJ incision (slow):

https://youtu.be/siYndfkb2gY

Trapped water bubble created under fat tissue during high pressure wj incision

https://youtu.be/0zZuHgJxn0Q

Incision performed on cow hoof ssing 30,000 psi WJ pressure:

https://youtu.be/0jfMCu0Hra4

REFERENCES

[1] (August 12, 2018). *Types of Minimally Invasive Surgery*. Available: http://www.hopkinsmedicine.org/minimally_invasive_robotic_surgery/types.html

[2] I. Wright. (2016, August 13, 2018). *An Engineer's Guide to Waterjet Cutting*. Available: https://www.engineering.com/AdvancedManufacturing/ArticleID/12716/An-Engineers-Guide-to-Waterjet-Cutting.aspx

[3] H. Shimizu, *Shimizu's Textbook of Dermatology*, 1 ed. Hokkaido University Press, Nakayama Shoten, 2007.

[4] R. Raghavan, P. Arya, P. Arya, and S. China, "Abdominal incisions and sutures in obstetrics and gynaecology," *The Obstetrician & Gynaecologist,* no. 16, pp. 13-18, 2014.

[5] L. M. Biga *et al*., *Anatomy & Physiology*. Corvallis, Oregon: Oregon State University, 2019.

[6] S. M. Arif, "Finite Element Analysis of Skin Injuries by Water Jet Cutting," Masters Thesis, Mechanical and Industrial Engineering Departement, New Jersey Institute of Technology, Newark, NJ, 1997.

[7] F. M. Hendriks, "Mechanical Behaviour of Human Epidermal and Dermal Layers in Vivo," Department of Biomedical Engineering, Technische Universiteit Eindhoven, Eindhoven, The Netherlands, 2005.

[8] J. Sandby-Moller, T. Poulsen, and H. C. Wulf, "Epidermal Thickness at Different Body Sites: Relationship to Age, Gender, Pigmentation, Blood Content, Skin Type and Smoking Habits," *Acta Derm Venereol,* vol. 83, pp. 410-413, 2003.

[9] O. Akkus, A. Oguz, M. Uzunlulu, and M. Kizilgul, "Evaluation of Skin and Subcutaneous Adipose Tissue Thickness for Optimal Insulin Injection," *Diabetes & Metabolism,* vol. 3, no. 8, 2012.

[10] A. Laurent *et al*., "Echographic measurement of skin thickness in adults by high frequency ultrasound to assess the appropriate microneedle length for intradermal delivery of vaccines," *Vaccine,* vol. 25, pp. 6423–6430, 2007.

[11] M. D. Alexander H, "Determining Skin Thickness with Pulsed Ultrasound", *Journal of Investigative Dermatology,* vol. 72, no. 1, 1979.

[12] R. K. Mlosek and S. Malinowska, "Ultrasound Image of the Skin, Apparatus and Imaging Basics," *Journal of Ultrasonography,* vol. 13, pp. 212-221, 2013.

[13] (June 25, 2018). *Pressure Ulcer Prevention*. Available: https://www.longportinc.com/episcan-i-200/high-resolution-ultrasound/10-main-website-pages#!Slide1

[14] M. Geerligs, "Skin Layer Mechanics," Technische Universiteit Eindhoven, Eindhoven, The Netherlands, 2009.

[15] K. B. Aisling Ni Annaidh, Michel Destrade' Michael D. Gilchrist, Melanie Ottenio, "Characterising the Anisotropic Mechanical Properties of Excised Human Skin," *Journal of the Mechanical Behavior of Biomedical Materials,* vol. 5, pp. 139-148, 2013.

[16] (2014, January 21, 2019). *Minimally Invasive Total Hip Replacement*. Available: https://orthoinfo.aaos.org/en/treatment/minimally-invasive-total-hip-replacement/

[17] (2015, January 21, 2019). *Laparoscopy*. Available: https://www.acog.org/Patients/FAQs/Laparoscopy?IsMobileSet=false#how

[18] (2016, January 24, 2019). *Musculoskeletal Key*. Available: https://musculoskeletalkey.com/wp-content/uploads/2016/11/F00019Xf019-002-9780443069918.jpg

[19] (2018, January 21, 2019). *Melbourne Oesophagogastric And General Surgery*. Available: http://www.moggs.com.au/laparoscopy/appendect-cholecty/

[20] J. Whitlock. (2018, December 22, 2018). *Burr Hole Surgery Information*. Available: https://www.verywellhealth.com/burr-hole-surgery-information-3157273

[21] (2018, May 3, 2018). *Debridement*. Available: https://surgery.ucsf.edu/conditions--procedures/debridement.aspx

[22] H.-O. Rennekampff, H.-E. Schaller, D. Wisser, and M. Tenenhaus, "Debridement of burn wounds with a water jet surgical tool," *Burns,* vol. 32, pp. 64-69, 2006.

[23] D. Smeak and L. N. Hill, "Core Surgical Skills: Basic Instrument Use," Texas A&M University, College Station, Texas2011.

[24] A. Schneider and H. Feussner, *Biomedical Engineering in Gastrointestinal Surgery*, 1st ed. Cambridge, Massachusetts: Academic Press, 2017.

[25] P. Wilder-Smith, R. Dent, A.-M. A. Arrastia, L.-H. Liaw, and M. Berns, "Incision Properties and Thermal Effects of Three CO2 Lasers in Soft Tissue," *Oral Surgery, Oral Medicine, Oral Pathology, Oral Radiology, and Endodontology,* vol. 79, no. 6, pp. 685-691, 1995.

[26] K. S. Jamali, N. A. Khan, M. Jawed, and U. Shaikh, "Diathermy Incisions vs. Surgical Scalpel Incisions; Outcome in General Surgery," *The Professional Medical Journal,* vol. 22, no. 11, pp. 1520-1524, 2015.

[27] D. K. Dutt and I. Dutta, "The Harmonic Scalpel," *The Journal of Obstetrics and Gynecology of India,* vol. 66, no. 3, pp. 209-210, 2016.

[28] J. Edward, F. Fitzgerald, M. Malik, and I. Ahmed, "A Single-blind Controlled Study of Electrocautery and Ultrasonic Scalpel Smoke Plumes in Laparoscopic Surgery," *Surgical Endoscopy,* vol. 26, no. 2, pp. 337–342, 2012.

[29] P. Hreha *et al*., "Water Jet Technology Used in Medicine," *Technical Gazette,* vol. 17, no. 2, pp. 237-240, 2010.

[30] J. Beard. (1994) Technology: Water Jet Puts Surgeons at the Cutting Edge. *NewScientist*. Available: https://www.newscientist.com/article/mg14319353-500-technology-water-jet-puts-surgeons-at-the-cutting-edge/

[31] G. Yildirim, "Using Water Jet Technology to Perform Skin Surgery," 2003.

[32] M. Hanna, "Waterjet Technology in Skin Incision," N. Atalla, Ed., ed. Newark, New Jersey, 2018.

[33] N. Areeratchakul, "Investigation of Water Jet Based Skin Surgery," 2002.

[34] G. Kraaij, R. G. H. H. Nelissen, E. R. Valstar, G. J. M. Tuijthof, and J. Dankelman, "Waterjet cutting of periprosthetic interface tissue in loosened hip prostheses: An in vitro feasibility study," (in English), *Medical Engineering and Physics,* Article vol. 37, no. 2, pp. 245-250, 02 / 01 / 2015.

[35] T. Bahls, F. A. Frohlich, A. Hellings, B. Deutschmann, and A. O. Albu-Schaffer, "Extending the Capability of Using a Waterjet in Surgical Interventions by the Use of Robotics," *IEEE Transactions on Biomedical Engineering,* Article vol. 64, no. 2, pp. 284-294, 2017.

[36] P. DN and B. R, "Resection of the liver with a water jet," *British Journal of Surgery,* vol. 69, no. 2, pp. 93-94, 1982.

[37] K. Vichyavichien, "Interventions of Water Jet Technology on Skin Surgery," Masters Thesis, Mechanical and Industrial Engineering, New Jersey Institute of Technology, Newark, New Jersey, 1999.

[38] B. RF, D. N, and W. P, "Use of Water Jet Resection in Organ-Sparing Kidney Surgery," *Journal of Endourology,* vol. 14, no. 6, pp. 501-505, 2000.

[39] M. Wanner, S. Jakob, F. Schwarzl, M. Oberholzer, and G. Pierer, "Optimizing the Parameters for Hydro-Jet Dissection in Fatty Tissue - A Morphological Ex Vivo Analysis," *Eur. Surg.,* vol. 34, no. 2, 2002.

[40] S. H *et al.*, "Hydro-Jet-assisted Laparoscopic Cholecystectomy: A Prospective Randomized Clinical Study," *Surgery,* vol. 133, no. 6, pp. 635-640, 2003.

[41] M. Honl *et al.*, "The Water Jet as a New Tool for Endoprosthesis Revision Surgery – An in vitro Study on Human Bone and Bone Cement," *Bio-Medical Materials and Engineering,* vol. 13, pp. 317–325, 2003.

[42] M. Tenenhaus, D. Bhavsar, and H.-O. Rennekampff, "Treatment of deep partial thickness and indeterminate depth facial burn wounds with water—jet debridement and a biosynthetic dressing," *Injury, International Journal of The Care of the Injured,* p. 7, 2007.

[43] H. G. Rau, A. P. Duessell, and S. Wurzbacher, "The Use of Water-jet Dissection in Open and Laparoscopic Liver Resection," *Hepato Pancreato Biliary,* vol. 10, no. 275-280, 2008.

[44] D. Keiner, J. Oertel, M. R. Gaab, V. Backhaus, and J. Piek, "Water jet dissection in neurosurgery: An update after 208 procedures with special reference to surgical technique and complications," (in English), *Neurosurgery,* vol. 67, no. SUPPL. 2, pp. 342- 354, 2010.

[45] T. C. S. Cubison, S. A. Pape, and S. L. A. Jeffery, "Dermal preservation using the Versajet hydrosurgery system for debridement of paediatric burns," *Burns,* vol. 32, pp. 714-720, 2006.

[46] (April 2, 2018). *Specific Energy*. Available: http://www.idc-online.com/technical_references/pdfs/chemical_engineering/Quantum_Mechanics_Specific_Energy.pdf

[47] G. Abdou, "Analysis of Velocity Control of Waterjets for Waterjet Machining," presented at the Waterjet Cutting West, Lost Angeles, California, November 14-15, 1989,

[48] "A New Dimension in Water Jet Surgery: The ERBEJET 2 in the VIO System.," in *Waterjet Surgery*, ERBE, Ed., ed. Tübingen, Germany: Erbe Elektromedizin GmbH.

[49] "Helix Hydro-Jet Applicator System," in *Helix Hydro-Jet*, H. Med, Ed., ed. Schwerin, Germany: Human Med.

[50] "VERSAJET II Hydrosurgery System," I. Smith & Nephew, Ed., ed. London, United Kingdom: Smith & Nephew Medical Ltd., 2012.

[51] "The Mach 4c Series," F. I. Corporation, Ed., ed, 2018.

[52] "ABSOLUTE Coolant Proof Caliper Series 500 with Dust/Water Protection Conforming to IP67 Level," in *Product Information*, M. A. Corporation, Ed., ed, 2018.

[53] O. S. Sasaki N, "Stress-strain curve and Young's modulus of a collagen molecule as determined by the X-ray diffraction technique," *Journal of Biomechanics,* vol. 29, no. 5, pp. 655-658, 1996.

[54] S. Pal, *Design of Artificial Human Joints & Organs*. Springer, 2014.